

NACA TN 4264 50901

0066904



TECH LIBRARY KAFB, NM

NATIONAL ADVISORY COMMITTEE FOR AERONAUTICS

TECHNICAL NOTE 4264

INTERNAL CHARACTERISTICS AND PERFORMANCE OF SEVERAL JET
DEFLECTORS AT PRIMARY-NOZZLE PRESSURE RATIOS UP TO 3.0

By Jack G. McArdle

Lewis Flight Propulsion Laboratory
Cleveland, Ohio



Washington

June 1958

AFMDC

TECHNICAL NOTE



TABLE OF CONTENTS

	Page
<u>SUMMARY</u>	1
<u>INTRODUCTION</u>	1
<u>APPARATUS AND INSTRUMENTATION</u>	2
BASIC JET EXHAUST SYSTEMS	3
JET DEFLECTORS	3
Swivelled Nozzles	3
Auxiliary Nozzles	4
Mechanical Deflectors	4
Miscellaneous Jet Deflectors	5
EXPERIMENTAL SETUP	6
INSTRUMENTATION	6
<u>PROCEDURE</u>	7
<u>DATA PRESENTATION AND APPLICATION</u>	7
<u>RESULTS AND DISCUSSION</u>	9
SWIVELLED-NOZZLE JET DEFLECTORS	9
Performance of Swivelled Tailpipe	10
Performance of Swivelled Convergent Nozzle	10
Performance of Plug Nozzle with Plug at Tailpipe Wall	10
AUXILIARY-NOZZLE JET DEFLECTORS	11
Performance of Tailpipe with Bleed Nozzle	11
Performance of Plug Nozzle with Auxiliary Jet from Plug	12
MECHANICAL JET DEFLECTORS	13
Performance of Swivelled Ejector Shroud	14
Performance of Ejector with Internal Flap	16
Performance of Ejector with External Flap	19
Performance of Modulating Cylindrical Target-Type Thrust Reverser	19
Performance of Ejector with Swivelled Primary Nozzle	20
Design Procedure	21
MISCELLANEOUS JET DEFLECTORS	21
<u>CONCLUDING REMARKS</u>	21
<u>APPENDIXES</u>	
A - <u>SYMBOLS</u>	23
B - <u>DEFINITIONS</u>	26
C - <u>SWIVELLED-NOZZLE JET DEFLECTORS</u>	28
ANALYSIS	28
ANALYTICAL PERFORMANCE	29

APPENDIXES - Continued

D - <u>AUXILIARY-NOZZLE JET DEFLECTORS</u>	30
ANALYSIS	30
ANALYTICAL PERFORMANCE	31
E - <u>MECHANICAL JET DEFLECTORS</u>	32
ANALYSIS	32
ANALYTICAL PERFORMANCE	36
APPLICATION OF ANALYSIS TO EJECTOR WITH SWIVELLED-PRIMARY-NOZZLE DEFLECTOR	36
GEOMETRIC FACTORS	37
<u>REFERENCES</u>	38

NATIONAL ADVISORY COMMITTEE FOR AERONAUTICS

TECHNICAL NOTE 4264

INTERNAL CHARACTERISTICS AND PERFORMANCE OF SEVERAL JET

DEFLECTORS AT PRIMARY-NOZZLE PRESSURE

RATIOS UP TO 3.0

By Jack G. McArdle

SUMMARY

Several model jet deflectors (devices which change the direction of resultant jet thrust) were tested in quiescent air to determine the effects of design variables on their performance and operating characteristics. The deflectors (swivelled nozzles, auxiliary nozzles, and mechanical deflectors) were designed to be adaptable to convergent-nozzle, plug-nozzle, and ejector turbojet exhaust systems.

Side force as high as 43 percent of the undeflected jet thrust was obtained, and, in general, the axial thrust was reduced to not less than 81 percent of the undeflected jet thrust. Analytical expressions relating the performance of each type deflector with significant design variables are also presented.

INTRODUCTION

The use of conventional aerodynamic surfaces to provide control forces under all flight conditions is increasingly troublesome as aircraft are required to operate in more varied flight regimes. At supersonic speeds the control surfaces may bring about undesirable coupling effects or excessive drag. At high altitude or very low speed, forces produced by the surfaces may be inadequate because of low dynamic pressure. Control would be improved in such cases by using forces produced by the powerplant to assist or supplant the aerodynamic surfaces. For jet-propelled vehicles, control moments can be produced by redirecting all or part of the engine exhaust. All devices which change the direction of the resultant thrust vector to produce control moments are herein called jet deflectors, whether or not the effect is brought about by actually deflecting the main exhaust stream. (The performance characteristics of thrust reversers, which are designed to produce a net rearward force rather than a moment, are summarized in ref. 1.)

Most of the work on jet deflectors thus far reported is concerned with devices designed for use with high-pressure-ratio convergent-divergent exhaust nozzles (e.g., refs. 2 to 9). These devices are more suited for rocket applications than for maneuvering a turbojet-powered aircraft at low speed and low altitude, as in jet vertical takeoff and landing. Because of current interest in the latter application, the NACA Lewis laboratory initiated a program to determine the effects of design variables on the internal characteristics and performance of several types of model jet deflectors operated at over-all pressure ratios near critical. Results of an investigation of some novel configurations are included in reference 10. Throughout the investigation reported herein emphasis was placed on devices which could be adapted to conventional turbojet exhaust systems suitable for supersonic propulsion. Analytical expressions relating the performance with significant design variables were developed, and performance data for a variety of configurations were obtained. The data served to verify the analytical expressions and, in certain cases, to provide necessary experimental coefficients. The results presented are, in general, restricted to over-all pressure ratios between approximately 1.4 and 3.0.

The experimental portion of this investigation was restricted to devices which produce side force (that component of the resultant thrust perpendicular to the original thrust axis) up to about 35 percent of the undeflected jet thrust. Tests were made with unheated pressurized air discharged to the atmosphere and no external flow. Most of the devices utilized a 4-inch-diameter primary exhaust nozzle. The deflectors have been classified as swivelled nozzles, auxiliary nozzles, and mechanical deflectors, types which are herein defined as follows:

(1) Swivelled nozzles. Devices which produce side force by means of a canted exhaust-nozzle exit. An example of this type is the swivelled convergent nozzle.

(2) Auxiliary nozzles. Devices which produce side force by means of a separate (auxiliary) jet exit. An example of this type is the plug nozzle with an auxiliary jet from the plug.

(3) Mechanical deflectors. Devices which produce side force by means of a flap or its equivalent immersed in the primary jet. Examples of this type are the ejector with internal or external flaps and the swivelled ejector shroud.

Jet deflectors utilizing immersed vanes are extensively treated in the literature and are not considered in the present report.

APPARATUS AND INSTRUMENTATION

Sketches, figure references, and the ranges of geometry variation for the jet-deflector models described in this section are summarized in

table I for convenience. All symbols and definitions used in this report are collected in appendixes A and B, respectively.

BASIC JET EXHAUST SYSTEMS

The model basic-jet-exhaust-system configurations used during this investigation are illustrated in figures 1 to 4.

Tailpipe and convergent nozzle. - The model tailpipe and convergent nozzle is shown in figure 1. The nozzle is 4 inches in diameter and has an 8° half-angle.

Tailpipe and plug nozzle. - The model tailpipe and plug nozzle are shown in figure 2. The nozzle is composed of a 30° half-angle plug and a 15° half-angle 4.5-inch-diameter shell. The effective flow area is approximately equal to that of a 3.8-inch-diameter convergent nozzle.

Ejector. - The model ejector is shown in figure 3. The configuration is built around a 15° half-angle 4-inch-diameter primary nozzle. The ejector is arranged to pump ambient air through a 3-inch-diameter secondary flow measuring orifice. The shrouds are secured to a shroud mounting spool extending from the fairing. Shroud details are shown in figure 4. Shroud geometry ranged as follows: half-angle, 0° to 15° ; diameter ratio D_{sh}/D_N , 1.1 to 1.4; and spacing ratio S/D_N , 0.84 to 1.04.

JET DEFLECTORS

The model jet deflectors used in conjunction with the basic jet exhaust systems are illustrated in figures 5 to 17.

Swivelled Nozzles

Swivelled tailpipe. - These devices simulate a swivelled engine or an engine in which the tailpipe is swivelled. The configurations were assembled from the basic tailpipe and convergent nozzle (fig. 1) and the elbows of figure 5. The maximum swivel angle tested is about 25° .

Swivelled convergent nozzle. - The model tested, shown in figure 6, is of spherical design and has a 3.5-inch-diameter exit and a maximum swivel angle of 20° . A full-scale nozzle for an afterburning engine would probably use two pairs of spherical "eyelids" to approximate this shape. With such an arrangement, movement of one of the pairs could produce side force, while movement of either or both pairs could vary the flow area.

4677

CB-1 back

Plug nozzle with plug at tailpipe wall. - This configuration, shown in figure 7, was obtained by altering the basic tailpipe and plug nozzle (fig. 2). The plug was translated transversely until it nearly touched the tailpipe wall and thus formed an exit which was neither normal to nor symmetric about the longitudinal axis.

Auxiliary Nozzles

Tailpipe with bleed nozzle. - This configuration, shown in figure 8, consists of a tailpipe, the basic convergent nozzle (fig. 1), and a perpendicularly mounted auxiliary nozzle. Air for the auxiliary nozzle is bled from the tailpipe through eight equally spaced $1\frac{1}{4}$ -inch-diameter ports. The auxiliary nozzles tested are of 15° half-angle and range in exit diameter from 1.22 to 2.03 inches.

Plug nozzle with auxiliary jet from plug. - In this configuration (fig. 9) the tailpipe, nozzle shell, and external plug shape are the same as the basic tailpipe and plug nozzle (fig. 2). The auxiliary air, supplied from an external source limited to 100 pounds per square inch gage and 1.5 pounds per second, is ducted through the plug mounting strut and exhausted through an orifice in the interchangeable conical portion of the plug. Orifice sizes and shapes are tabulated in figure 9. In each case the orifice is wholly downstream of the nominal primary-nozzle throat.

Mechanical Deflectors

Swivelled ejector shroud. - All swivelled ejector shroud configurations utilize the basic ejector (fig. 3) and ejector shrouds (fig. 4). The shroud is swivelled up to 15° relative to the longitudinal axis by means of one of the devices sketched in figure 10. The adjustable shroud mounting spool (fig. 10(a)) is similar to a stovepipe elbow in construction and operation and replaces the comparable part in the basic ejector. The 15° fixed extension for the shroud mounting spool (fig. 10(b)) increases the ejector spacing. For some of the configurations the entire ejector secondary flow passage (see fig. 3) was blocked with modelling clay to prevent gases flowing backward in the passage. For one of the deflectors the blockage was replaced with the baffle illustrated in figure 11. Significant geometric factors for all configurations of this type tested are listed in table II(a).

Ejector with internal flaps. - Ejectors with internal-flap configurations utilize the basic ejector (fig. 3) and one of the conical ejector shrouds (fig. 4(c) or (d)). The single-fixed-flap deflectors are illustrated in figure 12. One of the flaps (fig. 12(a) or (b)) is mounted

in the shroud to simulate a flap which has been pivoted into place from a stowed position against the shroud wall. The range of simulated actuation angles is from 9° to nearly 90° . For some tests, flow dams were added to the edges of a flap, as shown in figures 12(c) and (d). For certain tests with this type jet deflector only three-quarters of the secondary flow passage was blocked with modelling clay (similarly as was done with the swivelled-ejector-shroud models). Arrangement of the blockage in this case is illustrated in figure 12(f).

A device of this type incorporating two pivoted flaps is shown in figure 13. Either flap can be actuated independently up to $47\frac{1}{2}^\circ$, or both flaps can be actuated simultaneously up to $22\frac{1}{2}^\circ$, the point at which the flap edges coincide.

Significant geometric factors for all configurations of this type tested are listed in table II(b).

Ejector with external flap. - The ejector with external-flap configurations tested utilized the basic ejector (fig. 3) and one of the models illustrated in figure 14. For the shroud with one large flap (figs. 14(a) and (b)) the flap extends around half the shroud circumference and can be actuated up to 30° . For the shroud with two small flaps (fig. 14(c)) each flap extends around a quarter of the shroud circumference. One is fixed at 30° to the longitudinal axis, while the other is unactuated. Significant geometric factors for both configurations of this type are listed in table II(c).

Modulating cylindrical target-type thrust reverser. - This model, shown in figure 15, is the same one used in tests reported in reference 11. The stowed reverser acts as an ejector, but the pumping characteristics were not measured. For operation as a jet deflector, one of the reverser halves is actuated up to 38° from its stowed position. Significant geometric factors for this configuration are listed in table II(d).

Ejector with swivelled primary nozzle. - This model, shown in figure 16, simulates an exit configuration consisting of a swivelled primary nozzle, a convergent ejector, and a valve to prevent gas from flowing backward in the secondary flow passage. The swivelled convergent nozzle previously described (fig. 6) is used. Significant geometric factors for this configuration are listed in table II(e).

Miscellaneous Jet Deflectors

Miscellaneous deflector configurations investigated during the course of the program reported herein are illustrated in figure 17.

Plug nozzle with swivelled plug. - This configuration utilizes the basic tailpipe and plug nozzle (fig. 2). The plug is swivelled up to 30° from its normal position.

Ejector with partial blockage in secondary passage. - This configuration utilizes the basic ejector (fig. 3) and shroud (fig. 4(c)). Half the secondary flow passage is blocked with modelling clay as previously described.

Ejector with partly opened shroud. - This configuration utilizes the basic ejector (fig. 3) and a $D_{sh}/D_N = 1.2$ shroud of which half is opened to the equivalent of a $D_{sh}/D_N = 1.5$ shroud.

EXPERIMENTAL SETUP

The experimental setup on which all tests were conducted is shown in figure 18. The vertical inlet portion of the setup is joined to an air system through a bellows and is pivoted from a rigid steel supporting structure at pivot point A. Downstream of the elbow the inlet portion is connected to the horizontal duct on which the model is mounted through a labyrinth seal and pivot point B. This pivot, consisting of a spherical ball bearing and a quill rod, acts as a point about which the yaw, pitch, and roll torques are generated. Axial force passes through this pivot to the inlet portion. All torques are transmitted to and read from force-measuring cells connected to the setup through flexure members. The force-measuring cells are of the null-reading balanced-pressure-diaphragm type. Counterweights are used to ensure that the cells are always loaded.

INSTRUMENTATION

All airflows were measured with standard ASME thin-plate orifices. All total temperatures were measured at the respective orifices by thermocouples in the airstream. Pressure at the labyrinth seal surrounding pivot point B was measured by two total-pressure tubes spaced 180° apart.

The primary-nozzle inlet pressure was measured by eight total-pressure tubes on each of two diametral survey rakes spaced 90° apart just ahead of the nozzle. The ejector secondary inlet pressure was measured by two survey rakes spaced 180° apart in the secondary flow passage 2 inches ahead of the primary-nozzle exit on the ejector horizontal centerline. Each rake consisted of four total-pressure tubes, of which two tubes pointed upstream and two downstream. Ambient pressure was measured with a barometer.

The models were instrumented with wall static-pressure orifices as required. The orifices were 0.06 inch in diameter or less.

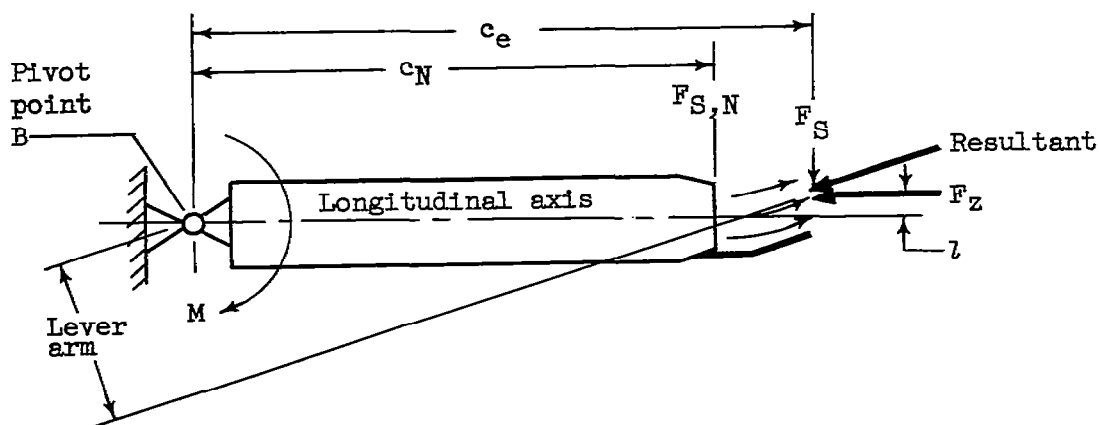
PROCEDURE

Calibration. - The force measuring systems were calibrated with dead weights. Leakage at the labyrinth seal was measured with air from an external source after the supply line near the orifice and the horizontal duct at the model mounting flange were blocked. The primary-nozzle air-flow was corrected for this leakage.

Tests. - The models were mounted to produce side force in the yaw direction only. The performance of each model was obtained over a range of primary-nozzle pressure ratios of about 1.4 to 3.0 using unheated pressurized air discharged to the atmosphere. Performance parameters were computed in terms of the undeflected performance of the same model except where noted.

DATA PRESENTATION AND APPLICATION

Method of data presentation. - The following sketch represents a model mounted on the experimental setup. The setup measures the axial



thrust along the longitudinal axis and the moment M about pivot point B. The moment is the product of the resultant jet force and the lever arm and, by resolving the resultant into components, can be written

$$M = F_S c_e - F_Z l \quad (1)$$

The distance l and the quantity $F_z l$ are called the offset distance and the counteracting moment, respectively. For many configurations the offset distance is indeterminate. For this reason the moment is considered to be wholly caused by an effective side force $F_{S,N}$ acting perpendicular to the longitudinal axis in the plane of the primary-nozzle exit. Thus

$$F_{S,N} = \frac{M}{c_N} \quad (2)$$

where both the moment and the distance c_N are easily measured. The axial component of the resultant F_z must, of course, lie along the longitudinal axis and is measured directly.

The axial and effective side components of the resultant force, the primary-nozzle corrected airflow and the ejector secondary-weight-flow ratio, are conveniently expressed in ratio form by dividing by the corresponding performance of the unactuated model. Thus

$$\text{Side-force ratio, } \mathcal{F}_S \equiv \frac{F_{S,N}}{F_{z,o}} \quad (3)$$

$$\text{Axial-thrust ratio, } \mathcal{F}_z \equiv \frac{F_z}{F_{z,o}} \quad (4)$$

$$\text{Airflow ratio} \equiv \left(\frac{w_N \sqrt{\theta_N}}{\delta_N} \right) / \left(\frac{w_N \sqrt{\theta_N}}{\delta_N} \right)_o \quad (5)$$

$$\text{Pumping ratio} \equiv \left(\frac{w_s \sqrt{T_s}}{w_N \sqrt{T_N}} \right) / \left(\frac{w_s \sqrt{T_s}}{w_N \sqrt{T_N}} \right)_o \quad (6)$$

In the following sections these parameters are shown as functions of the design variable which most significantly affects the performance. Experimental data, not corrected for changes in primary airflow, are presented at primary-nozzle pressure ratios of 2.0, 2.4, and 2.8 except where noted. Experimental and analytical results are often compared in the same figure to indicate the accuracy of the analyses. Analysis, discussion, and comparison of theoretical performance of the three types of deflectors are presented in appendixes C, D, and E.

Data application. - From equations (1) and (2),

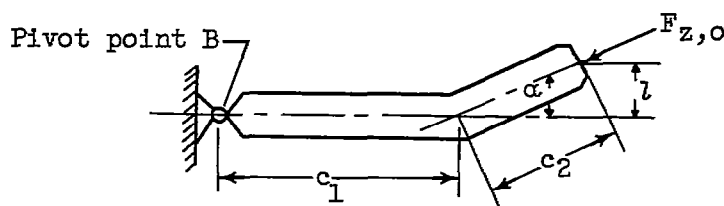
$$F_{S,N} = \frac{c_e}{c_N} F_S - \frac{l}{c_N} F_z \quad (7)$$

Thus, the effective side force $F_{S,N}$ may differ from the true value F_S by an amount dependent on geometric dimensions inherent in the configuration and on the distance c_N . For the configurations tested (except the swivelled tailpipe) both c_e and c_N are large compared to l , and therefore the difference can usually be neglected. (For example, c_N is $20.5 D_N$ for the ejector models, as found from figs. 18 and 3(a); whereas c_e is about $21.5 D_N$, and l is a fractional part of D_N . In a typical case $F_{S,N}$, l , and F_Z might be $0.25 F_{Z,O}$, $0.5 D_N$, and $0.87 F_{Z,O}$, respectively. Then, by equation (7), F_S is $0.258 F_{Z,O}$.) Corrections to reported values of $F_{S,N}$ are necessary only in applications in which the ratio c_e/c_N is significantly different from that of the setup used here, or in which the pivot point does not lie on the primary-exhaust-nozzle axis.

RESULTS AND DISCUSSION

SWIVELLED-NOZZLE JET DEFLECTORS

As previously defined, swivelled-nozzle jet deflectors are devices which produce side force by means of a canted exhaust-nozzle exit. The analysis of this type deflector in appendix C shows that for the general case in which there is a significant counteracting moment, as shown in the following sketch,



Counteracting
moment =
 $F_{Z,O} l \cos \alpha$

$$f \equiv c_2/c_1$$

the performance is

$$F_S = \frac{\sin \alpha}{1 + f \cos \alpha} \quad (C3)$$

$$F_Z = \cos \alpha \quad (C2)$$

If the counteracting moment is negligible, f approaches zero, and these equations reduce to

$$F_S = \sin \alpha \quad (8)$$

$$F_Z = \cos \alpha \quad (9)$$

In this case the deflector is said to follow the "cosine law", and the performance is the best obtainable for any deflector in which the whole jet is turned.

Performance of Swivelled Tailpipe

The performance of the swivelled-tailpipe (or swivelled-engine) deflector is shown in figure 19 for nozzle pressure ratios of 1.4, 2.0, and 2.8. These data, corrected to zero counteracting moment using the measured offset distance l and equation (7), follow the cosine law. These results illustrate that large values of side force can be obtained for relatively small decrements in axial thrust, and that the experimental setup is capable of measuring both side- and axial-force ratios within about ± 0.015 .

Performance of Swivelled Convergent Nozzle

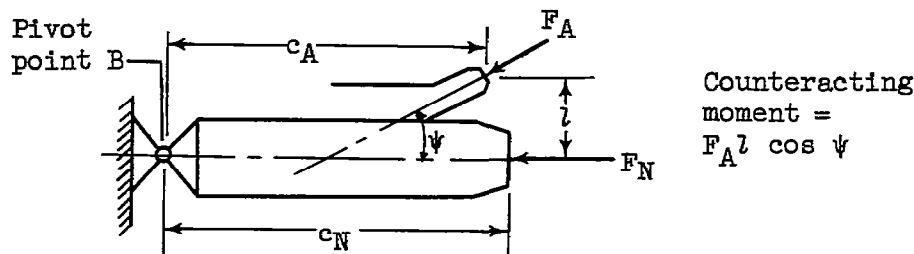
The performance of the swivelled convergent nozzle is shown in figure 20 as a function of the swivel angle α up to the maximum angle obtainable with this model, 20° . The airflow ratio (fig. 20(a)) does not vary from unity by more than 2 percentage points over the range of conditions tested. Values of \mathcal{F}_S (fig. 20(b)) are not corrected for the small counteracting moment. Although there is some difference, partly due to airflow, the performance is within ± 0.02 of the cosine law (indicated by dashed lines).

Performance of Plug Nozzle with Plug at Tailpipe Wall

In this configuration most of the gas is exhausted through an exit station having a maximum effective discharge angle of 22° . No intermediate plug positions were tested, and the basic plug nozzle (fig. 2) was used to obtain the unactuated performance. Test results are shown in figure 21 for a range of primary pressure ratios. The increased airflow ratio (fig. 21(a)) indicates that the effective throat area is enlarged when the plug is in this position. \mathcal{F}_S and \mathcal{F}_Z (figs. 21(b) and (c)) have approximately constant values of 0.10 and 1.0, respectively. By the cosine law, \mathcal{F}_S indicates that the average discharge angle of this device is 6° . The measured \mathcal{F}_Z is from 2 to 4 percentage points less than \mathcal{F}_Z computed from the cosine law and measured \mathcal{F}_S and airflow (dashed line).

AUXILIARY-NOZZLE JET DEFLECTORS

As previously defined, auxiliary-nozzle jet deflectors are devices which produce side force by means of a separate (auxiliary) jet exit. The analysis of this type deflector in appendix D shows that for the general case in which there is a significant counteracting moment, as shown in the following sketch,



the performance is

$$\mathcal{F}_S = \frac{F_A (c_A \sin \psi - l \cos \psi)}{c_N F_{Z,0}} \quad (D2)$$

$$\mathcal{F}_Z = \frac{F_N + F_A \cos \psi}{F_{Z,0}} \quad (D3)$$

Performance of Tailpipe with Bleed Nozzle

In this device side force is produced by an auxiliary nozzle perpendicular to and utilizing gas bled from the tailpipe wall. The undeflected jet thrust is the thrust that could be produced by the total air-flow w_T at tailpipe total pressure P_T and total temperature T . For this geometry, wherein $w_T = (w_A + w_N)$ and P_N is very nearly P_T , equations (D2) and (D3) are expressed in terms of flow variables as

$$\mathcal{F}_S = \frac{c_A}{c_N} \frac{w_A}{w_T} \sqrt{\frac{1 - \left(\frac{P_0}{P_A}\right)^{\frac{\gamma-1}{\gamma}}}{1 - \left(\frac{P_0}{P_T}\right)^{\frac{\gamma-1}{\gamma}}}} \quad (10)$$

$$\mathcal{F}_Z = 1 - \frac{w_A}{w_T} \quad (11)$$

The performance is shown in figure 22 as a function of the auxiliary-nozzle airflow ratio $\frac{w_A}{w_T}$. \mathcal{F}_Z (fig. 22(a)) closely follows equation (11). \mathcal{F}_S (fig. 22(b)) is corrected to unity c_A/c_N to eliminate the effect of this arbitrary variable. At larger values of w_A/w_T , \mathcal{F}_S is significantly less than it would be if the auxiliary-nozzle and tailpipe total pressures were equal (dot-dash line). The reason for this is shown in figure 22(c), where it can be seen that the auxiliary-nozzle total pressure is even less than tailpipe static pressure (dot-dash line) because of turning and friction losses and effects of flow-coefficient variations in the bleed ports.

Performance of Plug Nozzle with Auxiliary

Jet from Plug

In this device side force is produced by a small high-pressure auxiliary jet exhausted through an orifice in the surface of the plug. For this device, with the counteracting moment and differences in thrust coefficients neglected, equations (D2) and (D3) are expressed in terms of flow variables as

$$\mathcal{F}_S = \frac{w_A}{w_N} \sqrt{\frac{1 - \left(\frac{P_O}{P_A}\right)^{\frac{\gamma-1}{\gamma}}}{1 - \left(\frac{P_O}{P_N}\right)^{\frac{\gamma-1}{\gamma}}}} \sin 60^\circ \quad (12)$$

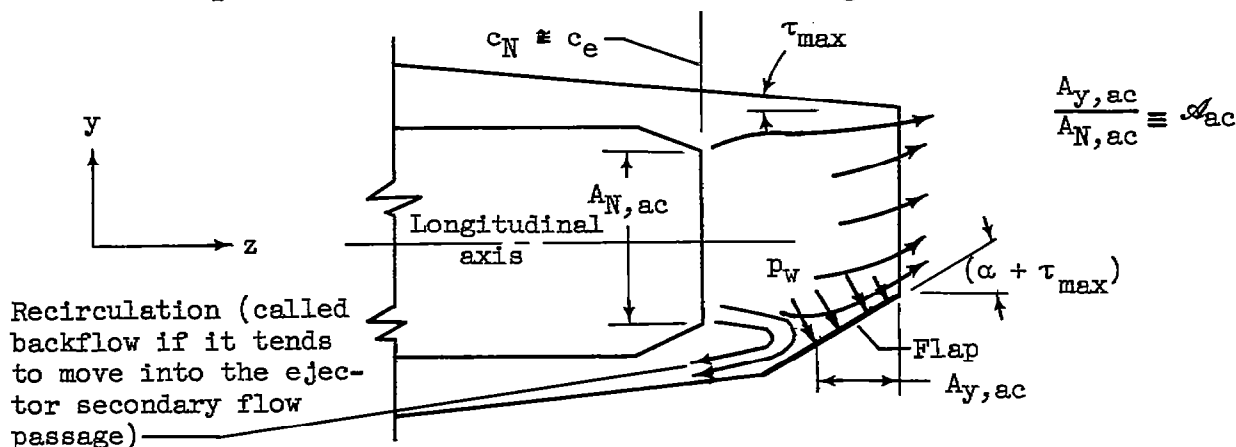
$$\mathcal{F}_Z = 1 + \frac{w_A}{w_N} \sqrt{\frac{1 - \left(\frac{P_O}{P_A}\right)^{\frac{\gamma-1}{\gamma}}}{1 - \left(\frac{P_O}{P_N}\right)^{\frac{\gamma-1}{\gamma}}}} \cos 60^\circ \quad (13)$$

The performance is shown in figure 23 as a function of the auxiliary-nozzle airflow ratio w_A/w_N . The uppermost parts of the figure show that in some cases the auxiliary jet caused a significant reduction in primary airflow ratio. For this reason, \mathcal{F}_S and \mathcal{F}_Z , shown in the other parts of figure 23, are based on the undeflected jet thrust that would be produced

by the measured primary airflow. The \mathcal{F}_S and \mathcal{F}_Z for all orifice configurations can be approximately represented by single curves (solid lines). This performance is always less than that which would be obtained if the airflow used by the orifice of cone number 1 were exhausted into still air under the same geometric and fluid conditions (dot-dash lines).

MECHANICAL JET DEFLECTORS

As previously defined, mechanical jet deflectors are devices which produce side force by means of a flap or its equivalent immersed in the primary jet. An analysis of this type deflector in appendix E shows that for a flow pattern like that shown in the following sketch



the general performance relation is

$$\mathcal{F}_Z = 1 - \mathcal{F}_S \tan(\alpha + \tau_{\max}) \quad (\text{E6})$$

When the flap is large enough to turn the whole jet, \mathcal{F}_S is $\sin(\alpha + \tau_{\max})$. For other cases,

$$\mathcal{F}_S = K \frac{\mathcal{A}_{ac}}{\mathcal{A}_{id}} \sin(\alpha + \tau_{\max}) = K \mathcal{F}_S \text{ Parameter} \quad (14)$$

and, using (E6),

$$\mathcal{F}_Z = 1 - K \frac{\mathcal{A}_{ac}}{\mathcal{A}_{id}} \frac{\sin^2(\alpha + \tau_{\max})}{\cos(\alpha + \tau_{\max})} = 1 - K \mathcal{F}_Z \text{ Parameter} \quad (15)$$

(See appendix B for definitions of \mathcal{F}_S and \mathcal{F}_Z Parameters.) Equations (14) and (15) are applied when \mathcal{F}_S is $\sin(\alpha + \tau_{\max})$ by limiting

$\frac{A_{ac}}{A_{id}}$ to unity in the Parameters. In these equations K is an experimentally determined factor, the ideal lateral area ratio A_{id} is found by equation (E8) or figure 47, and the actual lateral area ratio A_{ac} is determined by the method described in the section Geometric Factors in appendix E.

In the following sections \mathcal{F}_S and \mathcal{F}_Z for several deflectors will be presented as functions of their respective Parameters. A semi-empirical design procedure suggested for configurations not specifically covered by data is given following the experimental results.

Performance of Swivelled Ejector Shroud

\mathcal{F}_S and \mathcal{F}_Z . - The performance of the cylindrical ejector shroud swivelled up to 15° (called configuration A) is shown in figure 24. For this geometry the ratio A_{ac}/A_{id} is always greater than 3 (see table II(a)), and the \mathcal{F}_S and \mathcal{F}_Z Parameters are $\sin \alpha$ and $\sin^2 \alpha / \cos \alpha$, respectively. The solid symbols in this and following figures indicate that the entire secondary flow passage is blocked to prevent backflow. (The blockage simulates a high-temperature valve in the vicinity of the primary-nozzle exit. Alternate methods of providing cooling air to critical structures might have to be developed if the deflector is to be operated for substantial periods of time.) The dashed lines in the figure indicate the maximum theoretical \mathcal{F}_S and the corresponding \mathcal{F}_Z that this deflector can produce. Although deviations are present (probably because of aerodynamic losses and subambient pressures on the divergent portion of the shroud), most of the data points lie within 0.035 of these lines; therefore, this flap is large enough to turn the whole jet. For this case K , by equations (14) and (15), is unity.

Figure 25 shows the performance of deflectors in which the actual lateral area ratio is, in general, less than the ideal value. The reference configurations listed in the key for this and following figures are the configurations whose unactuated performance is used to compute the various performance parameters. The slope of the dashed line through the data gives the average value of the factor K for this group of deflectors; these values are intended for illustrative purposes only and should not be used in design. Precise values of the factor may, of course, be obtained for any individual deflector from the data of figure 25.

Comparison of the data of figure 25 reveals some of the characteristics of this type device. For any of the configurations \mathcal{F}_Z decreases

4677

and \mathcal{F}_S increases as their respective parameters increase at constant primary-nozzle pressure ratio. In general, a value of the \mathcal{F}_S Parameter of the order of 0.3 is required to produce 0.25 \mathcal{F}_S , and at this performance blockage appears necessary to prevent backflow. Performance is the same with or without blockage for operation in the region where backflow starts. Ejector spacing ratio has no appreciable effect on performance (see, e.g., configurations B and C). These results were obtained using a wide range of geometries which should be readily adaptable to conventional ejector-type jet exits.

The effect of recirculation in the shroud is illustrated in figure 26, which shows the wall pressure distribution in a plane through the longitudinal axis. (Although it is not shown in the figure, a continuous pressure gradient exists around the shroud circumference.) The recirculating gas pressurizes part of the shroud wall outside the cylinder of the jet, and thus effectively increases the lateral area. This tends to compensate for the fact that the wall pressure in the calculated lateral area is less than primary-nozzle total pressure.

Performance comparison. - The performance (at a primary-nozzle pressure ratio of 2.0) of all swivelled-ejector-shroud deflectors tested is compared on the basis of \mathcal{F}_Z in figure 27. The lines show the computed performance of configurations A and B. Although the computed performance of A is better than that of B, the losses associated with A are such that the actual performance of either deflector is about the same at higher values of \mathcal{F}_S .

The performance at a primary-nozzle pressure ratio of 2.0 of configurations A and B is compared on the basis of swivel angle in figure 28. Although either deflector can produce more than 0.25 \mathcal{F}_S , at swivel angles greater than 8° the conical shroud is better than the cylindrical shroud. However, with the cylindrical shroud, considerably more \mathcal{F}_S can be obtained before the secondary flow passage is blocked.

Primary airflow ratio. - Because the swivelled shroud acts to back-pressure the primary nozzle, the actual immersed area and the primary-nozzle pressure ratio would be expected to be the principal variables influencing the primary airflow ratio. As illustrated in figure 29, the airflow ratio was reduced only 3 percentage points in even the most extreme case, at a pressure ratio of 2.0. As the pressure ratio increases, the reduction becomes less.

Pumping ratio. - Ejector pumping characteristics are known to depend on many shroud geometric factors and primary and secondary fluid properties. The pumping data (fig. 30) are shown as a function of the actual immersed area ratio and should be used only as a guide to first-order

approximations when applied to other configurations. Comparison of these data shows that for all the configurations the pumping ratio decreases as the immersed area ratio increases. Greater pumping ratios are generally obtained with deflectors of small $(\alpha + \tau_{\max})$ and larger diameter ratio.

Backflow, which begins near zero pumping ratio, first occurs in that quadrant of the shroud which forms the immersed area and spreads rapidly circumferentially for small increments of immersed area. For this reason the entire secondary flow passage was blocked before performance tests were continued when backflow was detected.

In an attempt to improve the pumping ratio of this type deflector, blockage was replaced by a circumferential baffle (fig. 11) in configuration F. As shown in figure 30, small secondary flow was obtained at pressure ratios up to 2.8. When the baffle was faired on the aft side (see fig. 11), measurable backflow occurred at all pressure ratios greater than 1.8.

Performance of Ejector With Internal Flap

\mathcal{F}_S and \mathcal{F}_Z for 20° and 45° fixed flaps. - The performance of deflectors consisting of a single fixed flap having no flow dams and covering one quadrant of the shroud when stowed is presented in figure 31. Although K for the 45° flaps is greater than for the 20° flaps, performance trends for both types are similar. Single curves correlate \mathcal{F}_S for each type flap within about ± 0.02 up to the limit of the \mathcal{F}_S Parameter. At this limit for the 20° flaps (a numerical value of 0.342), \mathcal{F}_S for the flaps in the $1.4 D_{sh}/D_N$ shroud continues to rise as the actual lateral area is increased. If the flaps were made large enough to turn the whole jet, \mathcal{F}_S would theoretically rise to the value $\sin 20^\circ$. On the other hand, for the 20° flaps in the $1.2 D_{sh}/D_N$ shroud (configuration I) \mathcal{F}_S falls off under the same conditions. This decrease is caused by a pressure on the shroud wall opposite the flap, which tends to counteract the side force produced by the flap. However, the forces on the shroud and the flap act together to reduce \mathcal{F}_Z .

The dot-dash lines in the upper portions of figure 31 show \mathcal{F}_Z computed by equation (15) and the measured \mathcal{F}_S . The trends are as expected from the preceding discussion except that \mathcal{F}_Z for the 45° flaps is up to 0.07 greater (see configuration J) than the computed value. The reason for this can be seen in figure 32, which shows the pressure distribution on the flap and shroud wall. With the 45° flap (fig. 32(a)) the shroud wall is pressurized by recirculation and acts as an additional flap of small $(\alpha + \tau_{\max})$, although this effect is unaccounted for in equation (15). For the 20° flap geometry tested, this effect cannot occur, as illustrated in figure 32(b).

Effect of flow dams. - It was felt that the side force for a given geometry might be increased if the pressurized surfaces were isolated. Accordingly, flow dams designed to reduce circumferential flow in the shroud were mounted on the edges of 45° flaps (configurations J and L), as illustrated in figures 12(c) and (d). The effect of the flow dams was small; \mathcal{F}_S was increased by only 0.02 in the best case, and \mathcal{F}_Z was reduced a corresponding amount.

Effect of reducing flap chord (reducing β). - The effect of reducing the flap chord over the whole length (reducing the angle β , fig. 12(a)) was investigated by cutting away portions of a 45° flap used with the $D_{Sh}/D_N = 1.4$ ejector shroud. Results of the tests are shown in figure 33, with the performance of 90° β flaps in the same shroud indicated by dashed lines for reference. Comparison shows that the factor K is appreciably reduced when β is reduced to less than about 60° . However, when \mathcal{F}_Z is plotted as a function of \mathcal{F}_S , nearly identical results are obtained for all flaps.

\mathcal{F}_S and \mathcal{F}_Z for single pivoted flap. - The performance of the pivoted-flap deflector with one flap actuated up to $47\frac{10}{2}$ is shown in figure 34. As the actuation α is increased, both K and \mathcal{F}_S increase to a peak at $\alpha = 28^\circ$. After the peak, \mathcal{F}_S falls off rapidly because of pressure forces acting on the shroud wall opposite the flap. (This effect did not occur at such low actuation with the fixed flaps because the effective pivot point was farther from the primary nozzle. Thus, the performance of the pivoted-flap model might have been improved, both for this reason and because of the gains due to advantageous recirculation, by shortening the flap and moving the pivot downstream.) \mathcal{F}_Z continues to fall off as the actuation increases.

\mathcal{F}_S and \mathcal{F}_Z for two pivoted flaps. - When more than one flap is actuated in a deflector of this type, the resultant force depends on the forces acting normal to each flap. If two identical flat-plate flaps on mutually perpendicular pivots are each actuated the same amount, it can easily be shown by the trigonometric relations involved that

$$\mathcal{F}_S = 1.414 K (\mathcal{F}_S \text{ Parameter}) \quad (16)$$

$$\mathcal{F}_Z = 1 - 2K (\mathcal{F}_Z \text{ Parameter}) \quad (17)$$

where K, \mathcal{F}_S Parameter, and \mathcal{F}_Z Parameter are for a single flap.

The performance of the pivoted-flap model with both flaps actuated the same amount is shown in figure 35. The dashed lines show the performance computed from equations (16) and (17) and \mathcal{F}_S for a single

flap (fig. 34). The \mathcal{F}_S produced is greater than that computed at nearly all actuations. Although it was not definitely established, it is felt that this is due to interaction at the adjacent flap edges which effectively increases the β dimension on the downstream end. Peak \mathcal{F}_S produced by this configuration is about the same as that when a single flap is actuated, although the actuation required \mathcal{F}_Z and the point at which backflow starts are somewhat different.

\mathcal{F}_S and \mathcal{F}_Z for flaps normal to longitudinal axis. - The performance of deflectors consisting of flaps normal to the longitudinal axis in the plane of the ejector shroud exit, in which side force is produced by recirculation along the shroud wall, is shown in figure 36. Both \mathcal{F}_S and \mathcal{F}_Z are presented as functions of the actual immersed area ratio $\left(\frac{A_Z}{A_N}\right)_{ac}$. Performance of this sort of flap in the $1.2 D_{sh}/D_N$ shroud is always better than in the $1.4 D_{sh}/D_N$ shroud. For either shroud, \mathcal{F}_Z is poor for the \mathcal{F}_S produced (compare these results with fig. 27, for example). Comparison of configurations Q and R shows there is little change in performance when the ends of the flap are removed.

It was observed during the course of these tests that the forces produced are somewhat "jumpy," probably because of intermittent boundary-layer peeloff. This characteristic was not observed with the other types of flaps tested.

Performance comparison. - Data presented in the preceding figures for fixed-flap deflectors are compared at a primary-nozzle pressure ratio of 2.0 in figure 37. The lines show the performance for 20° and 45° flaps computed from equation (E6) and the measured \mathcal{F}_S . In general, the internal flaps tested are limited to about $0.17 \mathcal{F}_S$ and produce more than $0.85 \mathcal{F}_Z$. This is probably near the practical limit for jet deflectors of this type because of primary-airflow-ratio considerations, which are discussed in the following section.

Primary airflow ratio. - With an internal-flap jet deflector the flow area in the shroud is reduced as the flap is actuated. Figure 38 shows the primary airflow ratio for several configurations as a function of the effective-flow-area parameter, which is defined as the actual immersed area ratio $\left(\frac{A_Z}{A_N}\right)_{ac}$ divided by the residual area ratio $\frac{A_{res}}{A_N}$. As shown in the sketch in the figure, A_{res} is measured in a plane parallel to the primary-nozzle exit. Data scatter, probably due to flap size and

angle, is evident, but in general the primary airflow ratio is reduced 5 percentage points in the worst case, at a pressure ratio of 2.0. As the pressure ratio is increased, the reduction becomes less.

Pumping ratio. - The pumping ratio for several of the configurations of this type tested is presented in figure 39. The trends are similar to those of the swivelled-ejector-shroud deflectors (fig. 30), and the same discussion is applicable to these deflectors.

In an attempt to improve the pumping characteristics of configuration J, one quadrant of the secondary flow passage was left unblocked (fig. 12(f)). As shown in figure 39, this modification permitted a small secondary airflow up to a pressure ratio of 2.4.

Performance of Ejector with External Flap

The performance of both configurations of this type tested is presented in figure 40. The \mathcal{F}_S and \mathcal{F}_Z Parameters were computed neglecting the presence of the shroud, that is, assuming that neither the cross-sectional area nor the velocity of the primary jet is affected, as by overexpansion, as it passes through the shroud. In general, the performance follows the same trends as that for the mechanical deflectors previously discussed.

Some of the limitations inherent in the internal-flap deflectors can be overcome by using external flaps. One of the obvious advantages is that the flap can be made large enough to produce large side force. In addition, the primary airflow ratio is always unity and the pumping ratio is always greater than 85 percent because, for the geometries used, the shroud acts to isolate the flap. Shroud wall pressures were, of course, always about the same as when the flap was unactuated. A disadvantage of this type of configuration is that the undeflected jet thrust is reduced by about 1 percent because of flap internal drag.

Performance of Modulating Cylindrical

Target-Type Thrust Reverser

The performance of this model with one of the reverser halves actuated is shown in figure 41 for primary-nozzle pressure ratios of 2.0 and 2.4. The performance follows the same trends as the mechanical deflectors previously discussed, except that the primary airflow ratio is always unity. It was observed that at 45° ($\alpha + \tau_{\max}$) some backflow was discharged past the end plate.

It is interesting to compare the \mathcal{F}_S measured in this test with that which might be estimated from results of thrust-modulation tests in which both reverser halves are actuated. At 45° ($\alpha + \tau_{\max}$), reference 11 shows that a force sufficient to produce $0.49 \mathcal{F}_S$ acts on each reverser half, whereas, when only one half is actuated, about 40 percent of this value is obtained.

Performance of Ejector With Swivelled Primary Nozzle

Basic performance. - Figure 42 shows the basic performance of this device as a function of the primary-nozzle swivel angle. The reference configuration used to compute all performance parameters is the unshrouded primary nozzle, chosen because its performance is more nearly that which could be obtained with a conventional unactuated configuration than is the performance of the zero-secondary-flow ejector. The primary airflow ratio (fig. 42(a)) is reduced up to 5 percentage points. \mathcal{F}_z falls off almost linearly as actuation is increased and is poor for the \mathcal{F}_S produced. Maximum \mathcal{F}_S is obtained at 20° actuation; but, as shown by the extrapolations, no side force is produced for less than $\alpha \approx 6^\circ$. This characteristic occurs because the primary nozzle must be actuated $3\frac{1}{2}^\circ$ at a pressure ratio of 2.0 before the jet intercepts this shroud, and then an additional amount before positive side force is produced. Use of this configuration would probably be prohibited by this characteristic, which would, however, be minimized or perhaps even eliminated by using a longer ejector shroud of smaller diameter ratio.

Comparison with computed performance. - Equations (E12) and (E14), derived in appendix E, are analytical expressions pertaining to this device. By basing the \mathcal{F}_S Parameter on A_y and $(\alpha + \tau_{\max})$, equations (E12) and (E14) yield

$$\mathcal{F}_S + \sin \alpha = K \frac{\cos \tau_{\max}}{\cos(\alpha + \tau_{\max})} \mathcal{F}_S \text{ Parameter} \quad (18)$$

Computed and measured performance are compared at a primary-nozzle pressure ratio of 2.0 in figure 43. In figure 43(a) the higher curve is a plot of equation (18); from this curve the value of K is found to be 0.81. This is less than might be expected on the basis of other data, probably because of geometry effects. The lower curve in figure 43(a) shows that the positive \mathcal{F}_S produced is about one-third the sum $(\mathcal{F}_S + \sin \alpha)$. Inspection of equation (E12) shows that this fraction could be improved by increasing the shroud half-angle τ_{\max} .

As shown in figure 43(b), the measured \mathcal{F}_Z agrees satisfactorily with that computed from equation (E14) and the measured \mathcal{F}_S .

Design Procedure

If no precise data are available, the \mathcal{F}_Z and \mathcal{F}_S performance of flat-plate mechanical jet deflectors may be calculated by means of equations (14) and (15). The factor K is found from the design chart in figure 44. Computation of the \mathcal{F}_Z and \mathcal{F}_S in this manner correlates 65 percent of all the data points for configurations A to L and S to U presented herein to ± 0.020 , and 86 percent of the same data points to ± 0.035 . The larger deviations often occur in deflectors such as configuration J in which a large portion of the side force is developed on surfaces other than the flap (see fig. 32(a)) or in deflectors in which the pressure is not almost ambient on the wall opposite the flap.

The design chart may be used for primary-nozzle pressure ratios from 2.0 to 2.8 and for deflectors in which the β dimension is 90° or greater. If the β dimension is less than 90° , the reduction in K may be estimated from the data of figures 33 and 34. The primary airflow and pumping ratios may be estimated on the basis of considerations previously discussed.

MISCELLANEOUS JET DEFLECTORS

The miscellaneous jet deflectors sketched in figure 17 were tested during the course of the program reported herein. In each case the \mathcal{F}_S produced was insignificant; so the configurations are not discussed in detail. The direction of positive side force is shown on each sketch.

CONCLUDING REMARKS

Several model jet deflectors, classified into types called swivelled nozzles, auxiliary nozzles, and mechanical deflectors, were tested in quiescent air. Ratios of effective side force to undeflected jet thrust (called \mathcal{F}_S) as high as 0.43 were obtained. In general, the ratio of axial thrust to undeflected jet thrust (called \mathcal{F}_Z) was reduced to not less than 0.81. Analytical expressions relating the performance of each type deflector with significant design variables were developed.

The performance of swivelled-nozzle deflectors depends on the swivel angle and on the distance the center of the exhaust-nozzle exit is offset from the original axis. When the offset distance is negligible, the

performance of this type is the best obtainable for any deflector in which the whole jet is turned. For the swivelled convergent nozzle, a significant configuration of this type, \mathcal{F}_S and \mathcal{F}_Z can be computed within ± 0.02 by analytical expressions.

The performance of auxiliary-nozzle deflectors depends on the thrusts produced by the auxiliary and propulsion nozzles and on the distance and angle between these nozzles. For any specified \mathcal{F}_S , the \mathcal{F}_Z produced by this type is improved when more of the jet is turned and when the auxiliary nozzle is placed farther behind the propulsion nozzle. For the tailpipe with a bleed nozzle, a configuration of this type, \mathcal{F}_S and \mathcal{F}_Z can be computed within ± 0.01 by analytical expressions.

The performance of mechanical deflectors depends principally on the angle and the immersion of the deflecting flap. A wall opposite the flap or a small flap chord angle β can reduce performance, while jet recirculation in the vicinity of the flap can improve performance. At larger values of \mathcal{F}_S , ejector configurations often encounter reduced primary and secondary airflows, and may require blockage in the secondary flow passage. For most of the configurations of this type, \mathcal{F}_S and \mathcal{F}_Z can be computed within ± 0.035 by a semiempirical design method presented.

The performance of several configurations and the types and ranges of geometries tested are shown in the following table:

Type of deflector	Configuration	Actuation angle, deg	Maximum \mathcal{F}_S	\mathcal{F}_Z at maximum \mathcal{F}_S	Primary-airflow ratio at maximum \mathcal{F}_S
Swivelled nozzle	Swivelled tailpipe	24.6	0.43	0.915	1.00
	Swivelled convergent nozzle	20.0	.36	.936	1.01
	Plug nozzle with plug at tailpipe wall	-----	.10	1.00	1.05
Auxiliary nozzle	Tailpipe with bleed nozzle	-----	0.125	0.850	1.00
	Plug nozzle with auxiliary jet from plug	-----	.23	1.15	1.00
Mechanical deflector ^c	Swivelled ejector shroud; $D_{sh}/D_N = 1.1$; $S/D_N = 0.86$; cylindrical ejector	15	0.286	0.898	0.993
	Swivelled ejector shroud; $D_{sh}/D_N = 1.1$; $S/D_N = 0.87$; 15° conical convergent ejector	15	.370	.850	.981
	Ejector with internal flap; $D_{sh}/D_N = 1.4$; $S/D_N = 1.06$; 3° conical convergent ejector; 20° flap, $\beta = 90^\circ$	17	.21	.901	.997
	Ejector with external flap; $D_{sh}/D_N = 1.16$; 17.5° conical convergent ejector; one large flap around 180° of shroud	30	.41	.819	1.00
	Cylindrical thrust reverser, one-half actuated	38	.198	.815	1.00
	Ejector with swivelled primary nozzle; $D_{sh}/D_N = 1.1$; $S/D_N = 0.78$; 15° conical convergent ejector	20	.189	.827	.953

^aWhen primary nozzle is reduced.

^bWhen primary nozzle is enlarged.

^c D_{sh}/D_N , diameter ratio; S/D_N , spacing ratio; β , flap chord angle.

Lewis Flight Propulsion Laboratory
National Advisory Committee for Aeronautics
Cleveland, Ohio, February 11, 1958

APPENDIX ASYMBOLS

A	area, sq ft
A_y	lateral area, sq ft
A_z	immersed area, sq ft
\mathcal{A}	lateral area ratio, $\frac{A_y}{A_N}$
C_d	primary-nozzle discharge coefficient
C_F	primary-nozzle thrust coefficient
c	distance, ft
D	diameter, ft
D_{sh}	ejector shroud exit diameter, ft
F	jet thrust, lb
f	offset distance factor, dimensionless (see appendix C)
\mathcal{F}_S	side-force ratio, $F_{S,N}/F_{z,o}$
\mathcal{F}_z	axial-thrust ratio, $F_z/F_{z,o}$
g	acceleration due to gravity, ft/sec ²
K	experimentally determined factor, dimensionless
l	offset distance, ft
M	moment, ft-lb
P	total pressure, lb/sq ft abs
p	static pressure, lb/sq ft abs
R	gas constant, ft/ ^o R
S	ejector spacing, ft
T	total temperature, ^o R

V	velocity, ft/sec
w	weight-flow rate, lb/sec
α	actuation, deg
β	flap chord angle, deg
γ	ratio of specific heats
δ	ratio of total pressure to NACA standard sea-level pressure of 2116 lb/sq ft abs
θ	ratio of total temperature to NACA standard sea-level temperature of 518.7° R
τ	gas turning angle, deg
τ_{\max}	conical ejector shroud half-angle, deg
ϕ	nominal pipe diameter, in.
ψ	angle between auxiliary-nozzle axis and longitudinal axis, deg

Subscripts:

A	auxiliary nozzle
ac	actual
av	average
e	exit
f	flap
id	ideal
N	primary-nozzle exit
o	unactuated
res	residual
S	side
s	secondary

T tailpipe
w wall
y Cartesian coordinate perpendicular to longitudinal axis
y' Cartesian coordinate perpendicular to nozzle axis (specialized)
z Cartesian coordinate parallel to longitudinal axis
0 ambient
1,2,... stations or specialized locations

APPENDIX BDEFINITIONS

Actuation	Displacement of a jet deflector from the stowed condition in such a manner as to tend to produce side force. α is angular actuation.
Axial thrust	F_z is that component of the resultant force produced by an actuated jet deflector along the longitudinal axis.
Effective-flow-area parameter	$\left(\frac{A_z}{A_N}\right)_{ac} / \left(\frac{A_{res}}{A_N}\right)$
Effective side force	$F_{S,N}$ is the moment producing rotation divided by the axial distance from the pivot point to the center of the primary exhaust nozzle.
Ejector diameter ratio	D_{sh}/D_N
Ejector spacing ratio	S/D_N
\mathcal{F}_S Parameter	$\frac{\mathcal{A}_{ac}}{\mathcal{A}_{id}} \sin(\alpha + \tau_{max})$
\mathcal{F}_z Parameter	$\frac{\mathcal{A}_{ac}}{\mathcal{A}_{id}} \frac{\sin^2(\alpha + \tau_{max})}{\cos(\alpha + \tau_{max})}$
Immersed-area ratio	A_z/A_N
Lateral-area ratio	$A_y/A_N = \mathcal{A}$
Primary-airflow ratio	$\left(\frac{w_N \sqrt{\theta_N}}{\delta_N}\right) / \left(\frac{w_N \sqrt{\theta_N}}{\delta_N}\right)_o$
Pumping ratio	$\left(\frac{w_s}{w_N} \sqrt{\frac{T_s}{T_N}}\right) / \left(\frac{w_s}{w_N} \sqrt{\frac{T_s}{T_N}}\right)_o$

Residual area A_{res} is the shroud exit area less the projected area of the flap in a plane parallel to the primary-nozzle exit.

Side force F_S is that component of the resultant force produced by an actuated jet deflector acting perpendicular to the longitudinal axis.

Undeflected jet thrust $F_{z,0}$ is F_z at zero actuation.

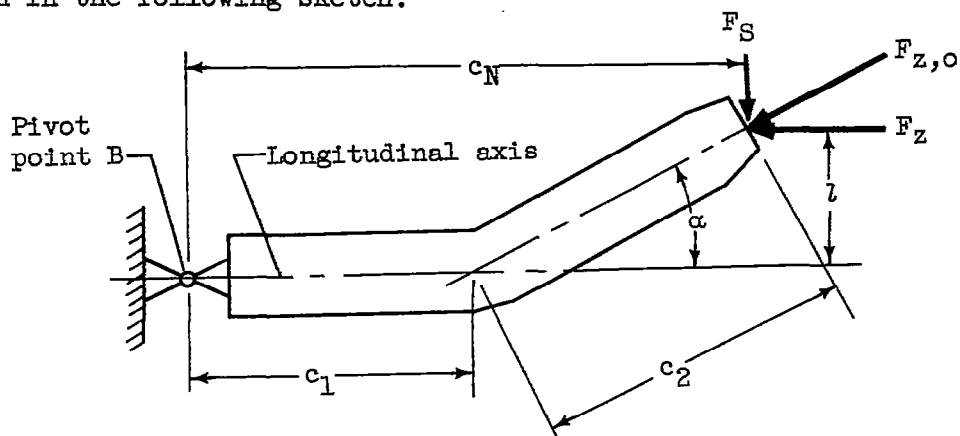
4677

CB-4 back

APPENDIX CSWIVELLED-NOZZLE JET DEFLECTORS

ANALYSIS

A swivelled-nozzle deflector mounted in the experimental setup is shown in the following sketch:



Summing moments about pivot point B and assuming no jet losses

$$M = F_S(c_N - F_Z)l \quad (C1)$$

The quantity $F_Z l$ is the counteracting moment. By definition (eqs. (3) and (2)),

$$\mathcal{F}_S = \frac{M}{c_N F_{Z,o}} = \frac{F_S c_N - F_Z l}{c_N F_{Z,o}} = \frac{F_S c_N - F_Z c_2 \sin \alpha}{c_N F_{Z,o}} \quad (C2)$$

By geometry, $c_N = c_1 + c_2 \cos \alpha$. Let $c_2/c_1 = f$. Then equation (C2) reduces to

$$\mathcal{F}_S = \frac{\sin \alpha}{1 + f \cos \alpha} \quad (C3)$$

There are no other axial jet forces, so that

$$\mathcal{F}_Z = \frac{F_Z}{F_{Z,o}} = \cos \alpha \quad (C4)$$

ANALYTICAL PERFORMANCE

Figure 45 shows the analytical performance of this type deflector. The double ordinate scale is drawn because \mathcal{F}_Z , by equation (C4), changes only as the swivel angle changes. \mathcal{F}_S , however, is dependent both on the swivel angle and the offset axis factor f . For constant swivel angle \mathcal{F}_S is significantly reduced as f is increased.

When f is zero the performance is the best obtainable for any deflector in which the whole jet is turned. For this case the deflector produces $0.35 \mathcal{F}_S$ and $0.936 \mathcal{F}_Z$ when swivelled $20\frac{10}{2}$.

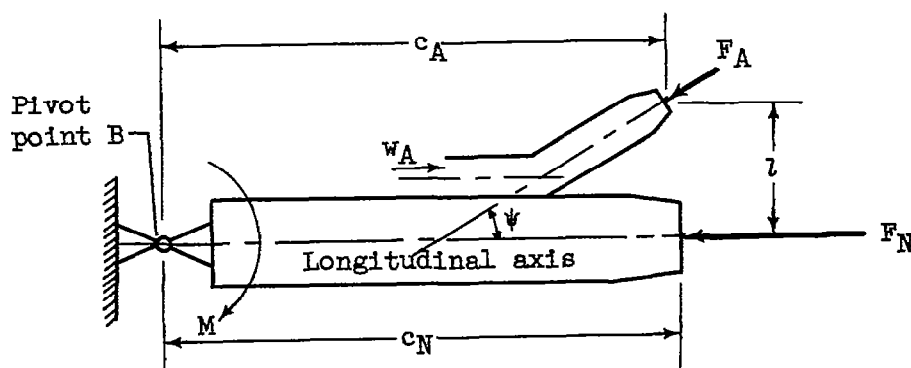
A swivelled-nozzle deflector using an ejector shroud and a swivelled primary nozzle would be difficult to achieve. To prevent jet impingement the shroud must be of very large diameter ratio or extremely short spacing ratio. Such a shroud is incompatible with good ejector design. An alternative might be found in translating the shroud.

APPENDIX D

AUXILIARY-NOZZLE JET DEFLECTORS

ANALYSIS

An auxiliary-nozzle jet deflector mounted in the experimental setup is shown in the following sketch:



Summing moments about pivot point B,

$$M = c_A F_A \sin \psi - l F_A \cos \psi \quad (D1)$$

The quantity $l F_A \cos \psi$ is the counteracting moment. By definition (eqs. (3), (2), and (4)),

$$\mathcal{F}_S = \frac{M}{c_N F_{Z,0}} = \frac{F_A (c_A \sin \psi - l \cos \psi)}{c_N F_{Z,0}} \quad (D2)$$

$$\mathcal{F}_Z = \frac{F_Z}{F_{Z,0}} = \frac{F_N + F_A \cos \psi}{F_{Z,0}} \quad (D3)$$

These relations can be expressed in terms of flow variables by substituting the following expression obtained from one-dimensional isentropic flow equations:

$$F = C_F \frac{W}{g} V_{id} = C_F \frac{W}{g} \sqrt{\frac{2\gamma g R T}{\gamma - 1} \left[1 - \left(\frac{p}{P} \right)^{\frac{\gamma-1}{\gamma}} \right]} \quad (D4)$$

ANALYTICAL PERFORMANCE

The analytical performance of an auxiliary-nozzle deflector assumed to operate under the following conditions is presented in figure 46:

- (1) Gas for the auxiliary nozzle is bled from the tailpipe with no total-pressure loss.
- (2) Primary-nozzle area is reduced to keep the engine operating point unchanged.
- (3) Auxiliary and primary thrust coefficients are always equal.
- (4) The ratio c_A/c_N is unity.
- (5) Counteracting moment is negligible.

With these assumptions equations (D2), (D3), and (D4) reduce to

$$\mathcal{F}_S = \frac{F_A \sin \psi}{F_{Z,O}} = \frac{w_A}{w_{N,O}} \sin \psi$$

$$\mathcal{F}_Z = \frac{F_N + F_A \cos \psi}{F_{Z,O}} = \frac{w_N + w_A \cos \psi}{w_{N,O}}$$

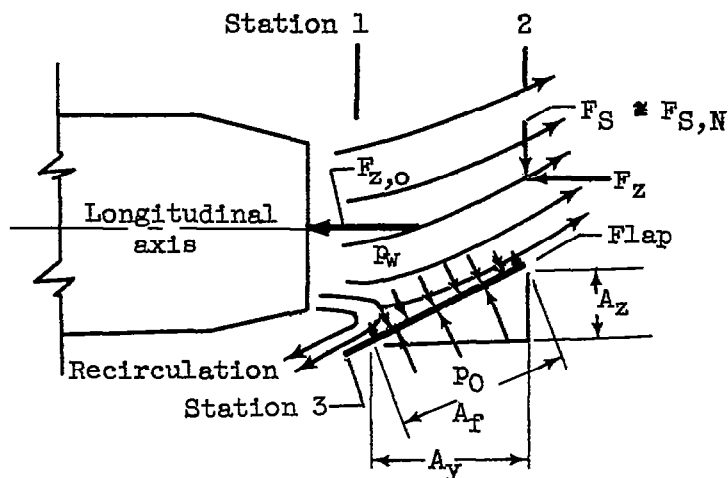
In figure 46 the lighter lines are lines of constant auxiliary-nozzle air-flow ratio $w_A/w_{N,O}$. The heavier lines represent deflectors having fixed auxiliary-nozzle discharge angle ψ . By comparison, it can be seen that the $45^\circ \psi$ deflector requires larger $w_A/w_{N,O}$ to produce the same \mathcal{F}_S as the $90^\circ \psi$ deflector, but at the same time \mathcal{F}_Z is significantly greater. In general, \mathcal{F}_Z is improved when more of the tailpipe flow is turned. When the whole jet is turned ($w_A/w_{N,O} = 1$), the performance is the same as for a swivelled-nozzle deflector following the cosine law. It should be emphasized that figure 46 is based on the assumption that the ratio c_A/c_N is unity. If this ratio were increased, \mathcal{F}_S would be increased in the same proportion, while \mathcal{F}_Z would remain unchanged.

The biggest advantage of auxiliary-nozzle deflectors is the inherent simplicity and reliability. The only moving parts necessary are valves to control the auxiliary flow and a conventional variable-area primary nozzle. Gas for the auxiliary nozzle could be obtained from an isolated source or from anywhere within the engine, as for example, the compressor. At least three auxiliary nozzles are needed to provide control forces in all directions. Principal disadvantages associated with this type deflector are that long large ducting may be necessary and that in certain cases, such as those discussed, large auxiliary nozzles and a primary nozzle capable of very large area changes may be required.

APPENDIX EMECHANICAL JET DEFLECTORS

ANALYSIS

The following sketch shows the forces involved as flow passes through a mechanical deflector:



Recirculation is necessary for flat-plate flaps in order to balance momentum parallel to the flap. The following analysis is applicable to the case in which the recirculated gas is discharged at station 3. In most of the deflectors tested, however, this gas returned to the main stream and left the system at the exit, station 2. Because either situation involves a momentum loss at the exit, the results of this analysis are applied to all deflectors, and any error is absorbed in necessary experimental coefficients.

The following assumptions are made:

- (1) The whole primary jet expands to ambient pressure p_0 at station 1 before intercepting the flap.
- (2) The flap, essentially two-dimensional, is frictionless and is the only surface affecting the flow.
- (3) Counteracting moment is negligible. (Therefore, $F_s = F_{s,N}$.)
- (4) Primary-airflow ratio is always unity.

(5) Ejector secondary flow is negligible.

(6) For the ejector configurations, the undeflected jet thrust $F_{z,o}$ is the same as the primary-nozzle jet thrust F_N . (This is a reasonable assumption for the ranges of geometry and pressure ratios tested.)

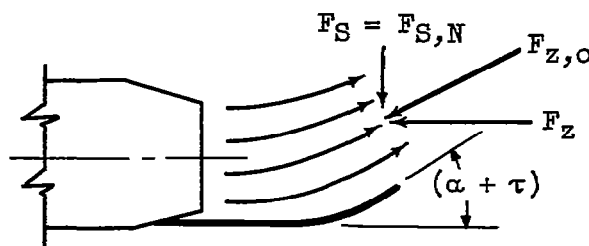
For those configurations having no momentum in the y-direction at station 1, the results of writing the momentum equations for a control volume around the jet at stations 1, 2, and 3 in terms of the side and axial components of the flap normal force are

$$F_{S,N} = \int_{A_F} (p_w - p_o) dA_y \quad (E1)$$

$$F_z = F_{z,o} - \int_{A_F} (p_w - p_o) dA_z \quad (E2)$$

These equations must be solved simultaneously.

Perfect Flap



In the ideal case the whole jet is turned through an angle $(\alpha + \tau)$ by a flap curved to prevent recirculation (which would bring about a momentum loss), as shown in the preceding sketch. Although equations (E1) and (E2) are valid, for this case the following is also true:

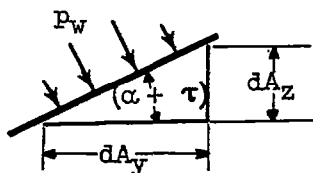
$$\mathcal{F}_S = \frac{F_S}{F_{z,o}} = \sin(\alpha + \tau) \quad (E3)$$

$$\mathcal{F}_z = \frac{F_z}{F_{z,o}} = \cos(\alpha + \tau) \quad (E4)$$

This is the same performance as that obtained for a swivelled-joint deflector having no counteracting moment (cosine law). In practice, the ideal case is not attained because of losses and geometry restrictions.

Practical Flap

For the mechanical deflectors tested the flap approximates a flat plate, and the relation between equations (E1) and (E2) is determined by the geometric relation between the surface elements dA_y and dA_z found in the flap. Thus, as shown in the following sketch,



$$dA_z = dA_y \tan(\alpha + \tau) \quad (E5)$$

Because the wall pressure is the same on both elements, equation (E5) can be substituted directly into (E1) and (E2) to obtain, after dividing by $F_{z,0}$,

$$\mathcal{F}_z = 1 - \mathcal{F}_g \tan(\alpha + \tau) \quad (E6)$$

This equation is the basic performance relation for flat-plate mechanical deflectors. It remains, however, to evaluate the relation in terms of design variables.

Evaluation and Application of Basic Performance Relation

The side force produced by a flat-plate deflector cannot exceed that produced by a perfect flap. Therefore, when the whole jet is turned parallel to the wall,

$$\int_{A_F} (p_w - p_0) dA_y = F_{z,0} \sin(\alpha + \tau) \quad (E7)$$

This expression can be evaluated in terms of design variables by assigning an ideal constant value, the nozzle total pressure P_N , to the wall

pressure term p_w . Combination of the integrated expression with

$$F_{z,0} = C_F C_d P_N A_N \left(\frac{2\gamma}{\gamma - 1} \right) \left[1 - \left(\frac{p_0}{P_N} \right)^{\frac{\gamma-1}{\gamma}} \right] \left(\frac{p_0}{P_N} \right)^{\frac{1}{\gamma}}$$

(from one-dimensional isentropic flow relations) yields

$$\left(\frac{A_y}{A_N} \right)_{id} = \mathcal{A}_{id} = \sin(\alpha + \tau) \left\{ \frac{C_F C_d \left(\frac{2\gamma}{\gamma - 1} \right) \left[1 - \left(\frac{p_0}{P_N} \right)^{\frac{\gamma-1}{\gamma}} \right] \left(\frac{p_0}{P_N} \right)^{\frac{1}{\gamma}}}{1 - p_0/P_N} \right\} \quad (E8)$$

In review, \mathcal{A}_{id} is the lateral-area ratio necessary to turn the whole jet parallel to the flap if the wall pressure were everywhere equal to nozzle total pressure. \mathcal{A}_{id} for a typical unheated-air model is shown in figure 47.

In practice, the wall pressure will obviously be something less than P_N . However, this difference can be made up by increasing the actual lateral area $A_{y,ac}$. Therefore, the foregoing principles are applied to flat-plate deflectors in the following manner:

(1) If the actual lateral-area ratio significantly exceeds the ideal value (i.e., if $\mathcal{A}_{ac}/\mathcal{A}_{id}$ significantly exceeds unity), $\mathcal{F}_S = \sin(\alpha + \tau)$.

(2) If $\mathcal{A}_{ac}/\mathcal{A}_{id}$ is less than unity, \mathcal{F}_S can be found by noting that if p_w were everywhere P_N , \mathcal{F}_S would be equal to $\mathcal{A}_{ac}/\mathcal{A}_{id} \sin(\alpha + \tau)$.

To allow for the difference between the assumed and actual wall pressures an experimentally determined factor K is necessary. In this case, therefore,

$$\mathcal{F}_S = K \frac{\mathcal{A}_{ac}}{\mathcal{A}_{id}} \sin(\alpha + \tau) \quad (E9)$$

(3) In each case \mathcal{F}_Z is given by equation (E6).

It was determined that for the three-dimensional geometries tested the mathematically averaged gas turning angle $\alpha + \tau$ is not appreciably different from the geometric angle $\alpha + \tau_{max}$. Accordingly, any of the preceding equations in this appendix can be written in terms of $\alpha + \tau_{max}$ with little error.

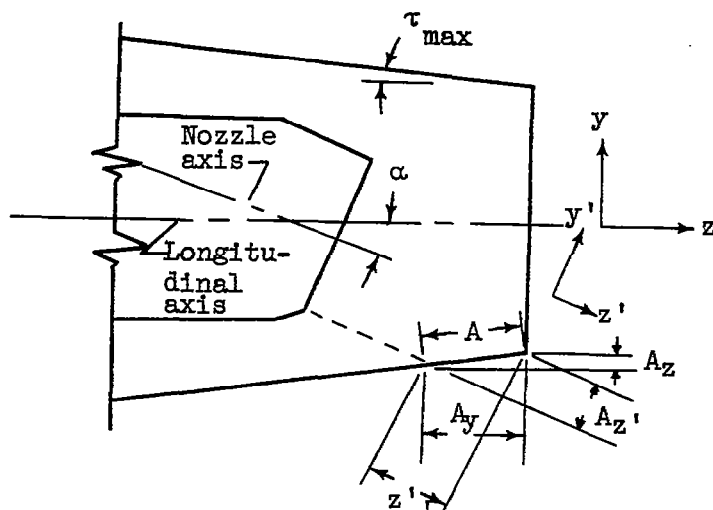
ANALYTICAL PERFORMANCE

The analytical performance of some deflectors meeting the assumptions stated at the beginning of the analysis is presented in figure 48. Sketches (a) and (b) show deflectors having geometry always sufficient to turn the whole jet parallel to the flap. Although \mathcal{F}_S is the same at any given flap angle for either of these deflectors, as indicated by the double abscissa scale, \mathcal{F}_Z for the flat-plate flap is always less than that for the perfect flap.

Sketches (c) and (d) show flat-plate deflectors in which the flap angle is constant and \mathcal{F}_S is varied by the immersion. Although \mathcal{F}_S for the 20° flap is limited to $\sin 20^\circ$, \mathcal{F}_Z is greater than for the 45° flap. In general, the best over-all performance is theoretically obtained when the flap angle is just large enough to produce the required side force.

Sketch (e) shows a deflector consisting of two flat-plate flaps in series, each of which completely turns the jet through half the total turning angle. This configuration more nearly approaches the performance of the perfect flap than the single flat-plate flaps.

Mechanical jet deflectors have the advantage of being, in principle, easily adapted to supersonic jet exits. Flaps may be portions of the rear fuselage skin, an ejector shroud, or a thrust-reverser component. Thus, great variety in design is possible. However, the flaps must be relatively large surfaces capable of withstanding high pressures.

APPLICATION OF ANALYSIS TO EJECTOR WITH
SWIVELLED-PRIMARY-NOZZLE DEFLECTOR

$$\cos(\alpha + \tau_{\max}) = \frac{A_{y'}}{A} = \frac{dA_{y'}}{dA}$$

$$\sin \tau_{\max} = \frac{A_z}{A} = \frac{dA_z}{dA}$$

$$\cos \tau_{\max} = \frac{A_y}{A} = \frac{dA_y}{dA}$$

In addition to the assumptions made in the preceding analysis it is assumed that the performance of the swivelled nozzle follows the cosine law even though the ejector shroud is present. The momentum equation for the flow through the deflector then reduces to

$$F_{S,N} = \int_{A_F} (p_w - p_0) dA_y - F_{z,o} \sin \alpha \quad (E10)$$

By the geometry, substitution gives

$$F_{S,N} = \frac{\cos \tau_{\max}}{\cos(\alpha + \tau_{\max})} \int_{A_F} (p_w - p_0) dA_y - F_{z,o} \sin \alpha \quad (E11)$$

For the configuration tested, A'_{ac}/A'_{id} is always less than unity. Evaluating (E11) in the same manner as previously,

$$\mathcal{F}_S = K \frac{\cos \tau_{\max}}{\cos(\alpha + \tau_{\max})} \frac{A'_{ac}}{A'_{id}} \sin(\alpha + \tau_{\max}) - \sin \alpha \quad (E12)$$

The momentum equation in the z-direction is

$$F_z = F_{z,o} \cos \alpha - \int_{A_F} (p_w - p_0) dA_z \quad (E13)$$

By the definition of \mathcal{F}_z , by geometry, and by substitution from (E11),

$$\mathcal{F}_z = \cos \alpha - (\mathcal{F}_S + \sin \alpha) \tan \tau_{\max} \quad (E14)$$

GEOMETRIC FACTORS

Because of the uncertainty of recirculation, the actual lateral area $A_{y,ac}$ is defined for use herein. Any difference between the defined area and the entire pressurized surface is absorbed in the experimentally determined factor K . As shown in figure 49, $A_{y,ac}$ is found graphically from the intersection of the flap and the "cylinder of the jet." (The diameter of the "cylinder of the jet" is determined by assuming that the jet expands isentropically to ambient pressure.) This procedure involves considerable layout work, and it was determined from some layouts that this area is reasonably approximated by

$$A_{y,ac} = A_{z,ac} \cot(\alpha + \tau_{\max}) \quad (E15)$$

where α is the swivel angle, τ_{\max} is the flap conical half-angle, and $A_{z,ac}$ is the actual immersed area, indicated in figure 49.

Equation (E15) and the mechanically integrated $A_{z,ac}$ were used to calculate all actual lateral areas reported herein. $A_{N,ac}$ is the physical flow area of the primary nozzle, and A_{id} , except in the case of the ejector with a swivelled primary nozzle, is given in figure 47.

For convenience, the geometric factors are grouped together in the \mathcal{F}_S and \mathcal{F}_Z Parameters, defined as follows:

$$\mathcal{F}_S \text{ Parameter} \equiv \frac{A_{ac}}{A_{id}} \sin(\alpha + \tau_{max}) \quad (E16)$$

$$\mathcal{F}_Z \text{ Parameter} \equiv \frac{A_{ac}}{A_{id}} \frac{\sin^2(\alpha + \tau_{max})}{\cos(\alpha + \tau_{max})} \quad (E17)$$


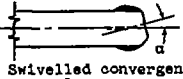

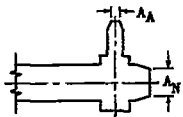
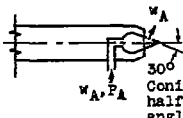

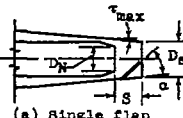
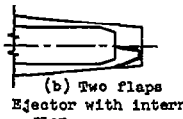
For a given geometry, both parameters tend to increase with pressure ratios above critical because A_{ac} increases because of jet expansion while A_{id} decreases (fig. 47). The quantity A_{ac}/A_{id} is arbitrarily limited to unity in computing each parameter.

REFERENCES

1. Povolny, John H., Steffen, Fred W., and McArdle, Jack G.: Summary of Scale-Model Thrust-Reverser Investigation. NACA TN 3664, 1956.
2. Rowe, P.: Supersonic Jet Deflection. Pt. I - Methods of Jet Deflection and a Review of Previous Work. MOS EMR/52/4, Imperial College of Sci. and Tech. (London), Sept. 1952.
3. Eisenklam, P., and Rowe, P.: Supersonic Jet Deflection. Pt. II - Deflection by Inclined Tubular Extensions. MOS EMR/52/5, Imperial College of Sci. and Tech. (London), Sept. 1952.
4. Rowe, P.: Supersonic Jet Deflection. Pt. III - Deflection by Beveling the Nozzle Exit Plane. MOS EMR/53/1, Imperial College of Sci. and Tech. (London), Feb. 1953.
5. Rowe, P. N.: Supersonic Jet Deflection. Pt. IV - Deflection by Vanes. MOS EMR/55/2, Imperial College of Sci. and Tech. (London), Nov. 1954.
6. Rowe, P. N.: Supersonic Jet Deflection. Pt. V - Deflection by Vanes with Particular Reference to Small Angles. MOS EMR/57/4, Imperial College of Sci. and Tech. (London), Feb. 1957.
7. Friedman, Henry: Summary Report on A-4 Control and Stability. Rep. No. F-SU-2152-ND, Headquarters Air Materiel Command, Wright Field, Dayton (Ohio), June 1947.

8. Main, J. H., and Winer, R.: Studies of Jet-Vanes in Rockets, III. Prog. Rep. ABL/R-29, Allegany Ballistics Lab., Hercules Powder Co., Jan. 1950. (Contract NOrd 10431.)
9. Blackaby, James R., Jr.: An Investigation of the Effects of Jet-Outlet Cut-Off Angle on Thrust Direction and Body Pitching Moment. NACA TN 2379, 1951.
10. von Glahn, Uwe H., and Povolny, John H.: Consideration of Some Jet-Deflection Principles for Directional Control and for Lift. Paper presented at SAE Nat. Aero. meeting (Los Angeles), Oct. 3, 1957.
11. Steffen, Fred W., and McArdle, Jack G.: Performance Characteristics of Cylindrical Target-Type Thrust Reversers. NACA RM E55I29, 1956.

TABLE I. - SUMMARY OF MODELS TESTED

Configuration	Type	Detailed drawings and photographs shown in fig. -	Actuation, α , deg	Diameter ratio, D_{sh}/D_N	Spacing ratio, S/D_N	Conical-shroud half-angle, τ_{max} , deg	Remarks
 Swivelled tailpipe (swivelled engine)	Swivelled nozzle	1 and 5	0 to 24.6	-----	-----	-----	
 Swivelled convergent nozzle	Swivelled nozzle	1 and 6	0 to 20	-----	-----	-----	
 Plug nozzle with plug at tailpipe wall	Swivelled nozzle	2 and 7	-----	-----	-----	-----	Only position tested
 Tailpipe with bleed nozzle	Auxiliary nozzle	1 and 8	-----	-----	-----	-----	Area ratio A_A/A_N varied from 0.093 to 0.257
 Plug nozzle with auxiliary jet from plug	Auxiliary nozzle	2 and 9	-----	-----	-----	-----	Pressure ratio P_A/P_0 varied from 1.0 to 7.7; eight auxiliary-flow-orifice configurations tested
 Swivelled ejector shroud	Mechanical	3, 4, 10, and 11	0 to 15	1.1 to 1.4	0.84 to 1.48	0 to 15	Ejector secondary-flow passage blocked for some tests; baffle added in shroud for one test (see fig. 11)
 (a) Single flap	Mechanical	3, 4, and 12	9 to 87	1.2 to 1.4	0.84 to 1.06	3 to 11	Flow dams added to some flaps; secondary-flow passage only partially blocked for some tests
 (b) Two flaps Ejector with internal flap	Mechanical	3, 4, and 13	0 to 47.5	1.4	1.06	3	

4677

TABLE I. - CONCLUDED. SUMMARY OF MODELS TESTED

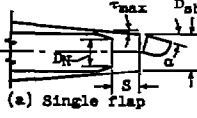

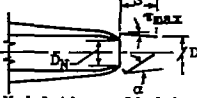
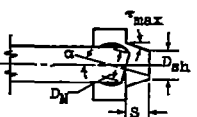
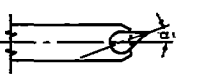
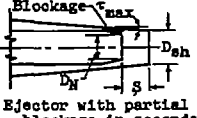
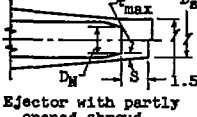
Configuration	Type	Detailed drawings and photographs shown in fig. -	Actuation, α , deg	Diameter ratio, D_{sh}/D_N	Spacing ratio, S/D_N	Conical-shroud half-angle, τ_{max} deg	Remarks
 (a) Single flap	Mechanical	3, 4, and 14(a)	0 to 30	1.16	0.82	17.5	
 (b) Two flaps Ejector with external flap	Mechanical	3, 4, and 14(c)	30	1.2	0.84	11	
 Modulating cylindrical target-type thrust reverser	Mechanical	15	0 to 38	1.29	1.17	7	
 Ejector with swivelled primary nozzle	Mechanical	6 and 16	0 to 20	1.1	0.78	15	Model simulates ejector with blocked secondary-flow passage
 Plug nozzle with swivelled plug	-----	2 and 17(a)	0 to 30	---	---	---	
 Ejector with partial blockage in secondary flow passage	-----	3, 4, and 17(b)	-----	1.2	0.84	11	
 Ejector with partly opened shroud	-----	3, 4, and 17(c)	-----	1.2	0.84	11	Half of shroud opened to equivalent of 1.5 D_{sh}/D_N shroud

TABLE II. - GEOMETRIC DATA FOR JET DEFLECTORS

(a) Ejectors with swivelled shroud.
 Primary-nozzle pressure ratio, 2.0

4677

Configuration	Diameter ratio, D_{sh}/D_N	Spacing ratio, S/D_N	Conical-shroud half-angle, τ_{max} , deg	$(\alpha + \tau_{max})$, deg	Area ratio, $(A_Z/A_N)_{ac}$	\mathcal{A}_{ac} (a)	$\mathcal{A}_{ac}/\mathcal{A}_{id}$
A	1.1	0.86	0	1.5	0	0	0
				5	.043	.492	3.93
				7.5	.130	.990	5.24
				10	.170	.966	3.87
				12.2	.232	1.071	3.53
				15	.302	1.130	3.06
B	1.1	0.87	15	20	0.047	0.129	0.264
				25	.162	.348	.578
				30	.283	.491	.689
C	1.1	1.28	15	30	0.281	0.487	0.682
D	1.2	0.84	11	16	0	0	0
				21	.100	.262	.515
				26	.194	.398	.638
E	1.2	1.07	15	30	0.136	0.236	0.331
F	1.2	1.27	11	26	0.208	0.427	0.685
G	1.4	1.06	3	8	0	0	0
				13	.038	.165	.512
				18	.159	.490	1.11
H	1.4	1.48	3	18	0.138	0.424	0.961

$$^a \mathcal{A}_{ac} = \left(\frac{A_Z}{A_N} \right)_{ac} \cot(\alpha + \tau_{max}).$$

TABLE II. - Continued. GEOMETRIC DATA FOR JET DEFLECTORS

(b) Ejectors with internal flap. Primary-nozzle pressure ratio, 2.0.

Configuration	Diameter ratio, D_{sh}/D_N	Spacing ratio, S/D_N	Flap chord angle, β , deg	Conical-shroud half-angle, τ_{max} , deg	$(\alpha + \tau_{max})$, deg	Area ratio, $(A_z/A_N)_{ac}$	\mathcal{A}_{ac} (a)	$\mathcal{A}_{ac}/\mathcal{A}_{id}$
I	1.2	0.84	90	11	20	0.045 .162 .250	0.124 .445 .687	0.254 .911 1.41
J	1.2	0.84	90	11	45	0.040 .084 .158	0.040 .084 .158	0.040 .083 .157
K	1.4	1.04	90	3	20	0.068 .153 .240	0.188 .421 .660	0.385 .861 1.35
L	1.4	1.04	90	3	45	0.040 .126 .183	0.040 .126 .183	0.040 .125 .181
M	1.4	1.04	60 45 30	3	45	0.174 .149 .099	0.174 .149 .099	0.172 .148 .098
N	1.4	1.04	(b)	3	12 17 20.5 25.5 31 40 50.5	0 .052 .104 .158 .228 .329 .445	0 .172 .278 .332 .379 .392 .366	0 .411 .559 .541 .518 .428 .331
O (c)	1.4	1.04	(b)	3	12 17 20.5 25.5	0 .052 .104 .158	0 .172 .278 .332	0 .411 .559 .541
P	1.2	0.84	54 72 88	11	90	0.041 .094 .167	----- ----- -----	----- ----- -----
Q	1.4	1.04	75	3	90	0.182	-----	-----
R	1.4	1.04	112 136 152	3	90	0.061 .182 .296	----- ----- -----	----- ----- -----

$$^a \mathcal{A}_{ac} = \left(\frac{A_z}{A_N} \right)_{ac} \cot(\alpha + \tau_{max}).$$

^b $\beta = 90^\circ$ at upstream end of each flap; $\beta = 41^\circ$ at downstream end of each flap.

^c Values for configurations O are given on the basis of single flap.

4677

CB-6 back

TABLE II. - Concluded. GEOMETRIC DATA FOR JET DEFLECTORS

(c) Ejectors with external flap. Primary-nozzle pressure ratio, 2.0.

Configuration	Diameter ratio, D_{sh}/D_N	Spacing ratio, S/D_N	Flap chord angle, β , deg	Conical-shroud half-angle, τ_{max} , deg	$(\alpha + \tau_{max})$, deg	Area ratio, $(A_z/A_N)_{ac}$ (a)	\mathcal{A}_{ac} (a), (b)	\mathcal{A}_{ac}/id
S	1.16	0.82	180	0	10	0.057	0.324	1.29
					20	.297	.818	1.67
					30	.595	1.03	1.45
T	1.2	0.84	90	0	30	0.062	0.108	0.152

^aParameter computed neglecting presence of ejector shroud.

$$^b \mathcal{A}_{ac} = \left(\frac{A_z}{A_N} \right)_{ac} \cot(\alpha + \tau_{max}).$$

(d) Modulating cylindrical target-type thrust reverser. Primary-nozzle pressure ratio, 2.0

Configuration	Diameter ratio, D_{sh}/D_N (a)	Spacing ratio, S/D_N (a)	Flap chord angle, β , deg	Conical-shroud half-angle, τ_{max} , deg	$(\alpha + \tau_{max})$, deg	Area ratio, $(A_z/A_N)_{ac}$	\mathcal{A}_{ac} (b)	\mathcal{A}_{ac}/id
U	1.29	1.17	130	7	22	0	0	0
					30	.079	.137	.193
					45	.220	.220	.218

^aEffective values.

$$^b \mathcal{A}_{ac} = \left(\frac{A_z}{A_N} \right)_{ac} \cot(\alpha + \tau_{max}).$$

(e) Ejector with swivelled primary nozzle. Primary-nozzle pressure ratio, 2.0

Configuration	Diameter ratio, D_{sh}/D_N (a)	Spacing ratio, S/D_N (a)	Conical-shroud half-angle, τ_{max} , deg	$(\alpha + \tau_{max})$, deg	Area ratio, $(A_z/A_N)_{ac}$	\mathcal{A}_{ac} (b)	\mathcal{A}_{ac}/id
V	1.1	0.78	15	25	0.169	0.364	0.687
				30	.328	.568	.905
				35	.480	.686	.953

^aBased on physical dimensions.

$$^b \mathcal{A}_{ac} = \left(\frac{A_z}{A_N} \right)_{ac} \cot(\alpha + \tau_{max}).$$

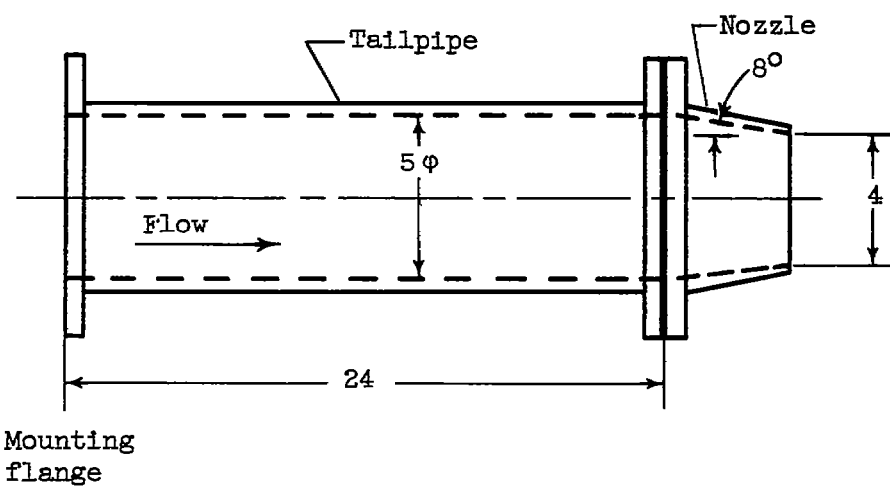


Figure 1. - Basic tailpipe and convergent nozzle. (All dimensions in inches.)

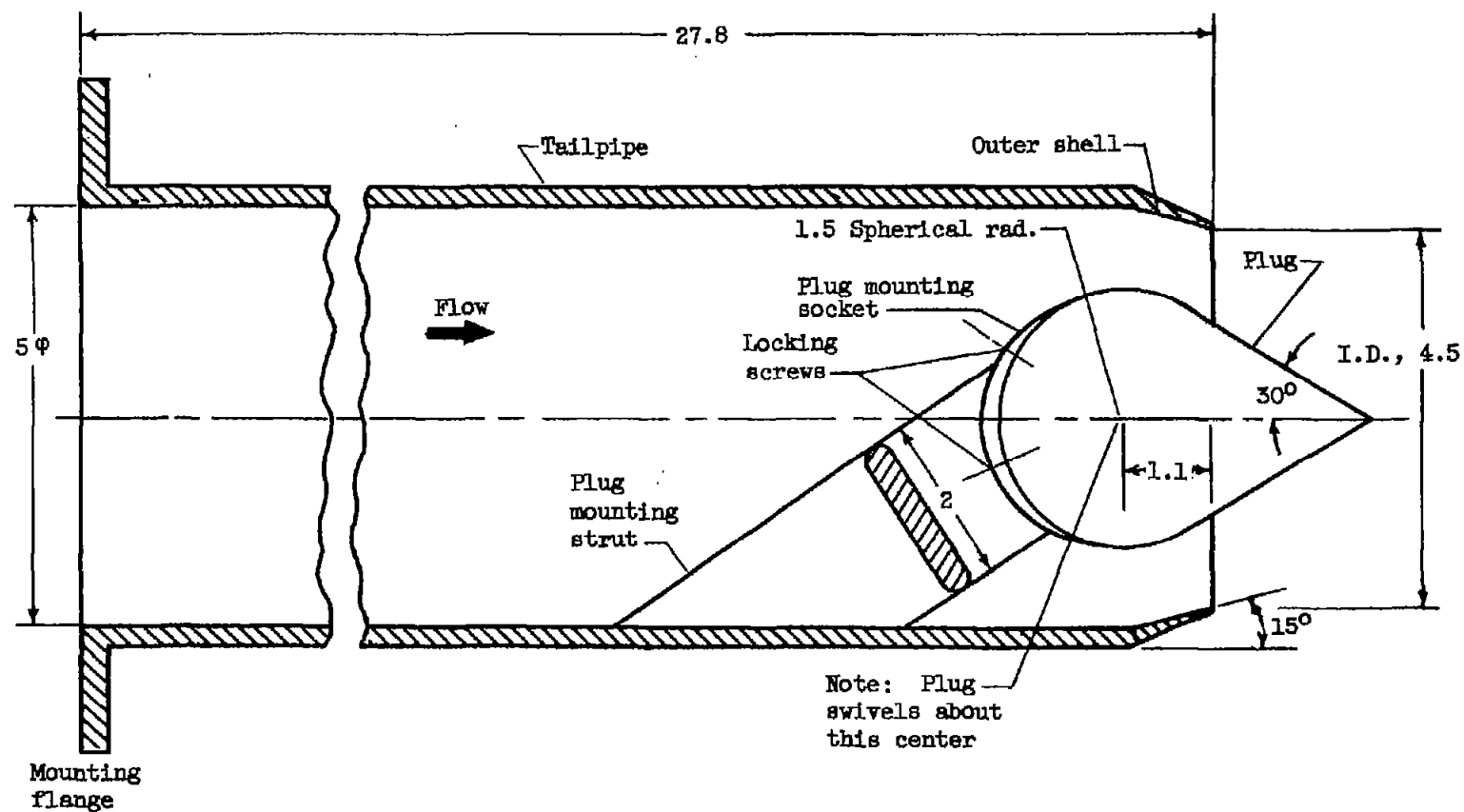
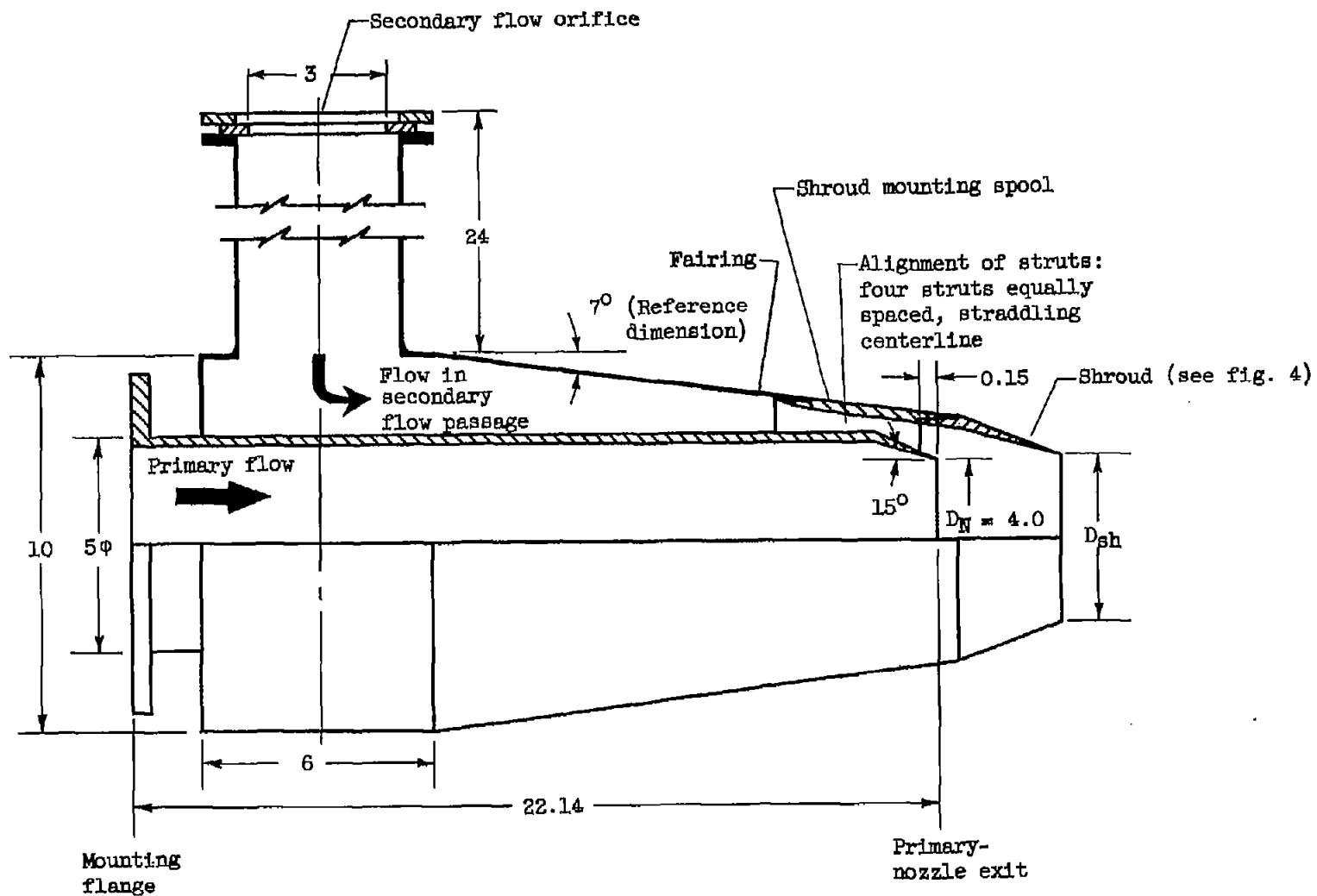
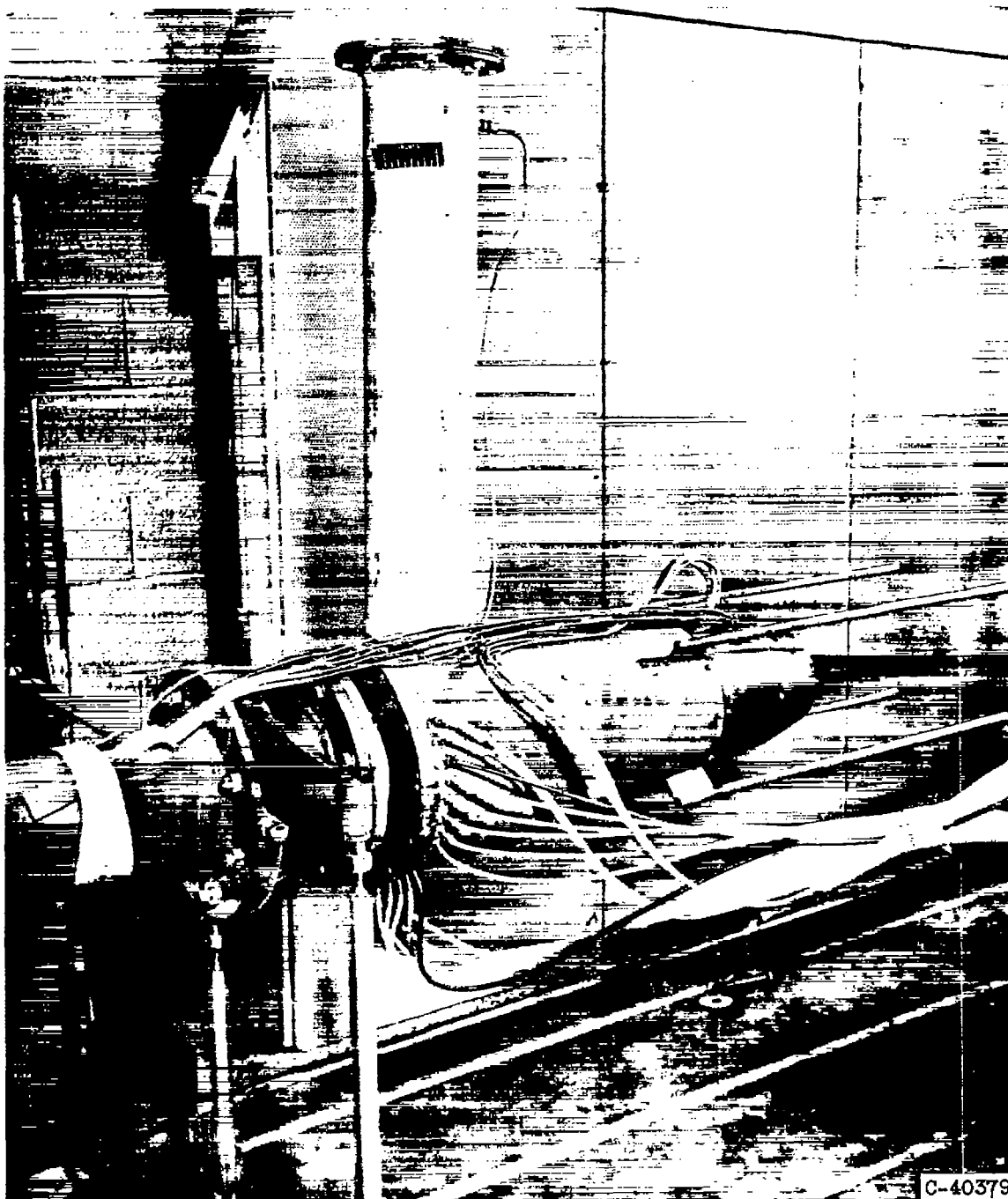


Figure 2. - Cutaway view of basic plug nozzle. (All dimensions in inches.)



(a) Cutaway cross section. (All dimensions in inches.)

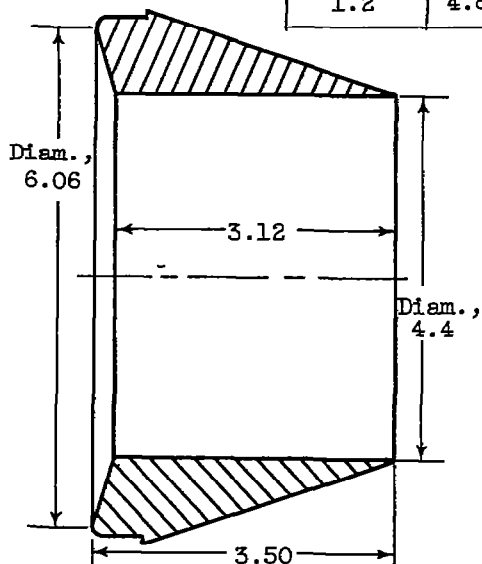
Figure 3. - Basic ejector.



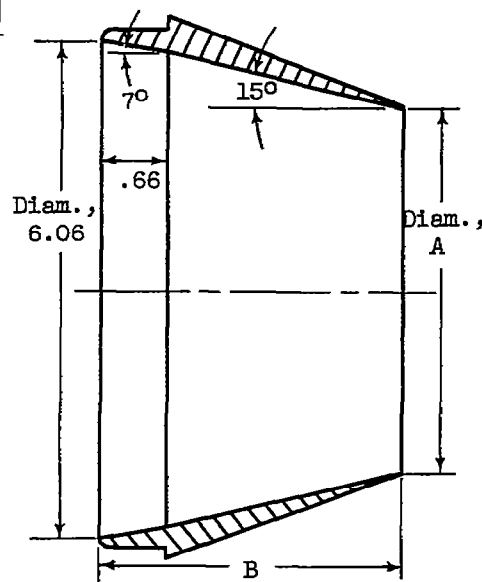
(b) Model mounted in experimental setup.

Figure 3. - Concluded. Basic ejector.

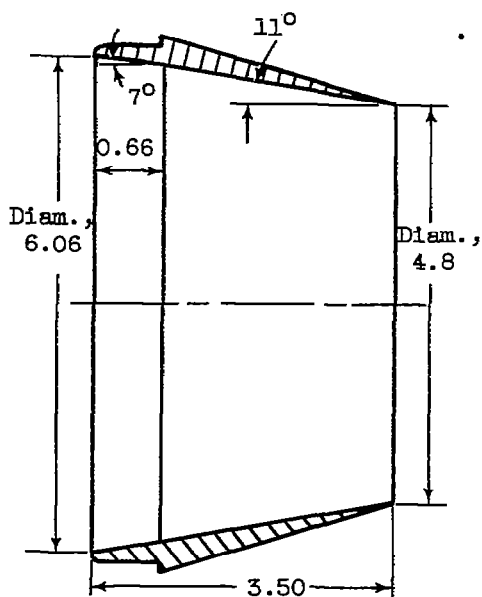
Diameter ratio, D_{sh}/D_N	A, in.	B, in.
1.1	4.4	3.5
1.2	4.8	2.6



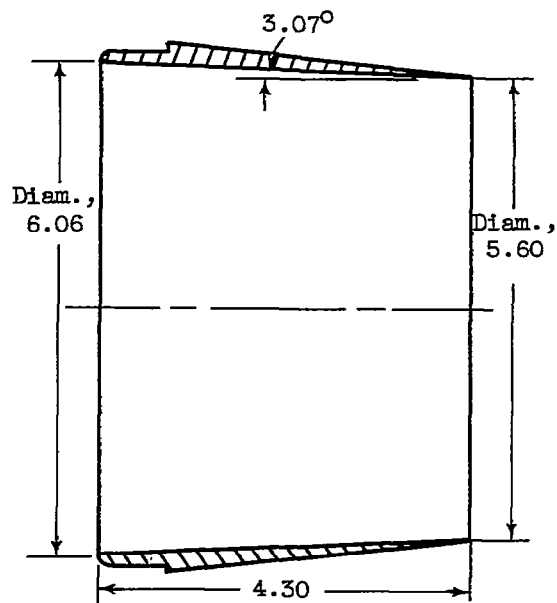
(a) $D_{sh}/D_N = 1.1$; cylindrical.



(b) 15° Conical.

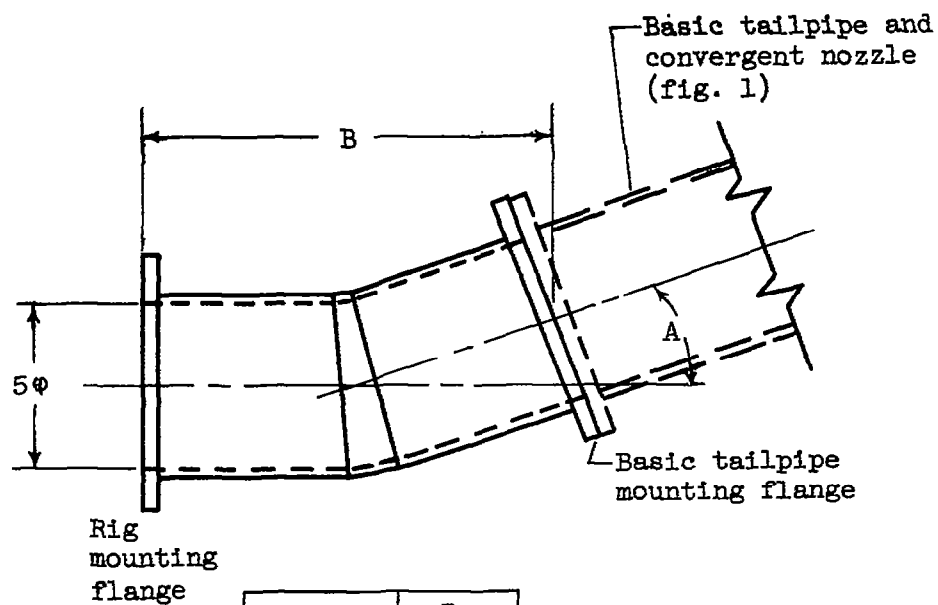


(c) $D_{sh}/D_N = 1.2$; 11° conical.



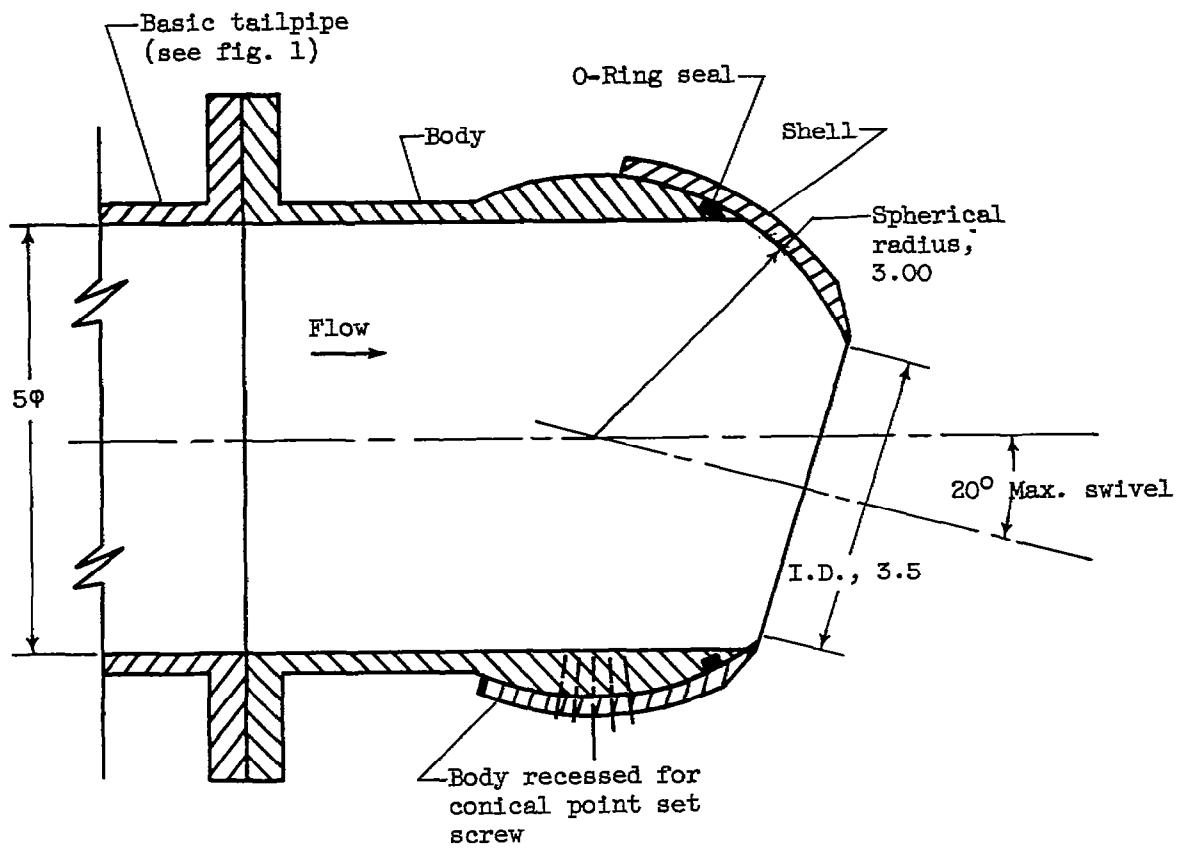
(d) $D_{sh}/D_N = 1.4$; 3° conical.

Figure 4. - Detailed geometry of shrouds used with basic ejector. (All dimensions in inches.)



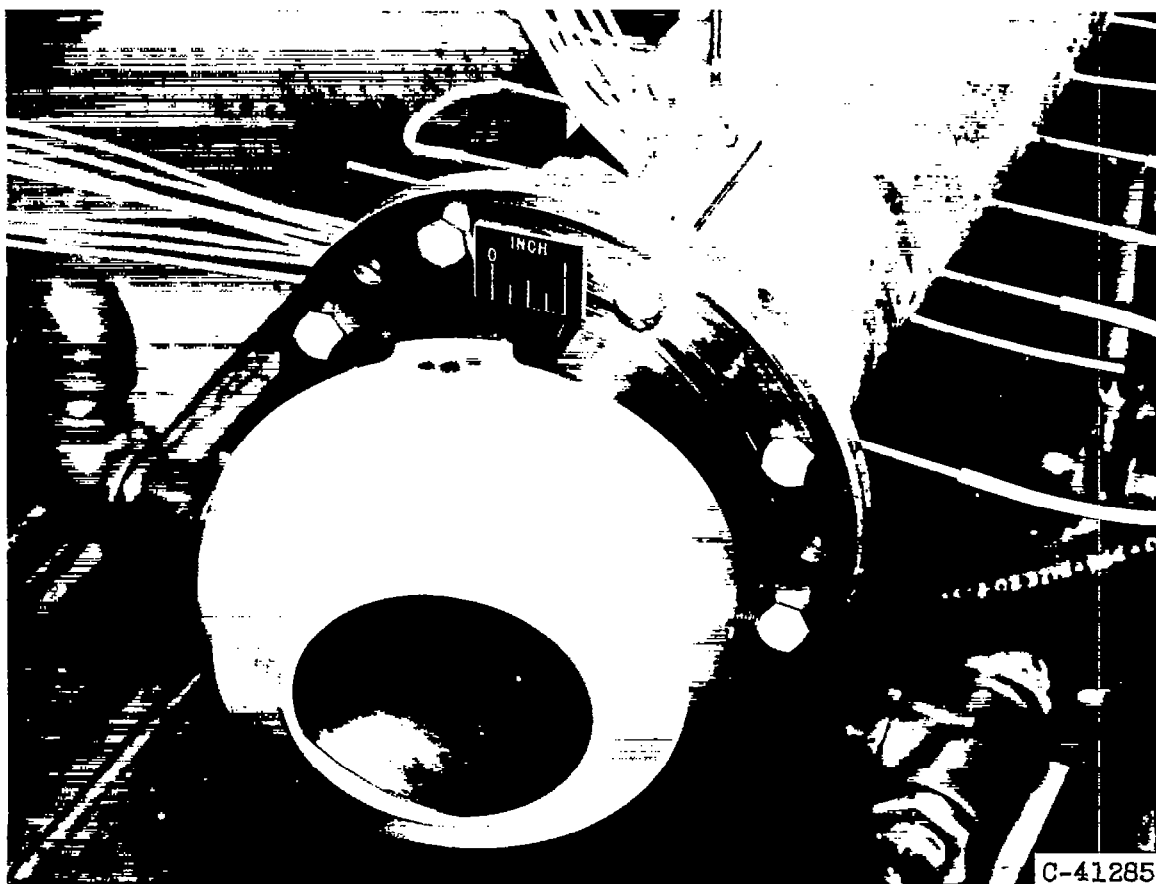
A	B, in.
5° 20'	8.82
10° 15'	8.77
14° 30'	8.69
19° 55'	8.57
24° 50'	8.50

Figure 5. - Elbows used in swivelled-tailpipe configurations.



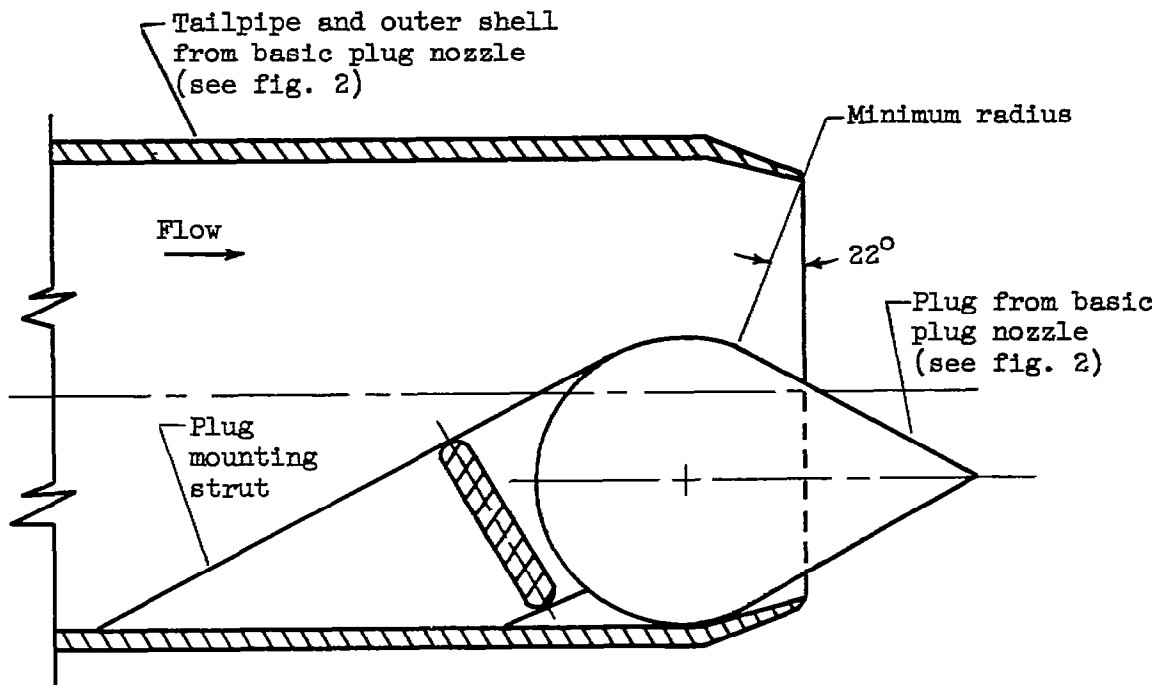
(a) Cross section. (All dimensions in inches.)

Figure 6. - Swivelled convergent nozzle.



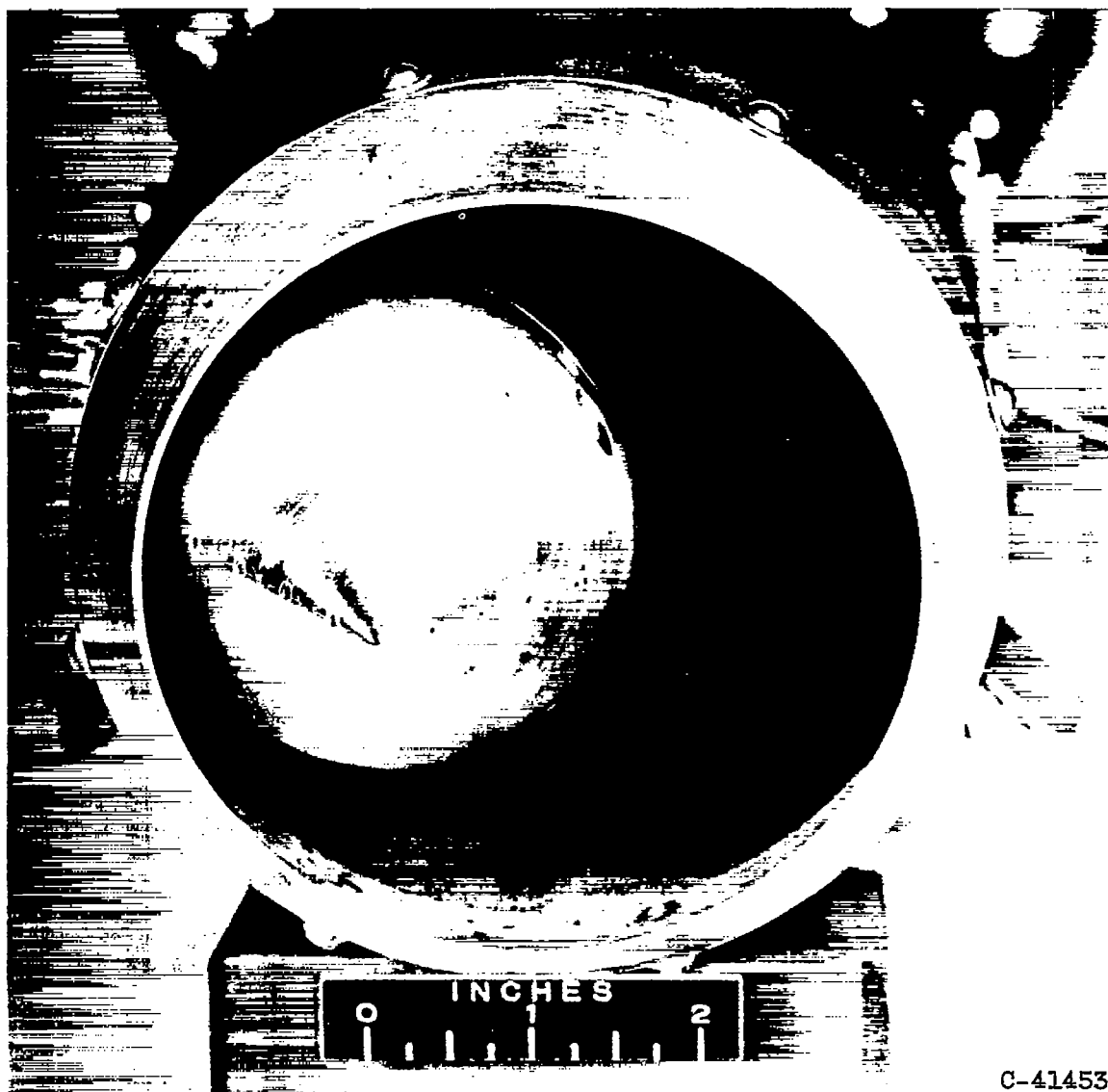
(b) Photograph of model.

Figure 6. - Concluded. Swivelled convergent nozzle.



(a) Cross section.

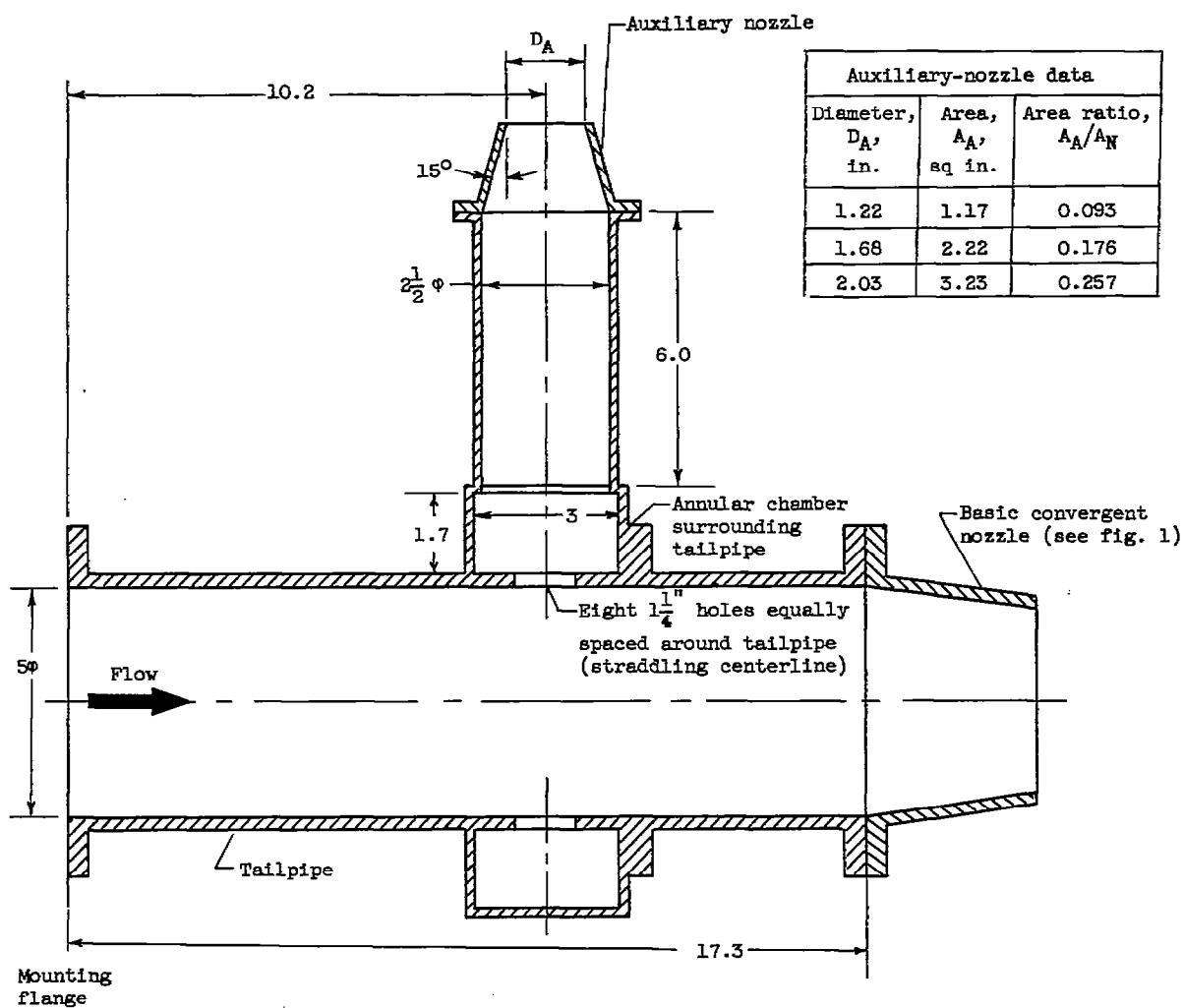
Figure 7. - Plug nozzle with plug at tailpipe wall.



C-41453

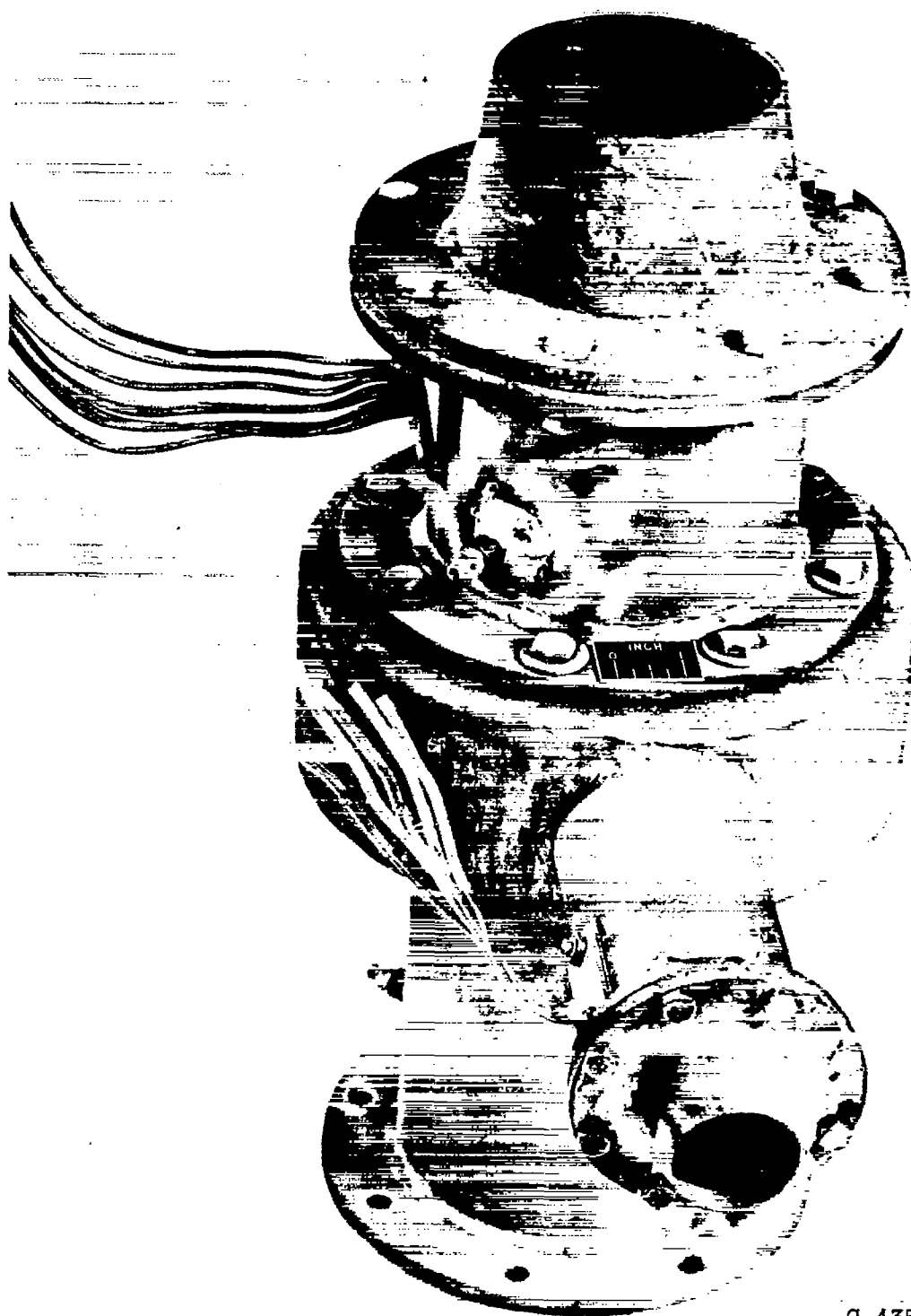
(b) Photograph of model.

Figure 7. - Concluded. Plug nozzle with plug at tailpipe wall.



(a) Cross section. (All dimensions in inches.)

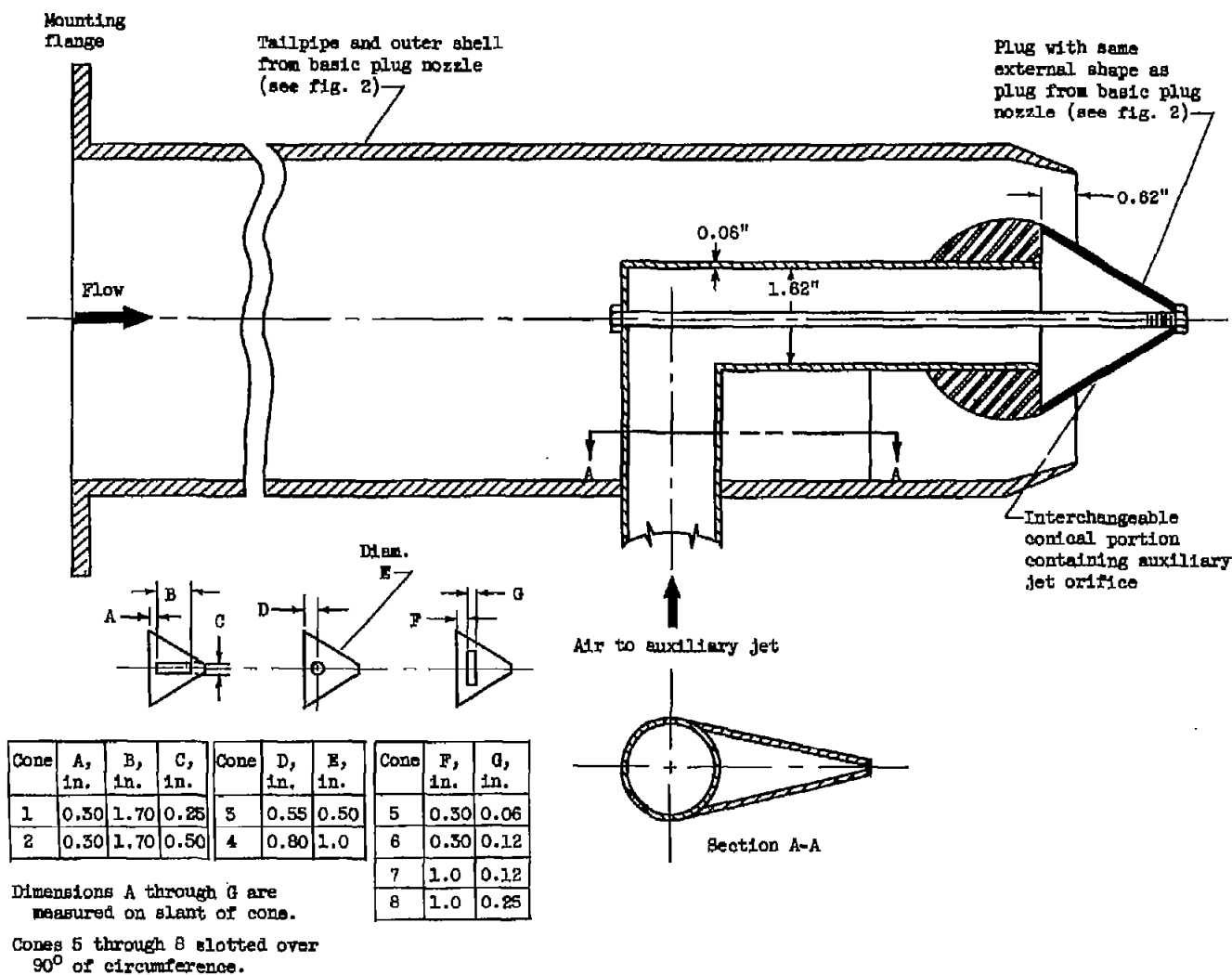
Figure 8. - Tailpipe with bleed nozzle.



C-43503

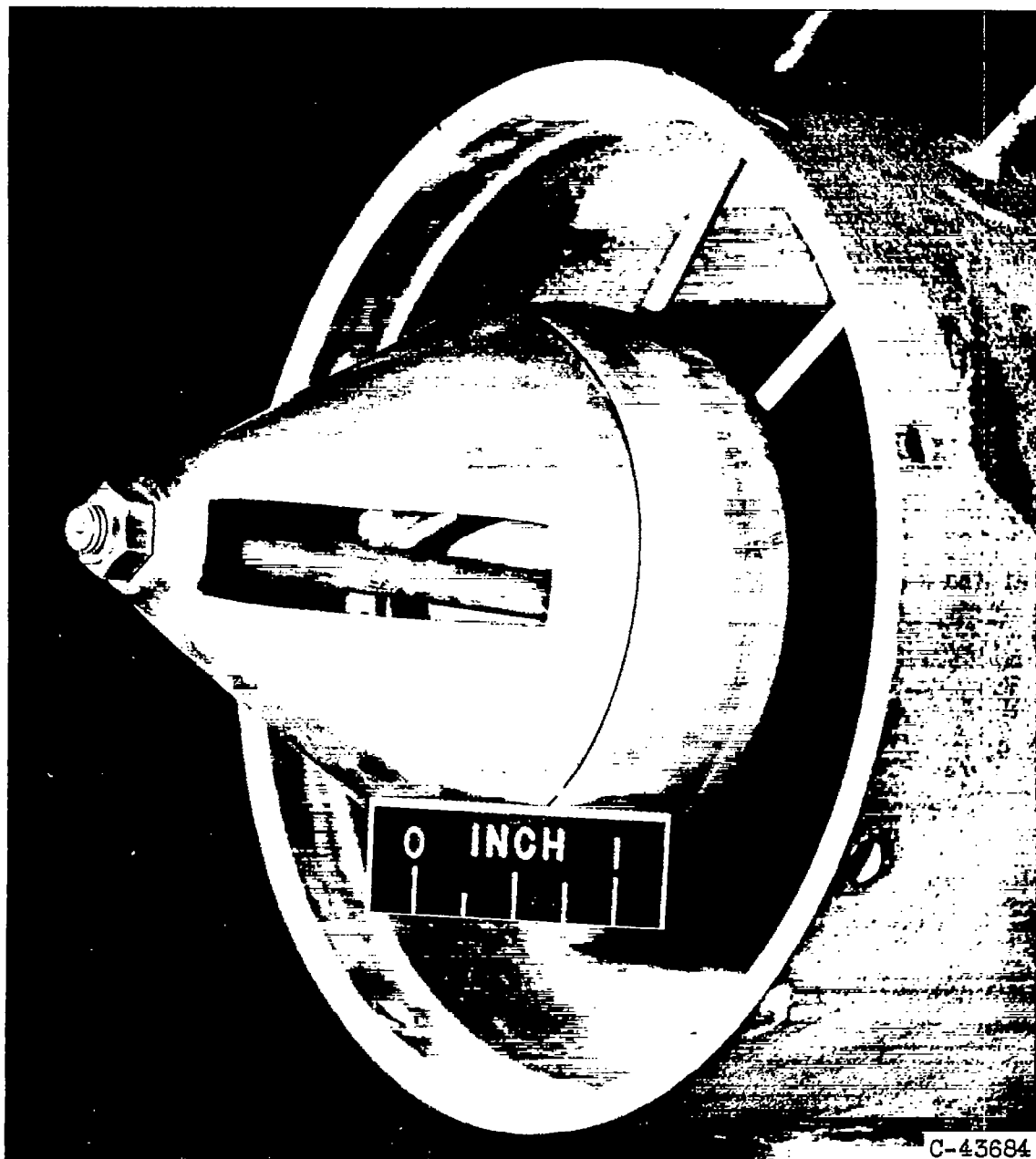
(b) Photograph of model.

Figure 8. - Concluded. Tailpipe with bleed nozzle.



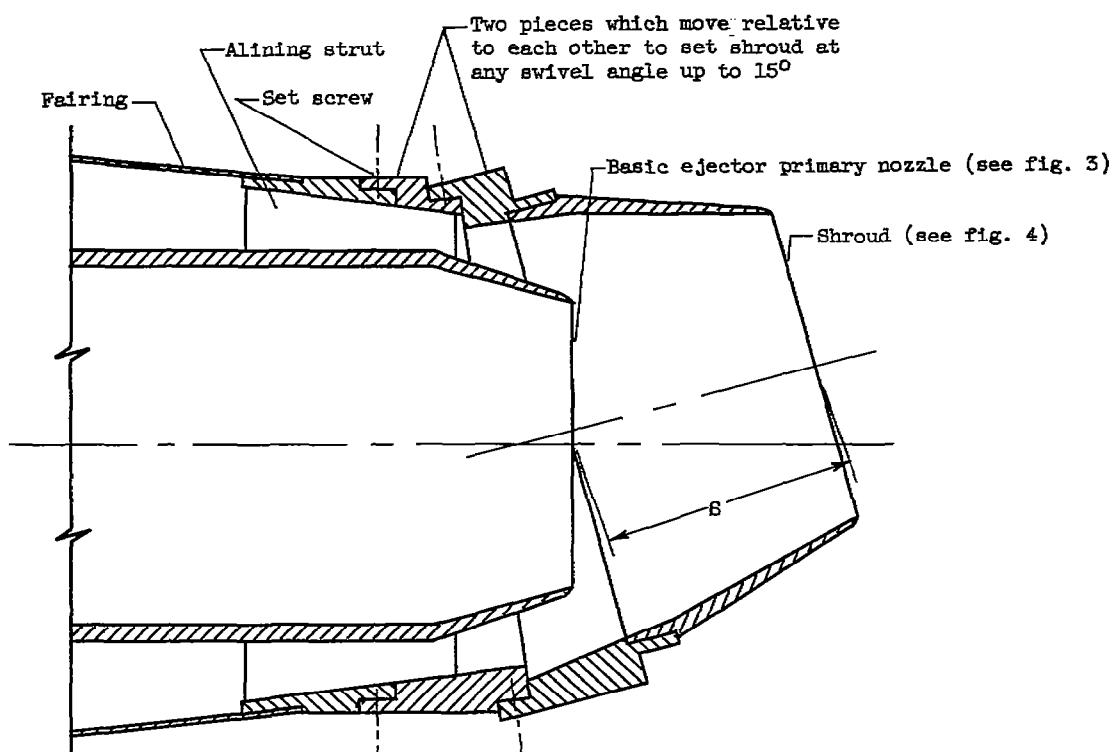
(a) Cross section.

Figure 8. - Plug nozzle with auxiliary jet from plug.

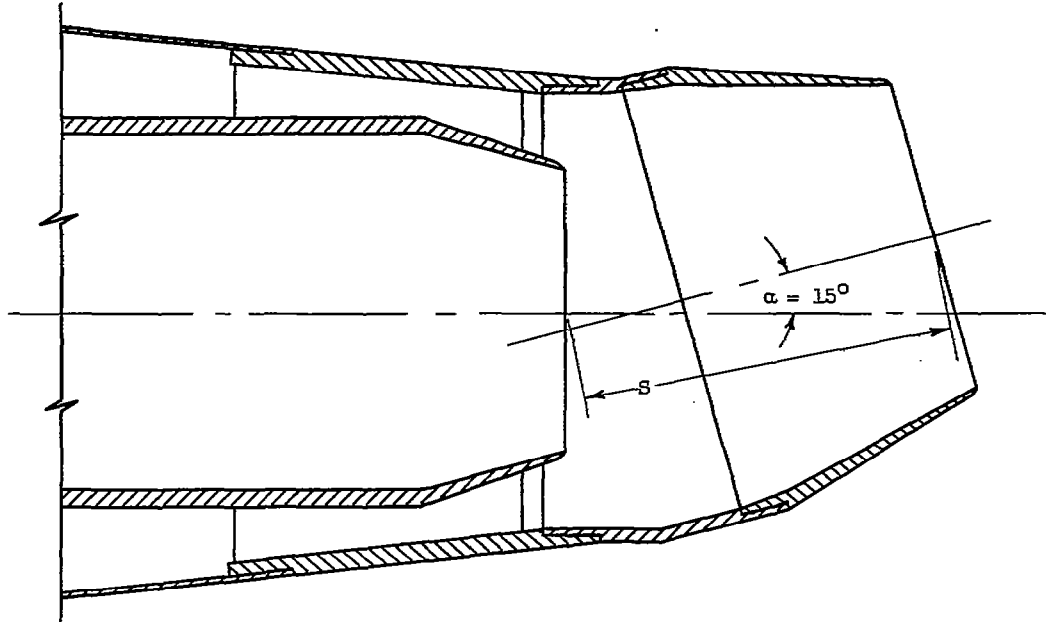


(b) Photograph of model. (Nozzle outer shell removed for clarity.)

Figure 9. - Concluded. Plug nozzle with auxiliary jet from plug.



(a) Adjustable shroud mounting spool (shown in maximum-swivel-angle position). Effective pivot point maintains approximately constant position for all swivel angles.



(b) 15° Fixed extension for shroud mounting spool.

Figure 10. - Variable aft geometry used with basic ejector to form swivelled-ejector-shroud jet deflectors.

4677

, CE-8 back

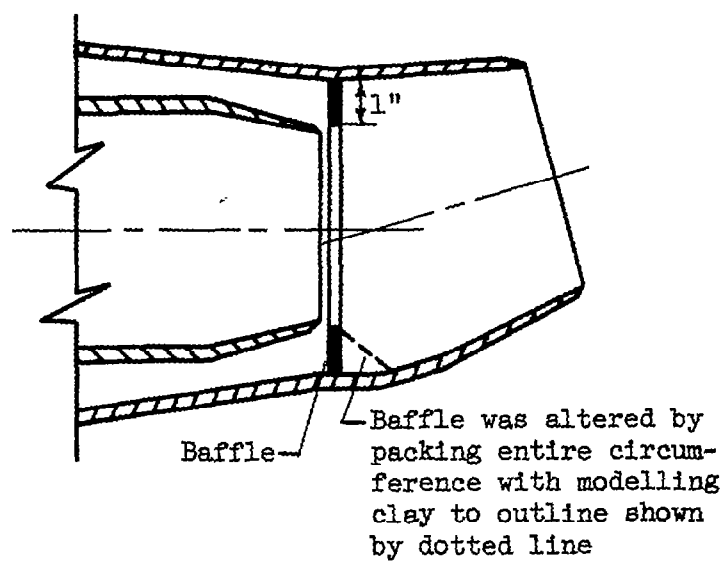
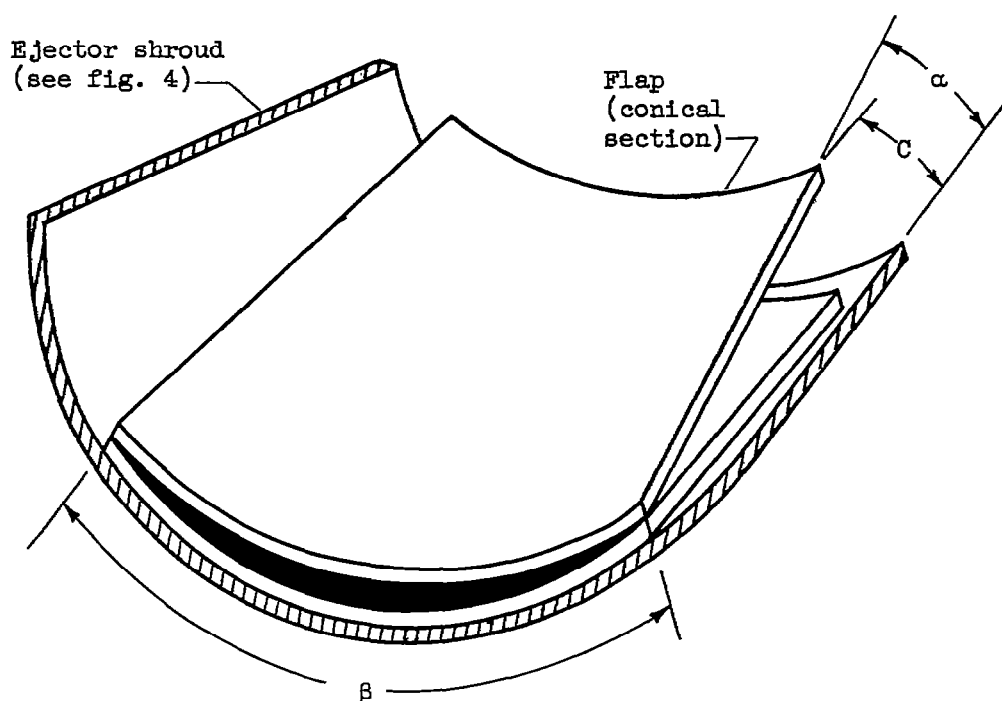


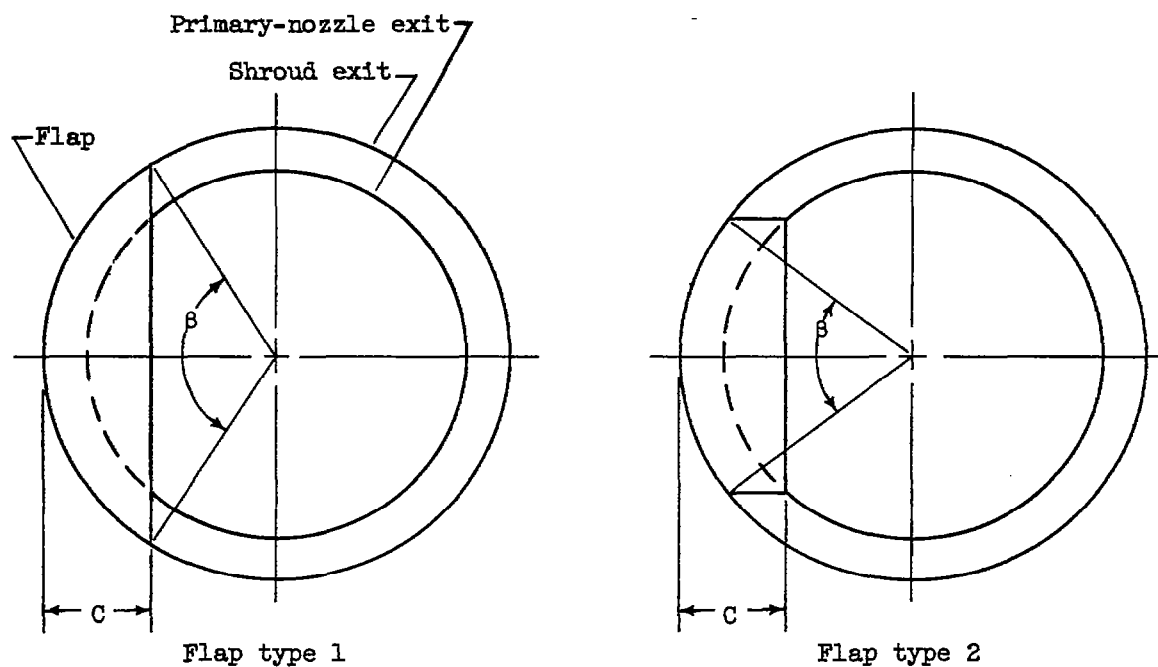
Figure 11. - Baffle added to swivelled ejector shroud (configuration F).



Configuration	Used with ejector shroud shown in fig. -	α , deg	C, in.	β , deg
I	4(c)	9	0.61	90
I	4(c)	9	1.06	90
I	4(c)	9	1.38	90
J	4(c)	34	0.65	90
J	4(c)	34	0.79	90
J	4(c)	34	1.04	90
K	4(d)	17	1.10	90
K	4(d)	17	1.41	90
K	4(d)	17	1.72	90
L	4(d)	42	1.04	90
L	4(d)	42	1.35	90
L	4(d)	42	1.62	90
M	4(d)	42	1.62	60
M	4(d)	42	1.62	45
M	4(d)	42	1.62	30

(a) Flaps not normal to longitudinal axis.

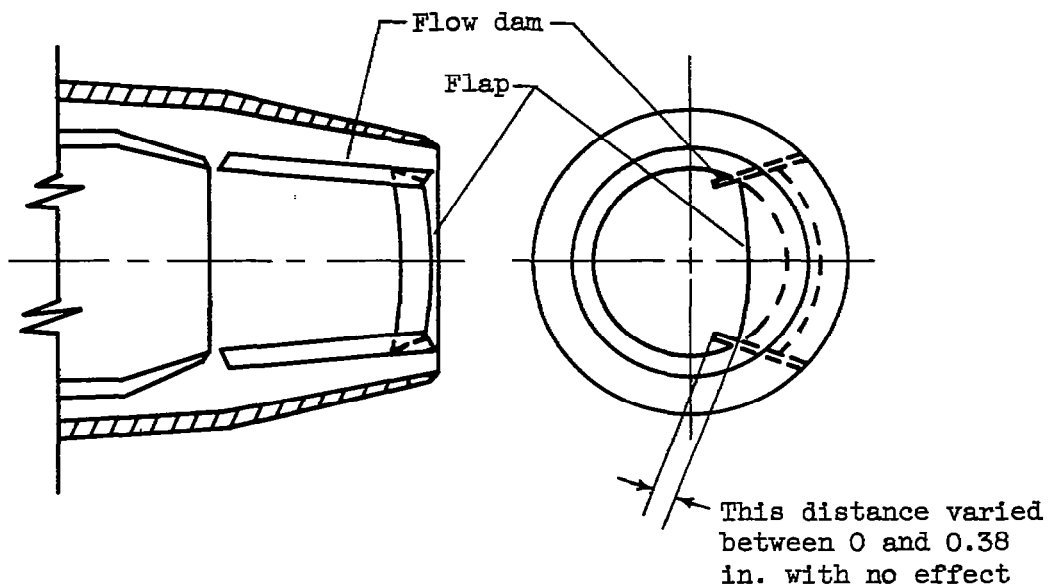
Figure 12. - Ejectors with internal fixed flap.



Configuration	Used with ejector shroud shown in fig. -	Flap type	C, in.	β , deg
P	4(c)	2	0.73	54
P	4(c)	2	0.98	72
P	4(c)	2	1.28	88
Q	4(d)	2	1.75	75
R	4(d)	1	1.24	112
R	4(d)	1	1.75	136
R	4(d)	1	2.13	152

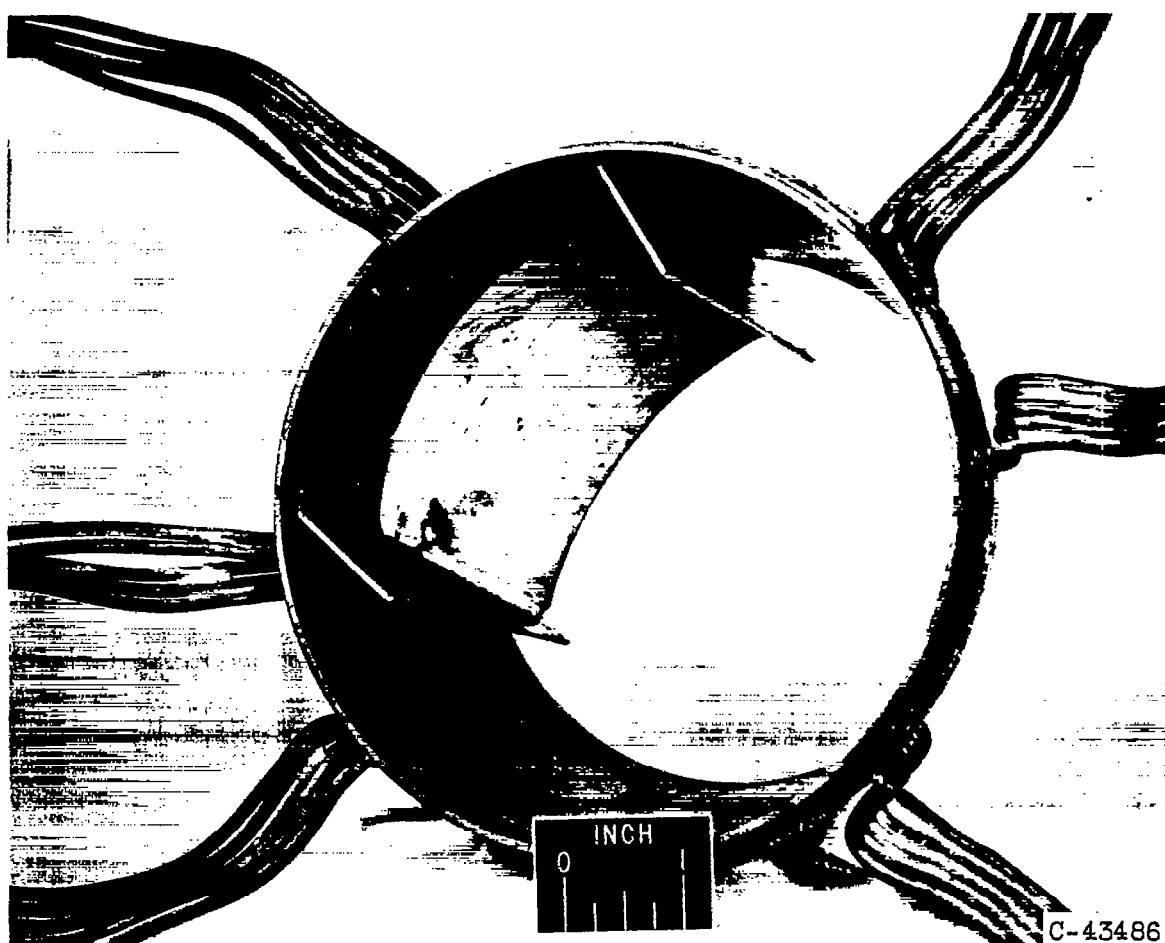
(b) Flaps normal to longitudinal axis at shroud exit.

Figure 12. - Continued. Ejectors with internal fixed flap.



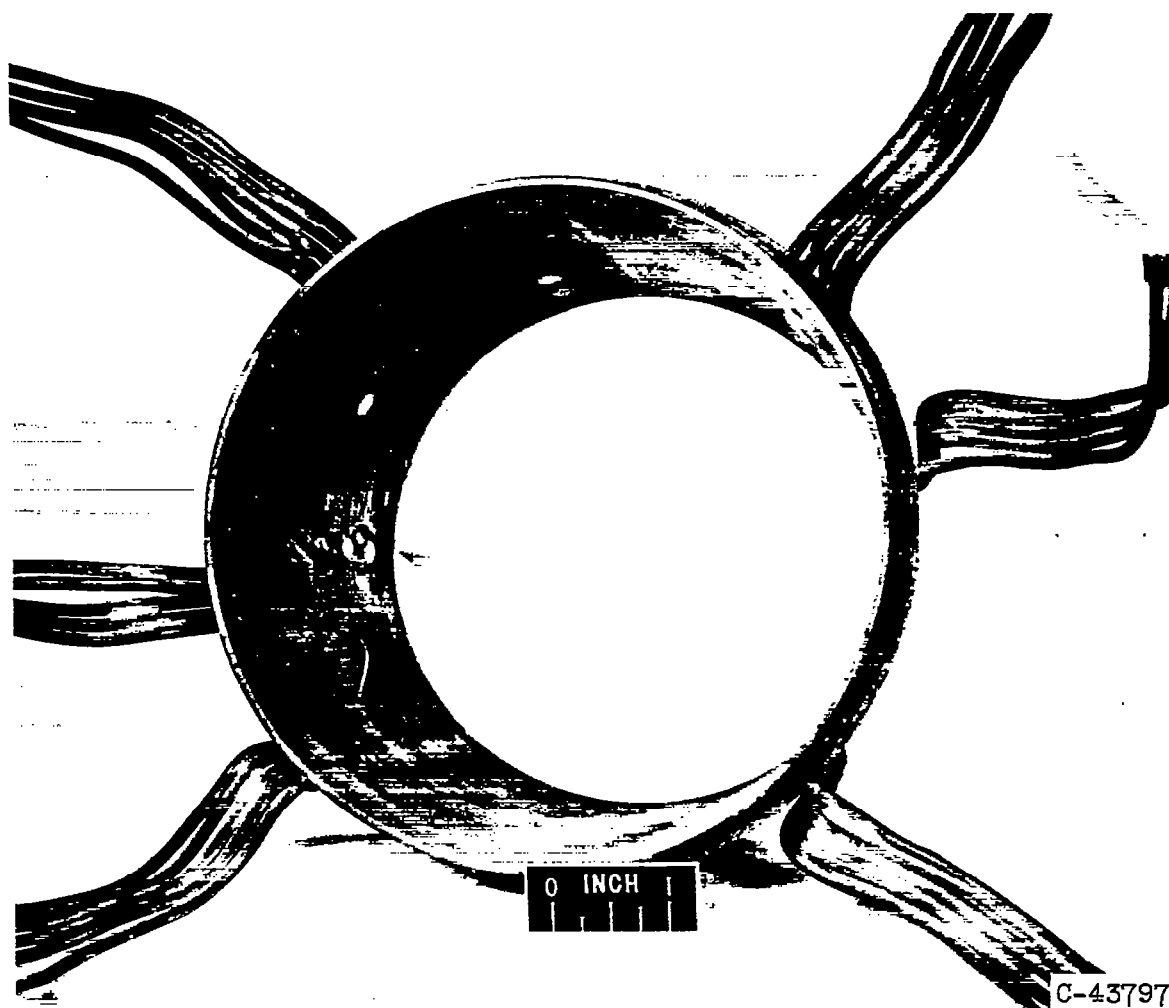
(c) Flow dams added to some configurations.

Figure 12. - Continued. Ejectors with internal fixed flap.



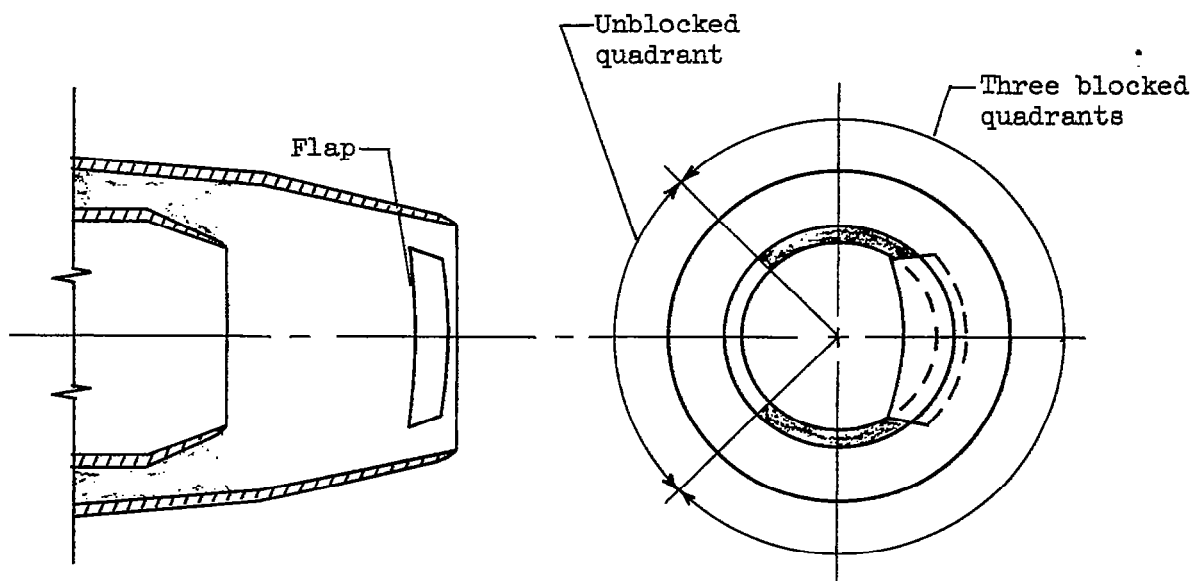
(d) 45° Flap, with flow dams on either edge of flap.

Figure 12. - Continued. Ejectors with internal fixed flap.



(e) Flap normal to longitudinal axis at shroud exit.

Figure 12. - Continued. Ejectors with internal fixed flap.



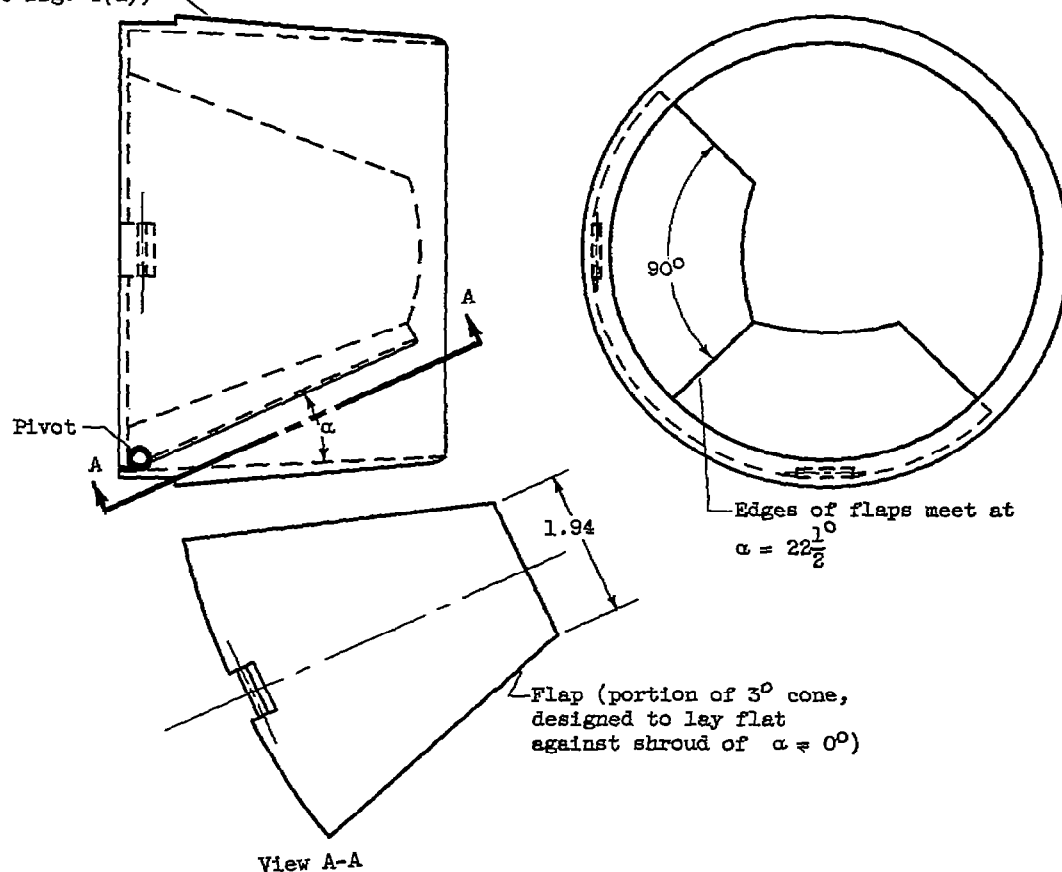
(f) Blockage in secondary flow passage as used with some configurations.

Figure 12. - Concluded. Ejectors with internal fixed flap.

4677

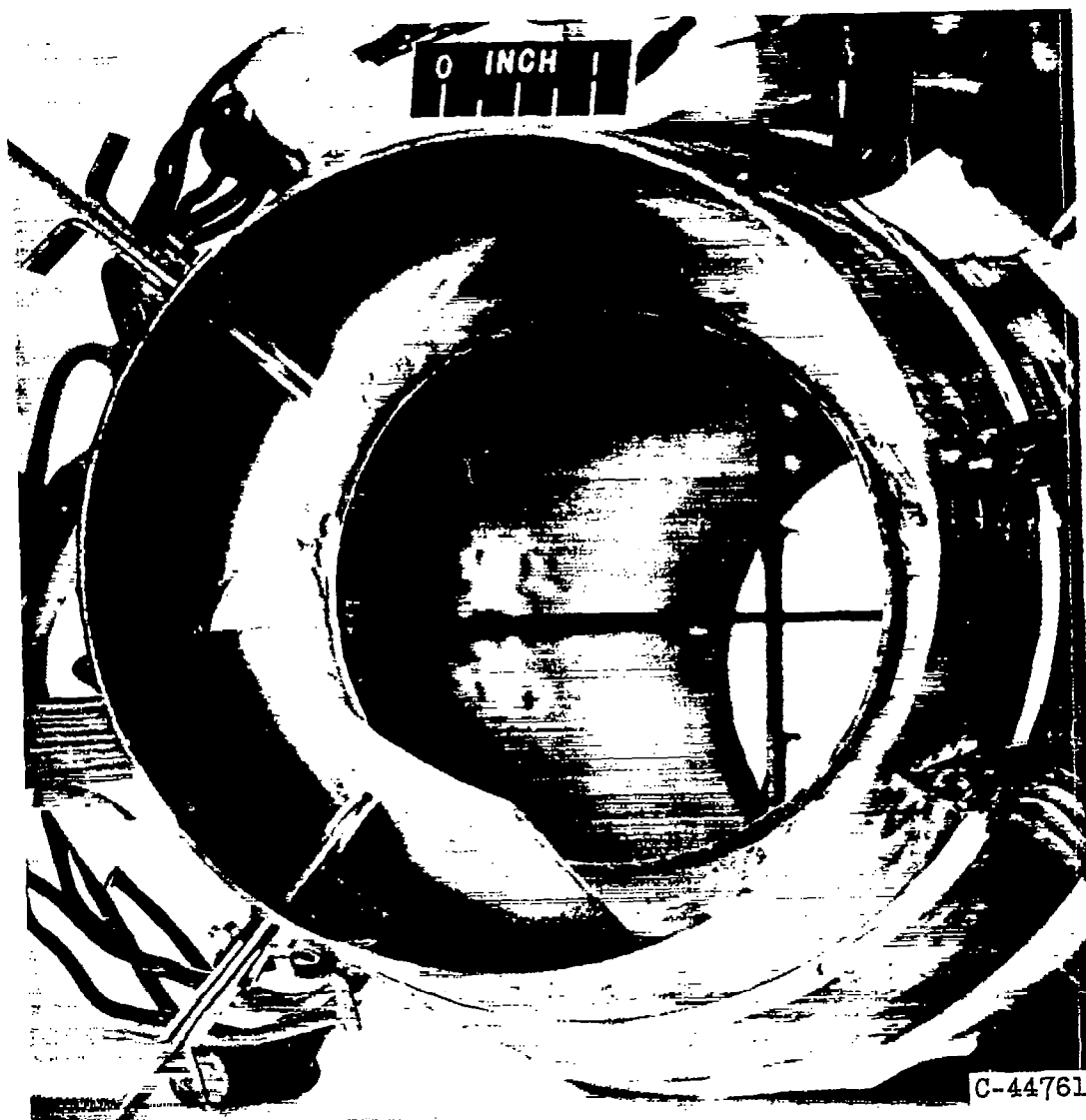
CB-9 back

$D_{sh}/D_N = 1.4$,
 3° conical
 ejector shroud
 (see fig. 4(d))



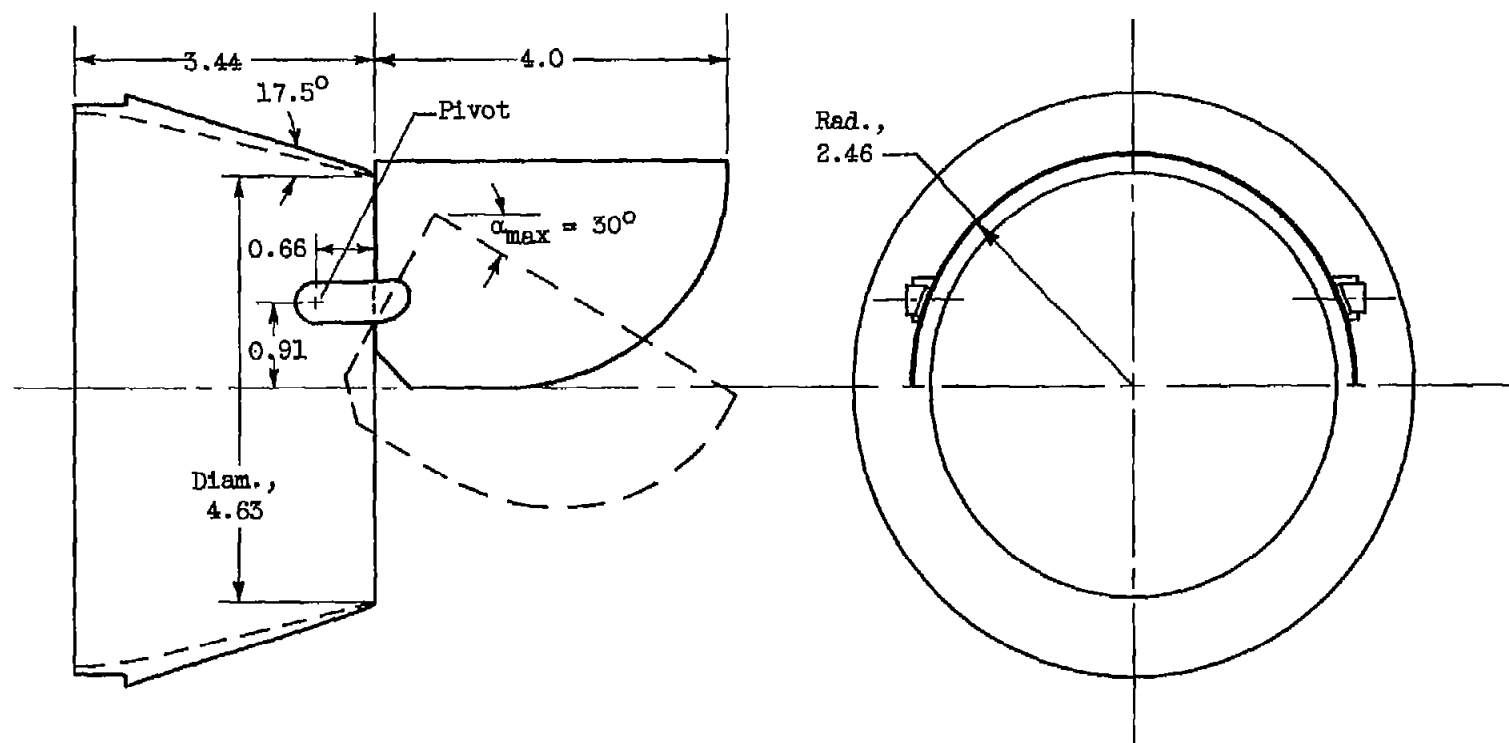
(a) Schematic drawing of shroud and flaps. Either flap may be actuated independently. Actuating and locking mechanism not shown. (All dimensions in inches.)

Figure 13. - Ejector with internal pivoted flap.



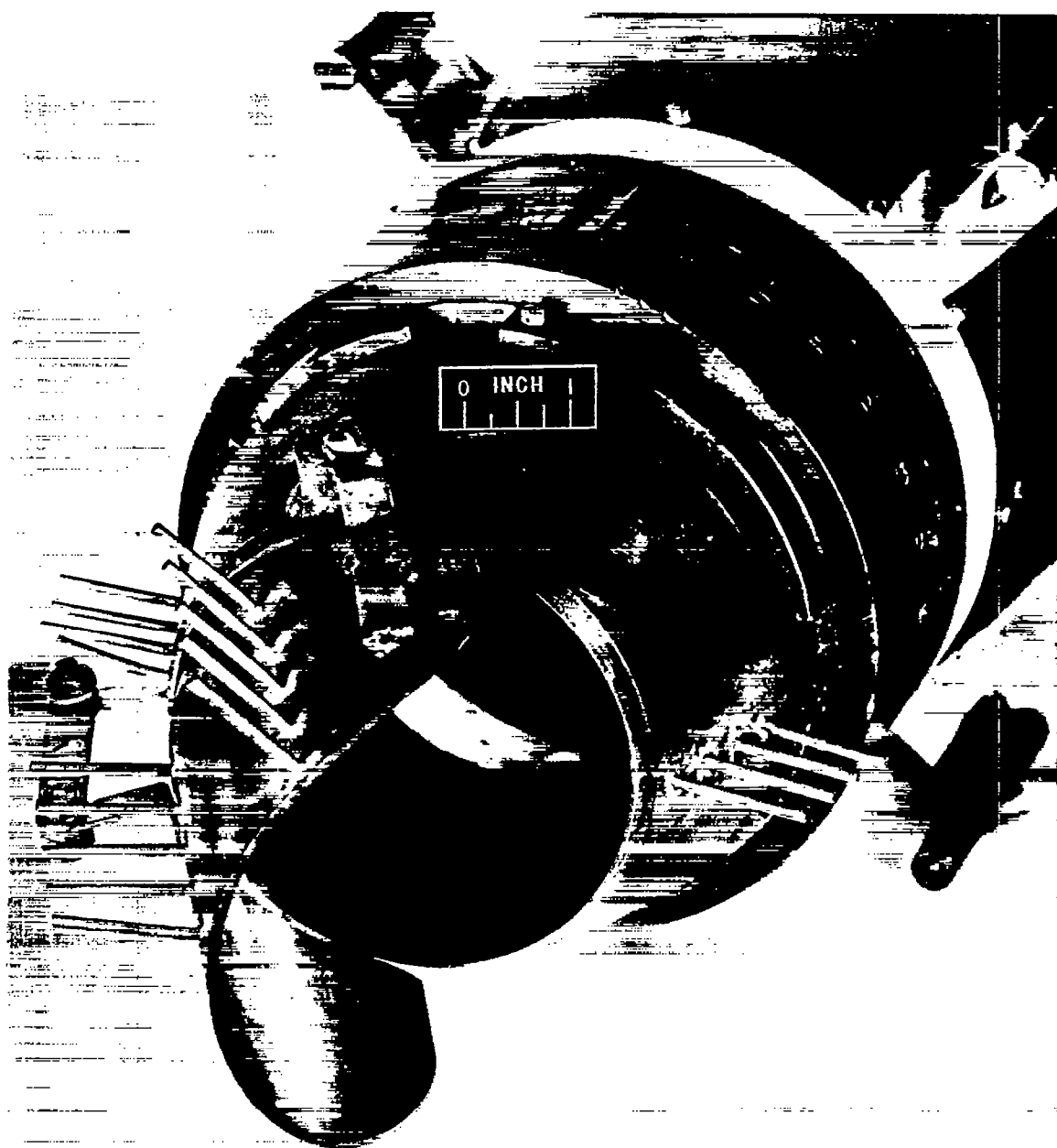
(b) Photograph of model. Both flaps actuated.

Figure 13. - Concluded. Ejector with internal pivoted flap.



(a) One large flap (configuration 5). Locking mechanism not shown. (All dimensions in inches.)

Figure 14. - Ejectors with external flap.

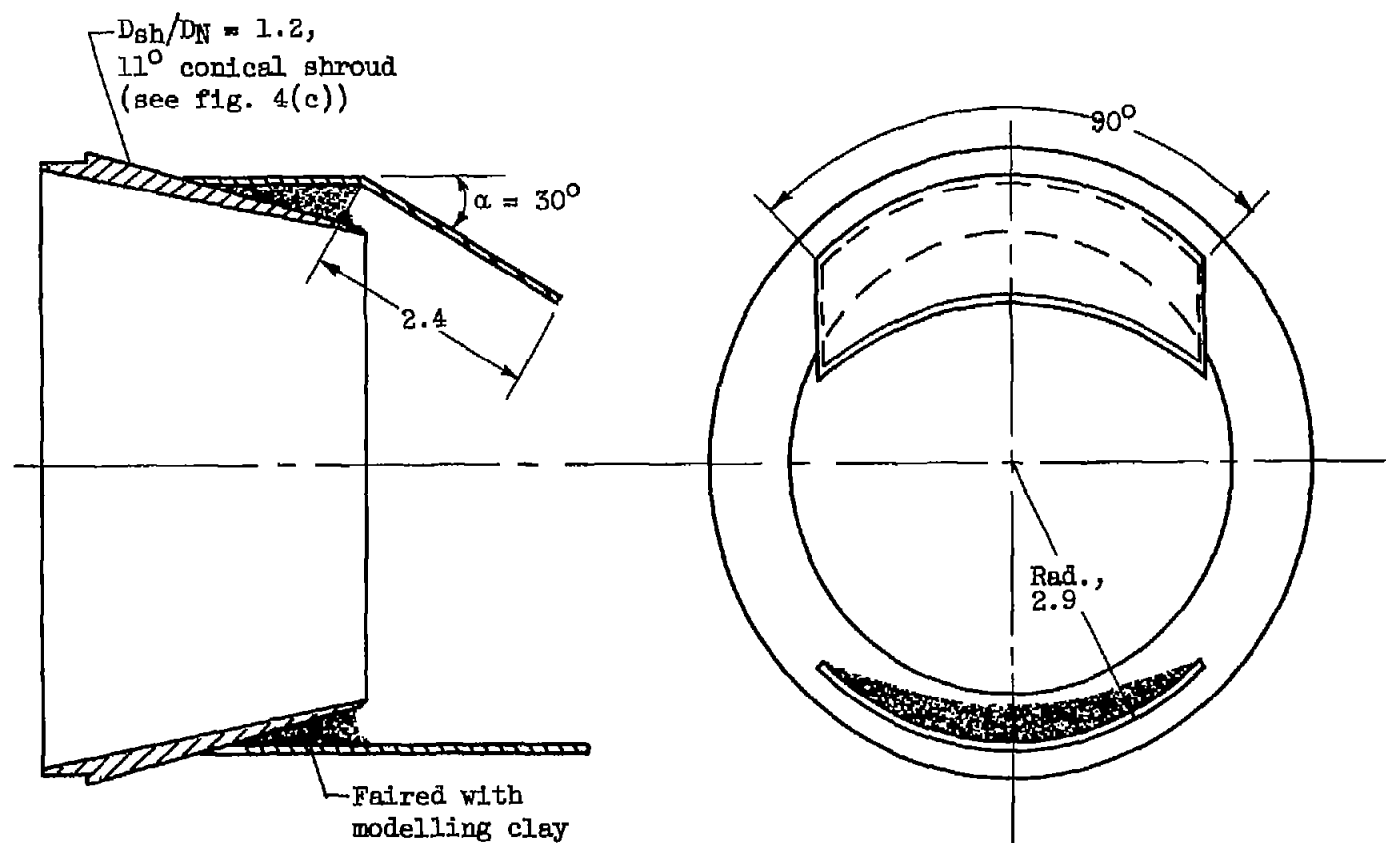


C-44762

(b) Photograph of model (configuration S).

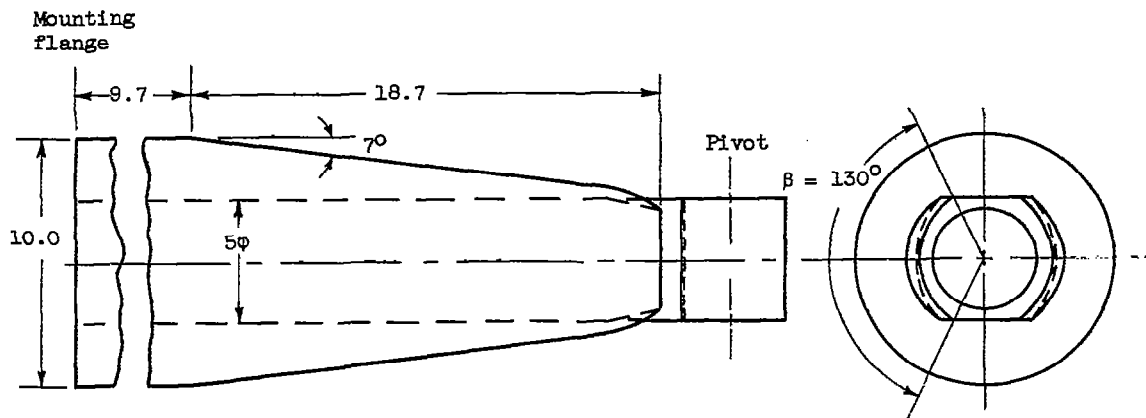
Figure 14. - Continued. Ejectors with external flap.

4677

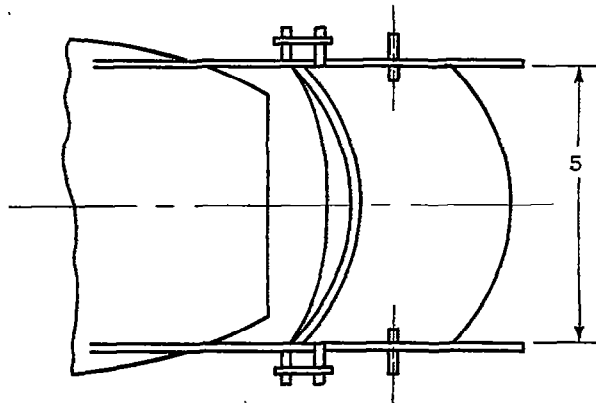


(c) Two small flaps (configuration T). (All dimensions in inches.)

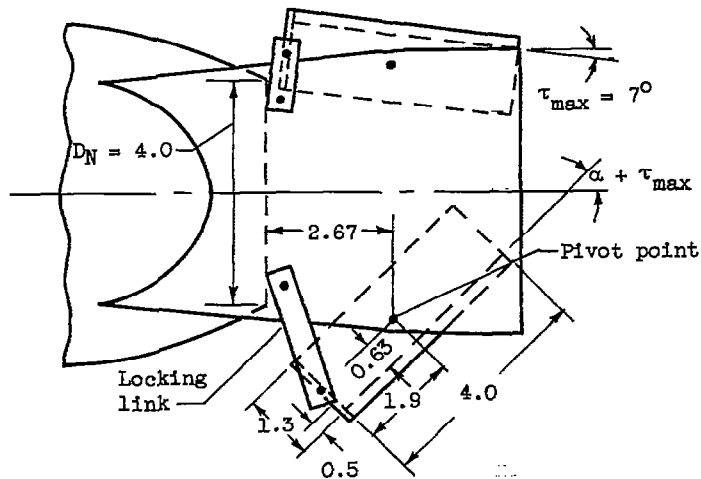
Figure 14. - Concluded. Ejectors with external flap.



(a) Side view of nozzle and fairing with reverser in stowed position.



(b) Side view of reverser with one half actuated.



(c) Top view of reverser with one half actuated. Reverser halves are made of 6" standard pipe.

Figure 15. - Modulating cylindrical target-type thrust reverser. Reverser in stowed position forms ejector. (All dimensions in inches.)



(d) Model mounted in experimental setup. One half actuated.

Figure 15. - Concluded. Modulating cylindrical target-type thrust reverser. Reverser in stowed position forms ejector. (All dimensions in inches.)

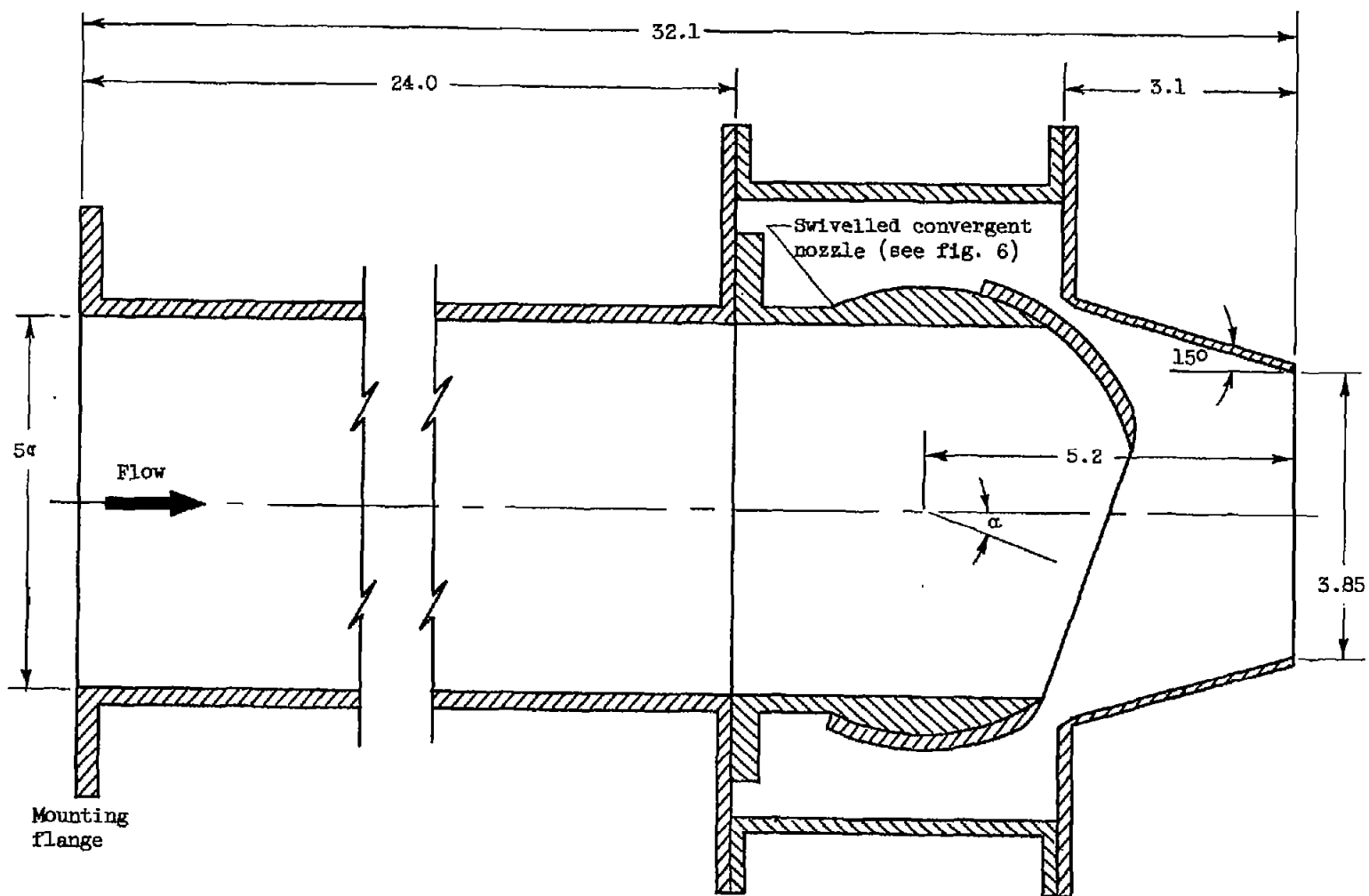
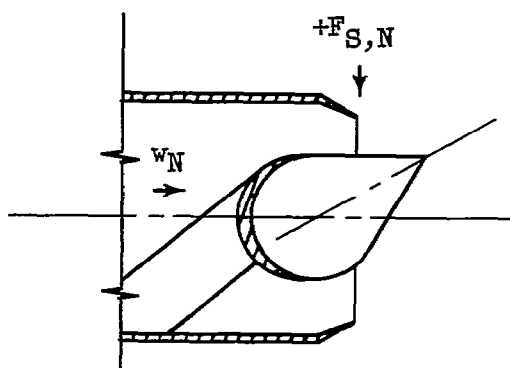
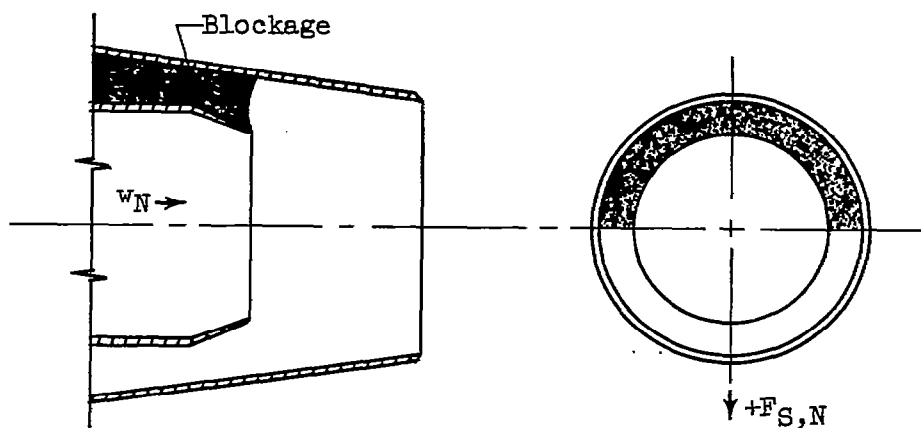


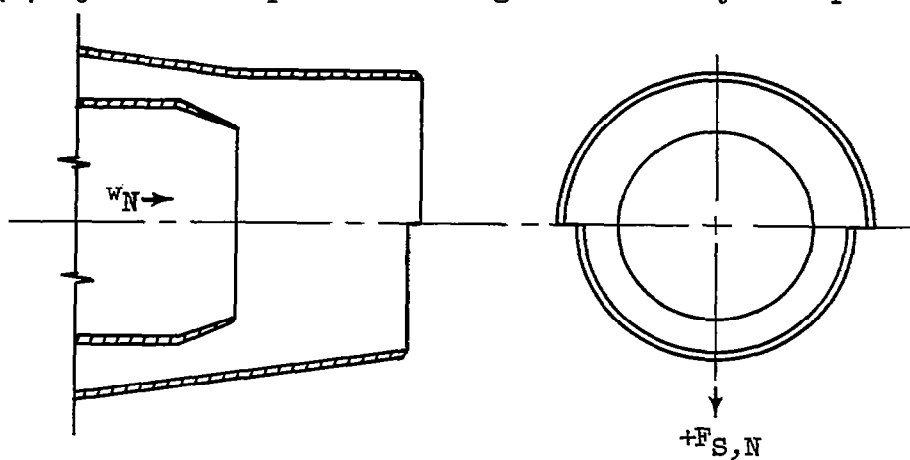
Figure 16. - Cross section of ejector with swivelled primary nozzle. (All dimensions in inches.)



(a) Plug nozzle with swivelled plug.



(b) Ejector with partial blockage in secondary flow passage.



(c) Ejector with partly opened shroud.

Figure 17. - Miscellaneous jet deflectors.

4677

CB-10 back

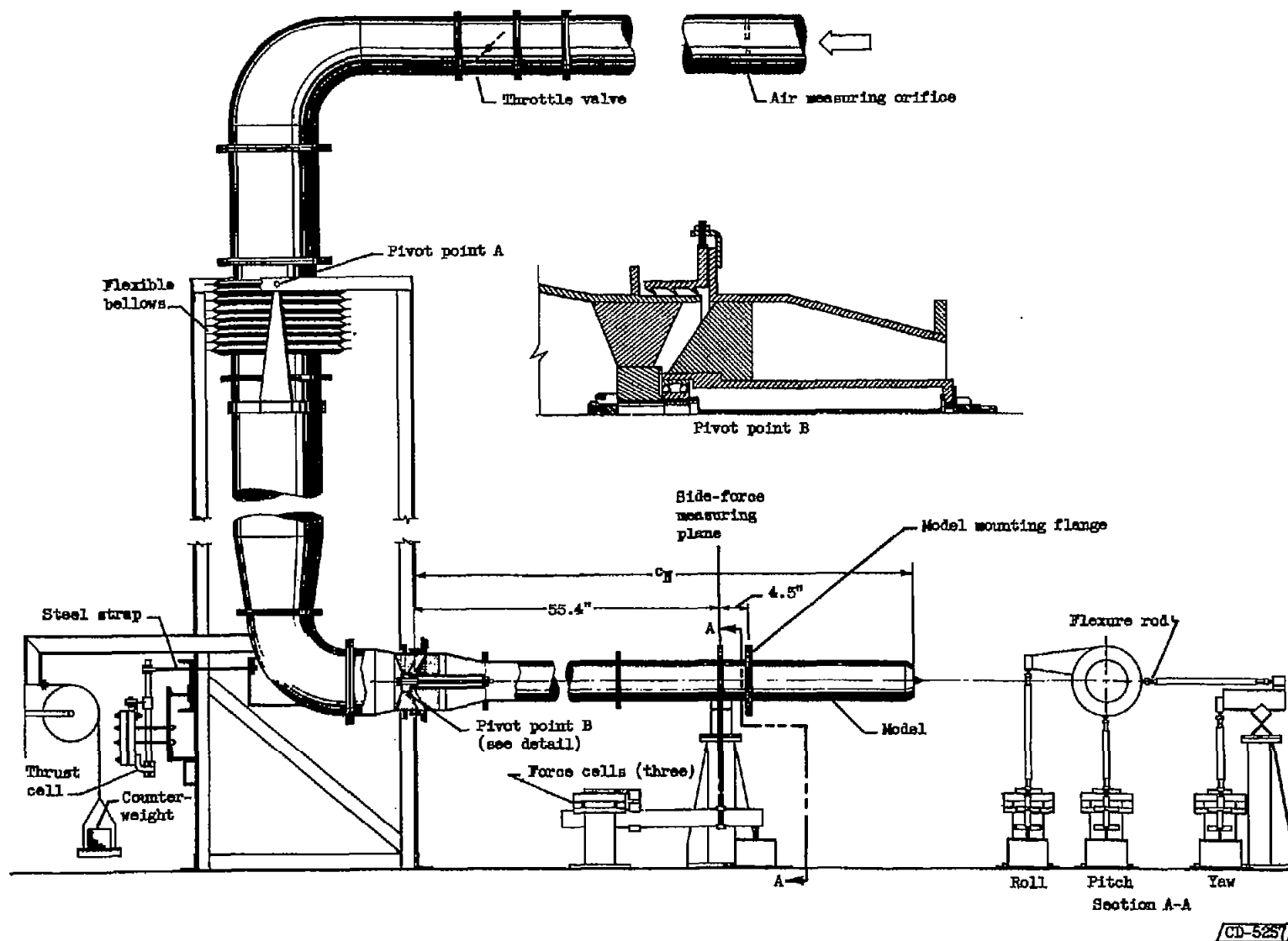


Figure 18. - Test rig used in experimental portion of jet-deflector investigation.

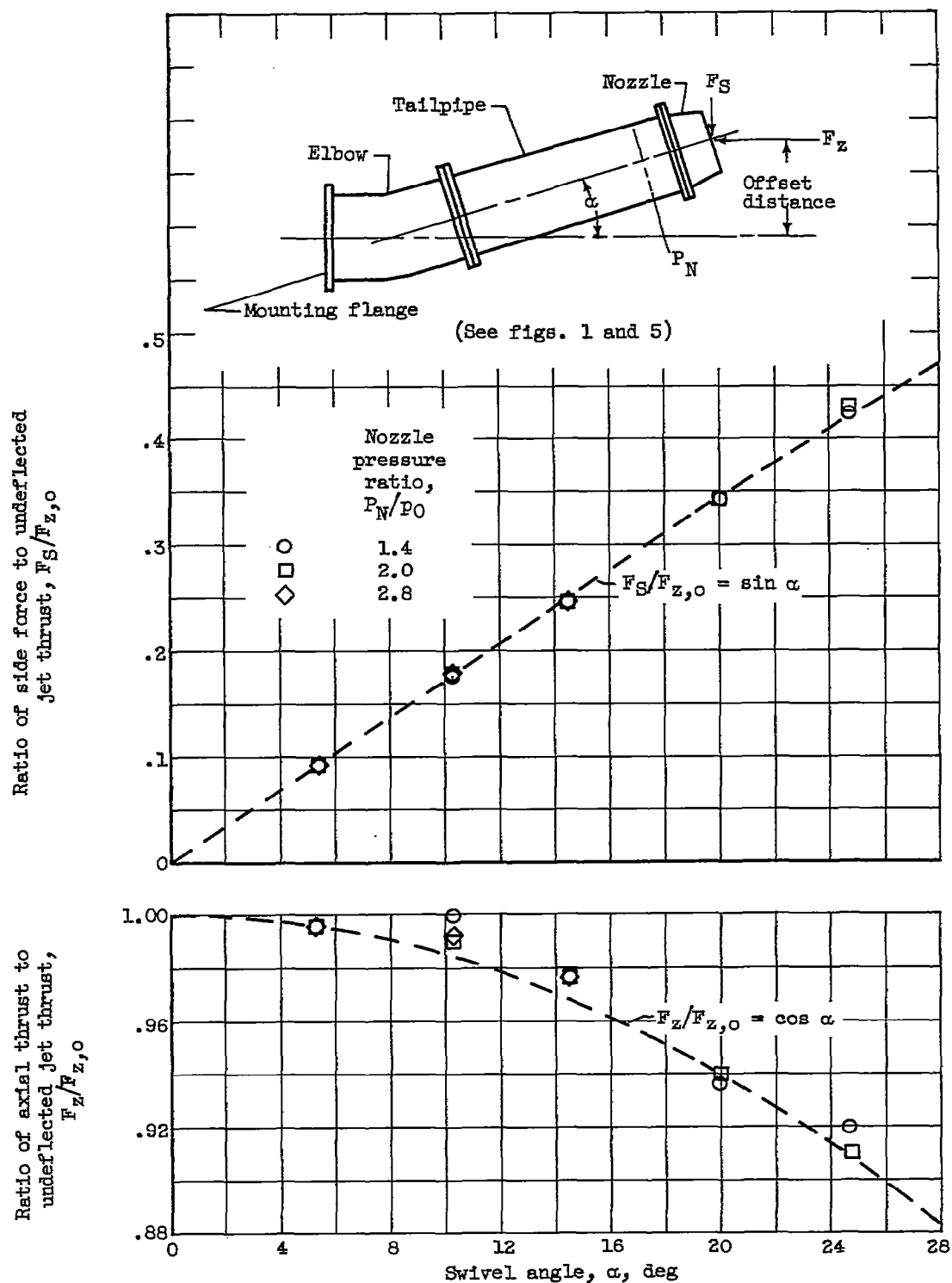


Figure 19. - Performance of swivelled-tailpipe (swivelled-engine) jet deflector having no counteracting moment.

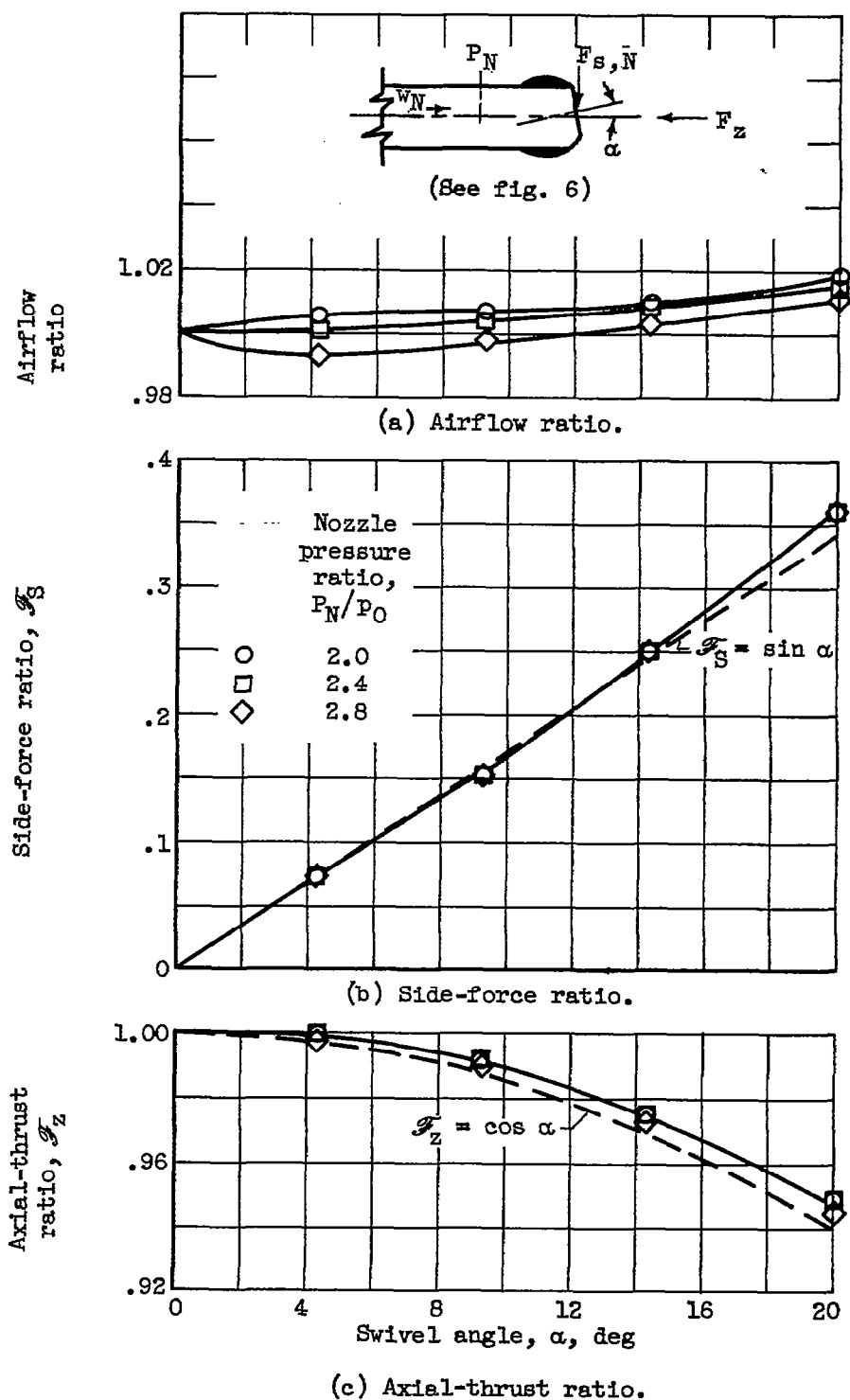


Figure 20. - Performance of swivelled convergent nozzle.

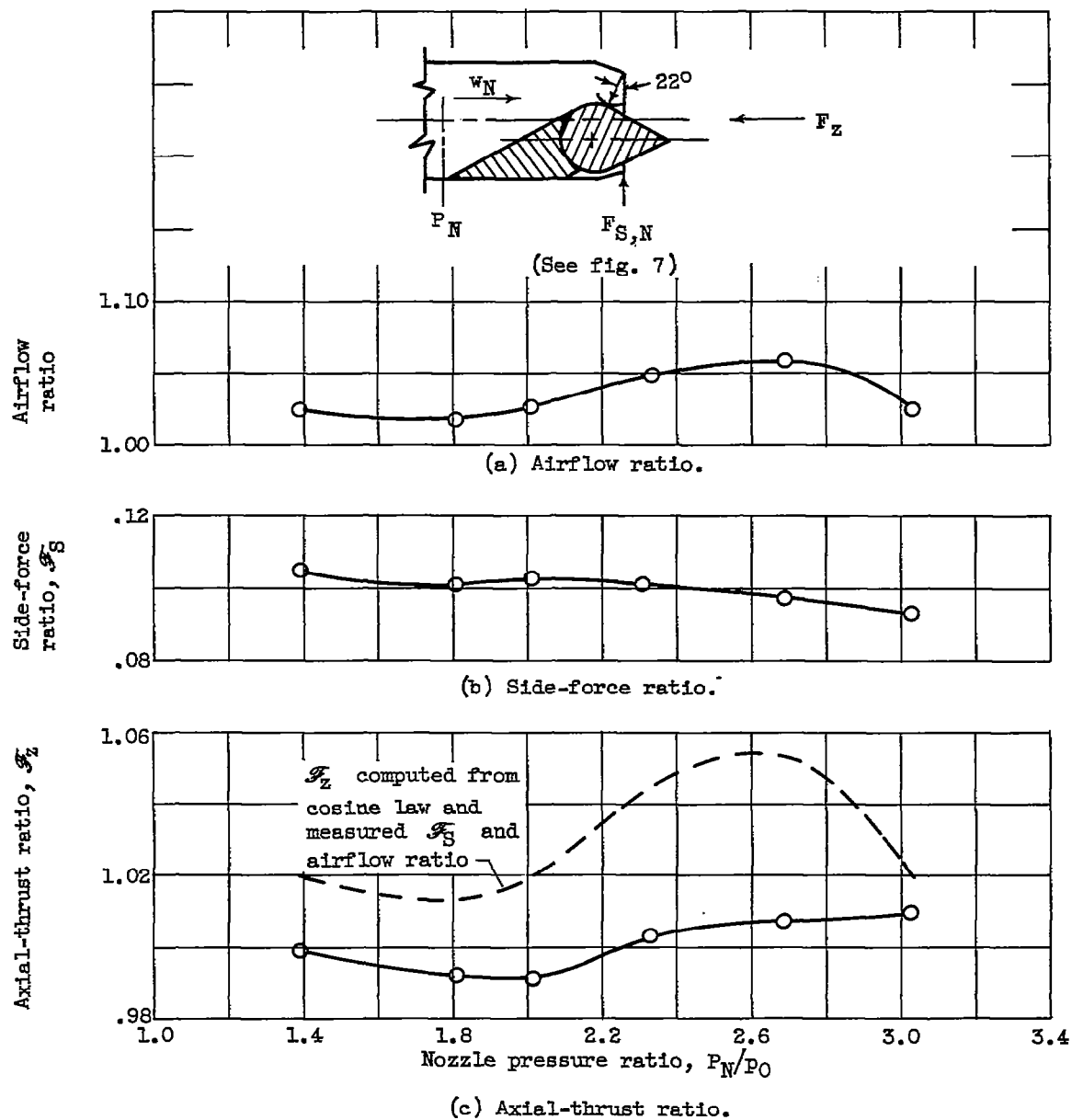


Figure 21. - Performance of plug nozzle with plug at tailpipe wall.

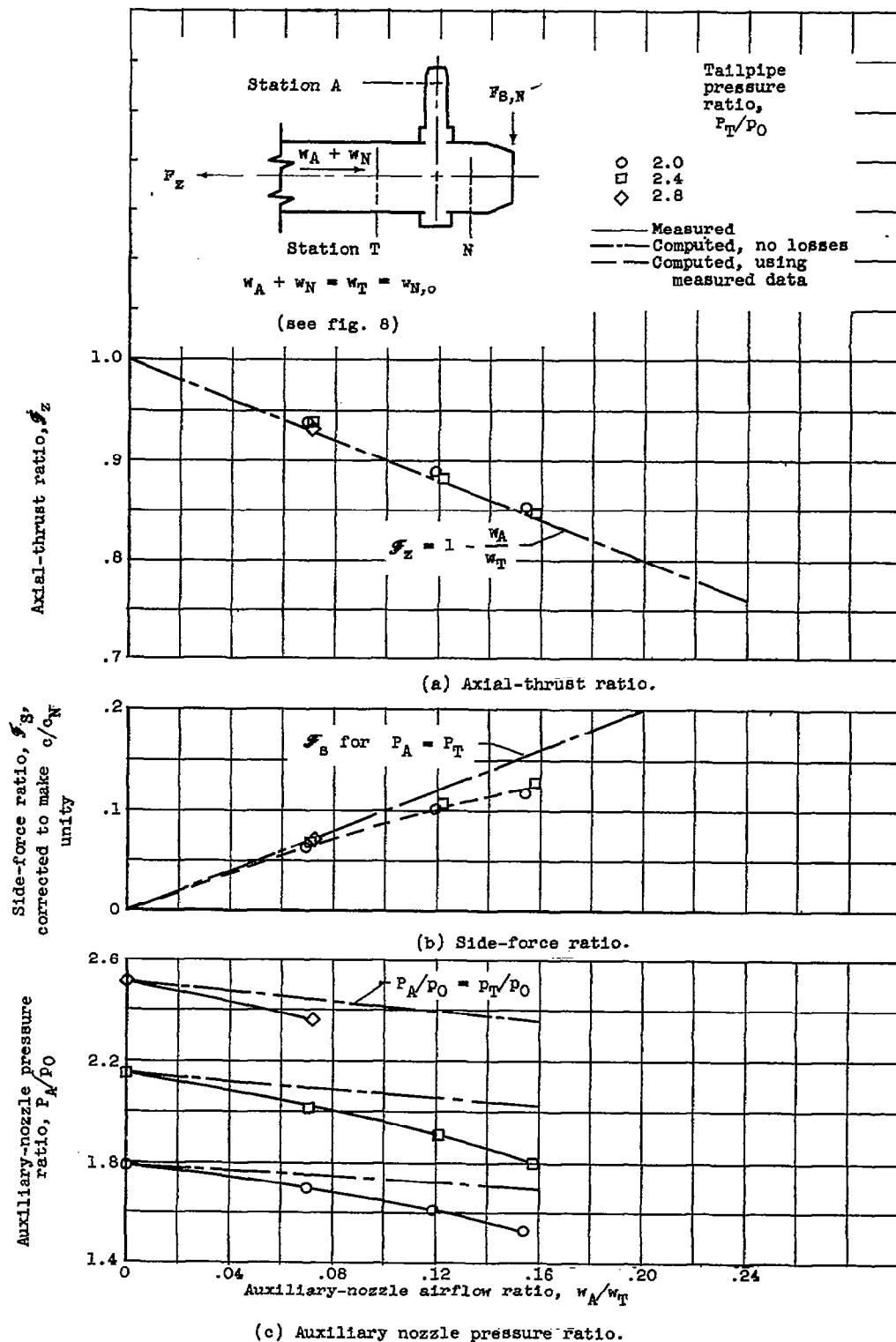


Figure 22. - Performance of tailpipe with bleed nozzle.

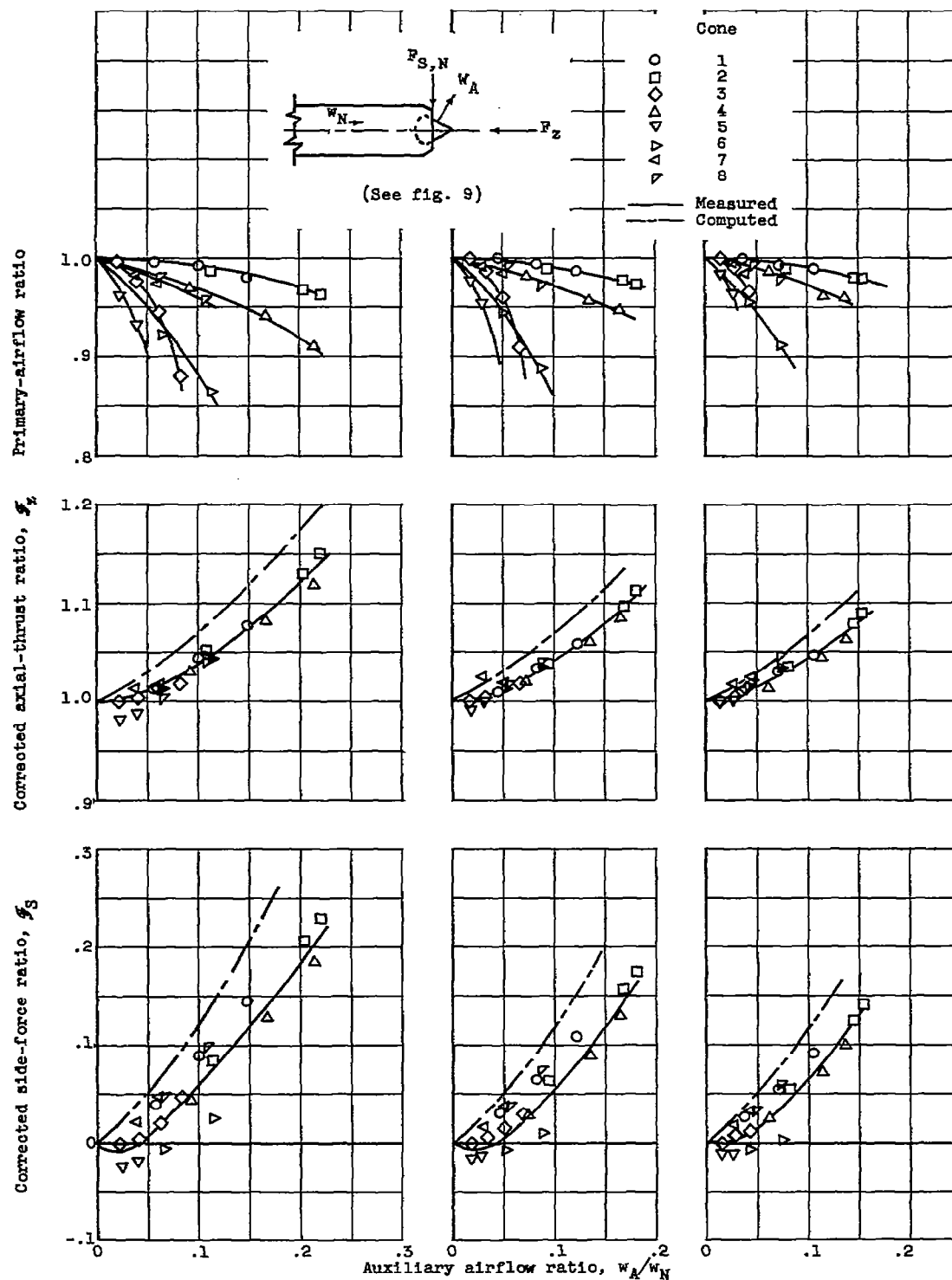


Figure 23. - Performance of plug nozzle with auxiliary jet from plug.

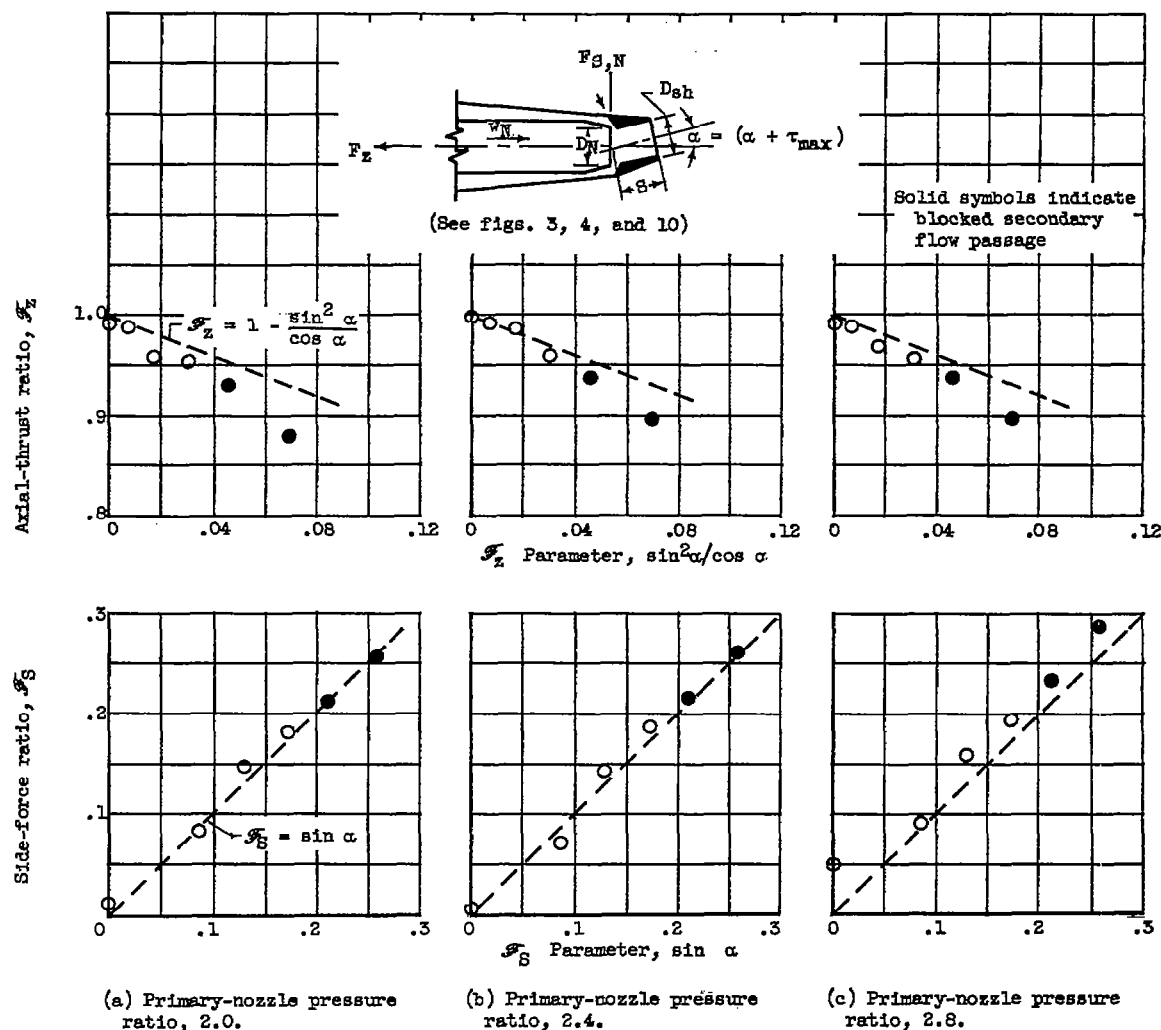
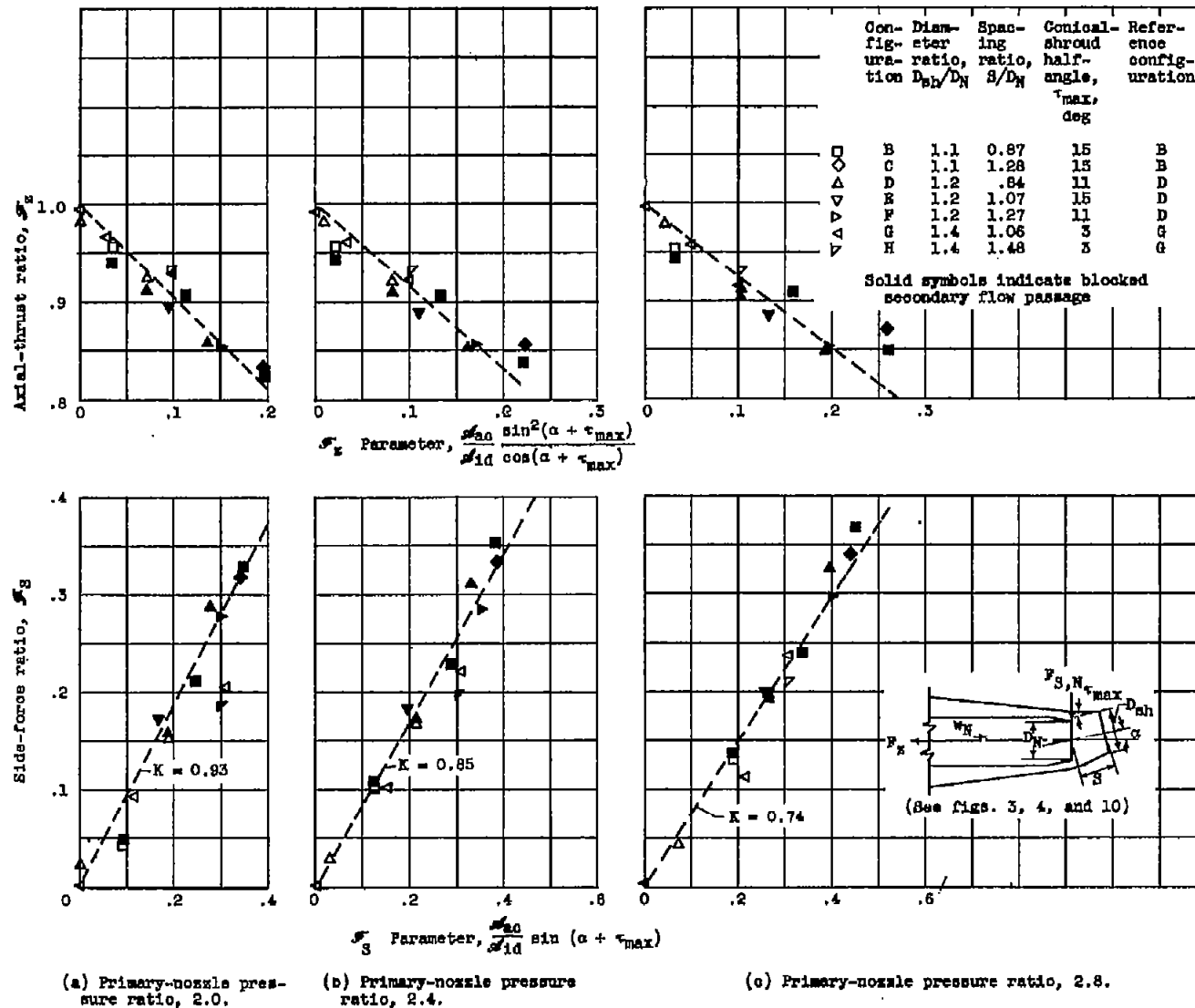


Figure 24. - Performance of swivelled-ejector-shroud jet deflector (configuration A). Ejector: diameter ratio, D_{sh}/D_N , 1.1; spacing ratio, S/D_N , 0.86; cylindrical shroud. For all data in this figure $\mathcal{M}_{ac}/\mathcal{M}_{id} > 3.0$.



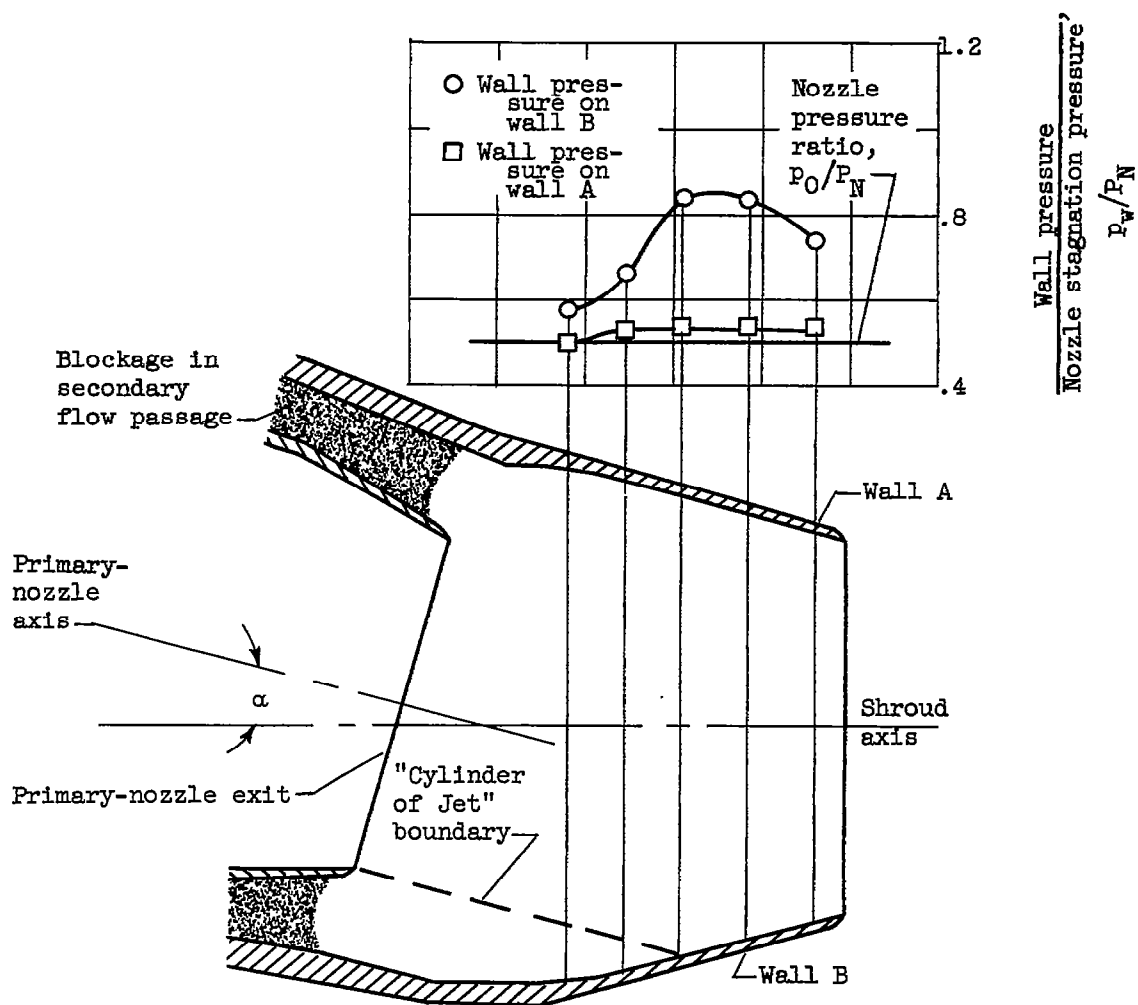


Figure 26. - Wall pressure distribution on shroud in plane through axis. Swivelled-ejector-shroud jet deflector; swivel angle, α , 15° ; primary-nozzle pressure ratio, 2.0; ejector: diameter ratio, D_{sh}/D_N , 1.1; spacing ratio, S/D_N , 1.28; 15° conical shroud.

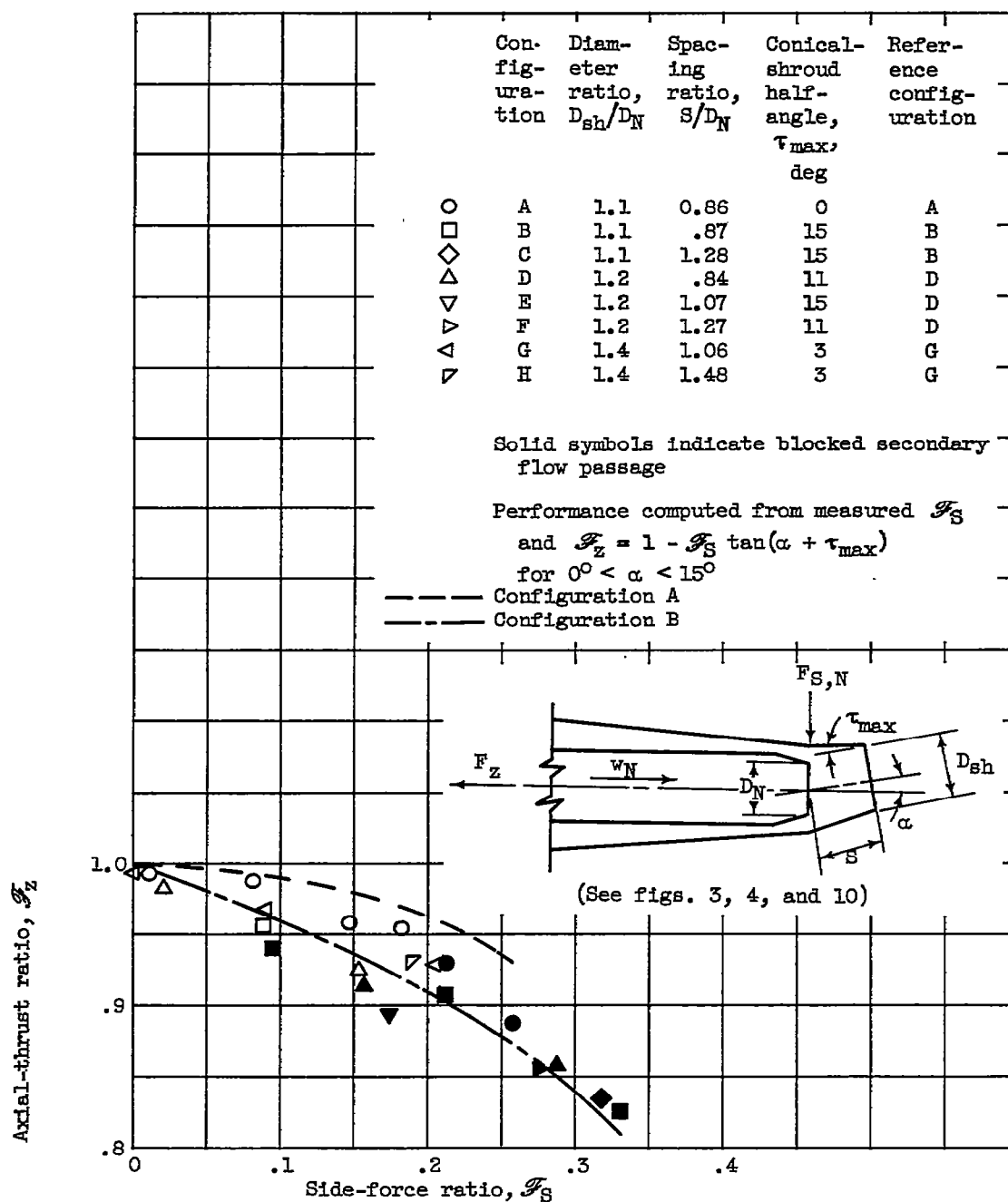


Figure 27. - Variation in axial-thrust ratio with side-force ratio for swivelled-ejector-shroud jet deflectors. Primary-nozzle pressure ratio, 2.0.

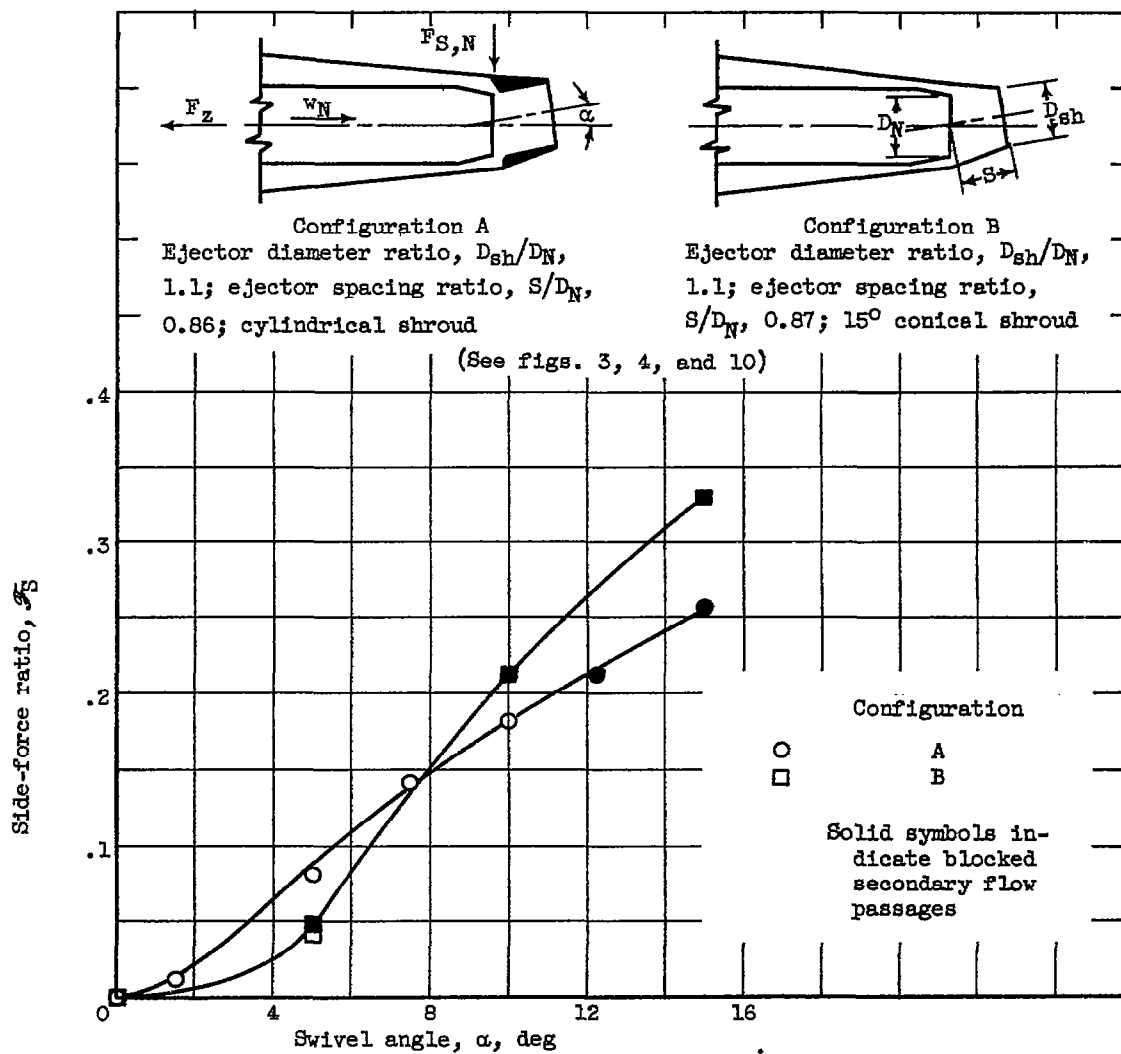


Figure 28. - Variation in side-force ratio with swivel angle for two swivelled-ejector-shroud jet deflectors. Primary-nozzle pressure ratio, 2.0.

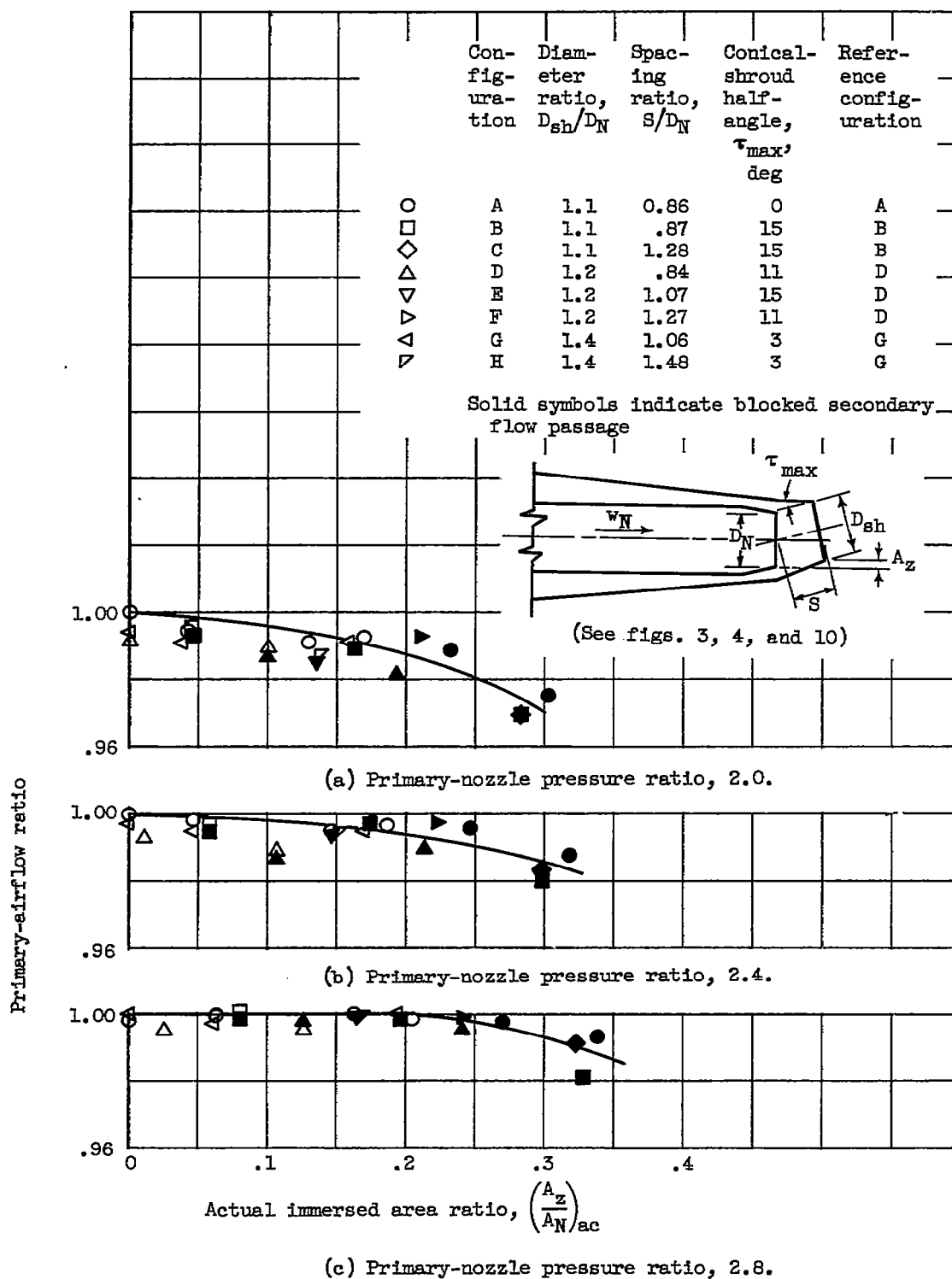


Figure 29. - Variation in primary-airflow ratio with immersed area for swivelled-ejector-shroud jet deflectors.

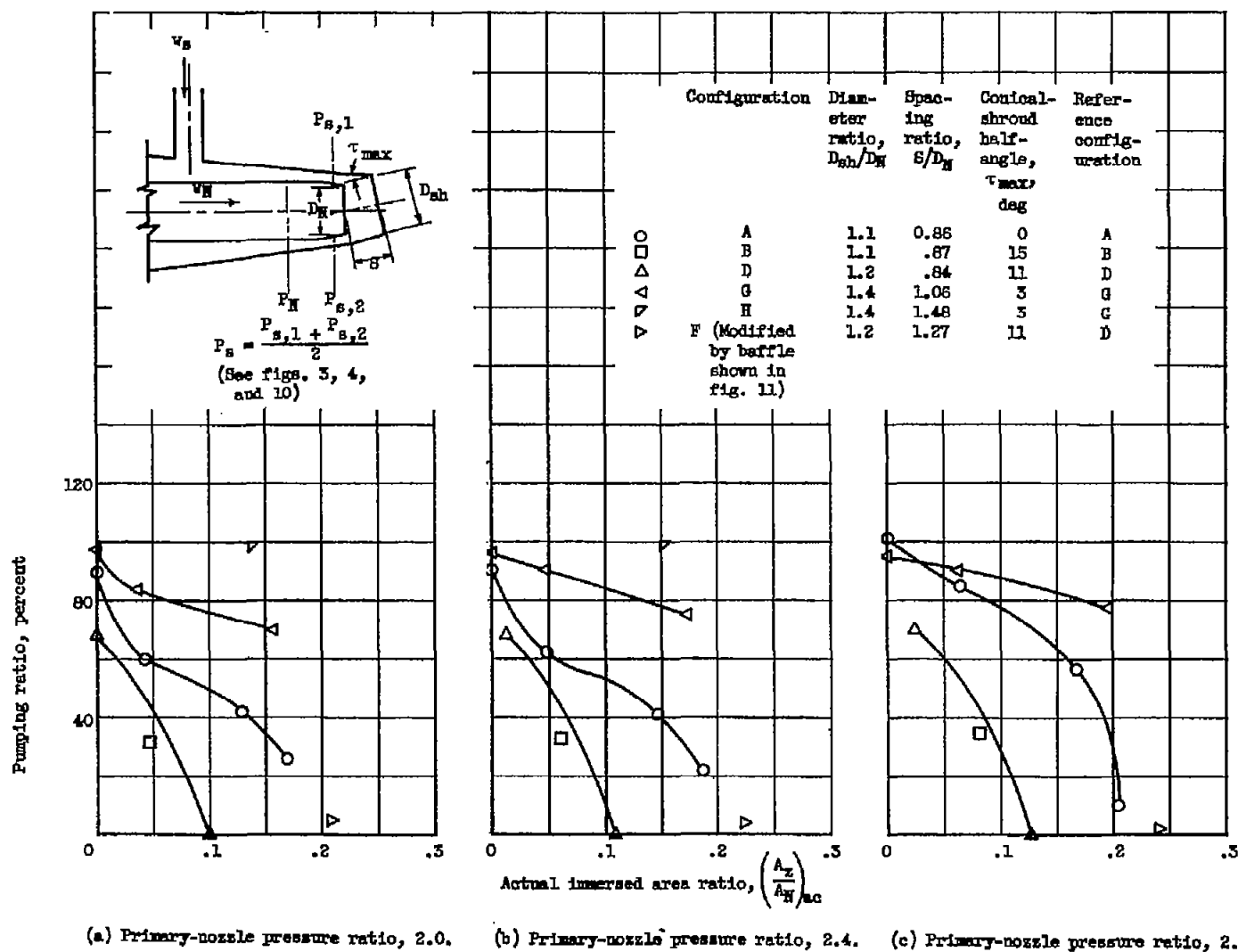
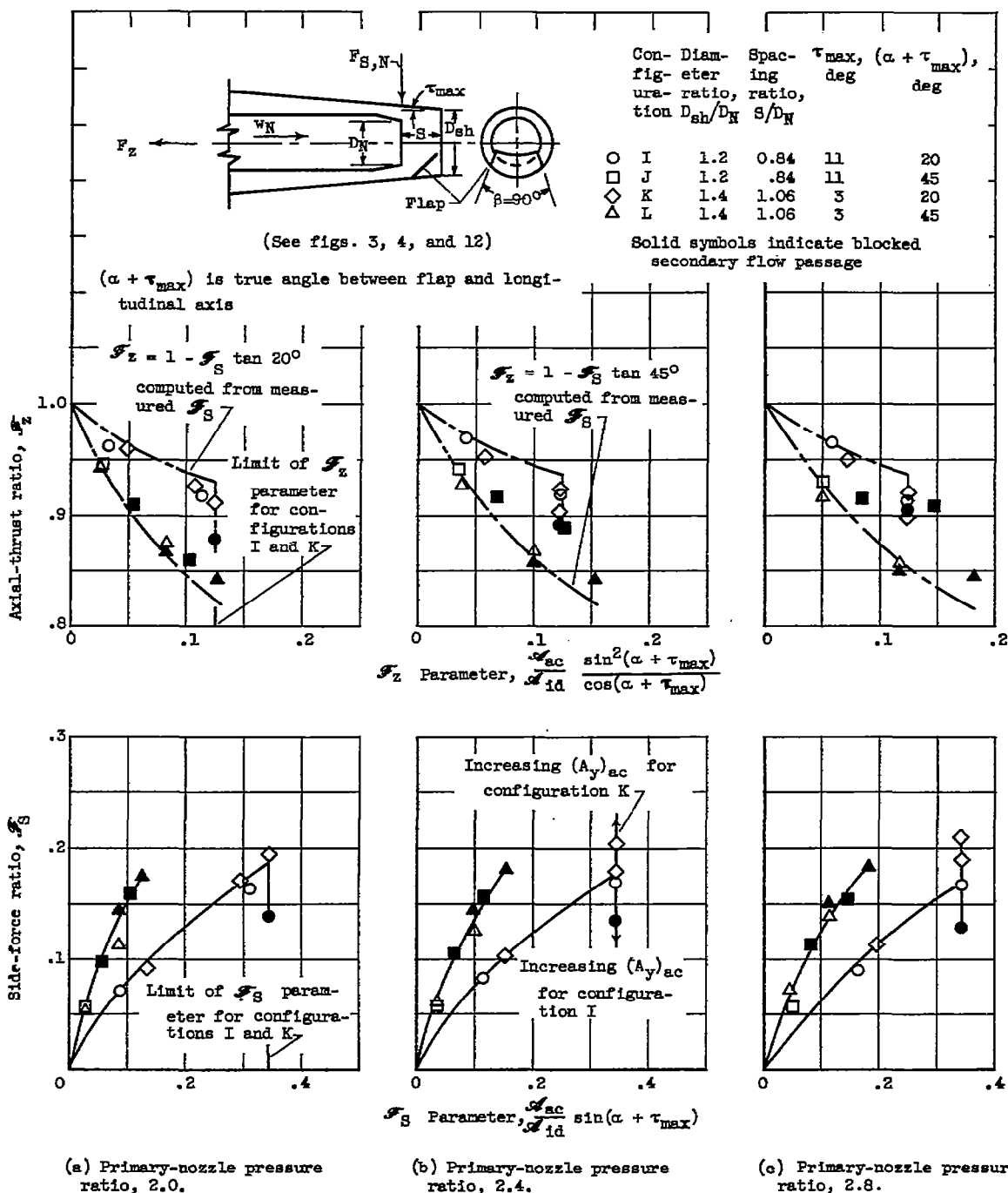
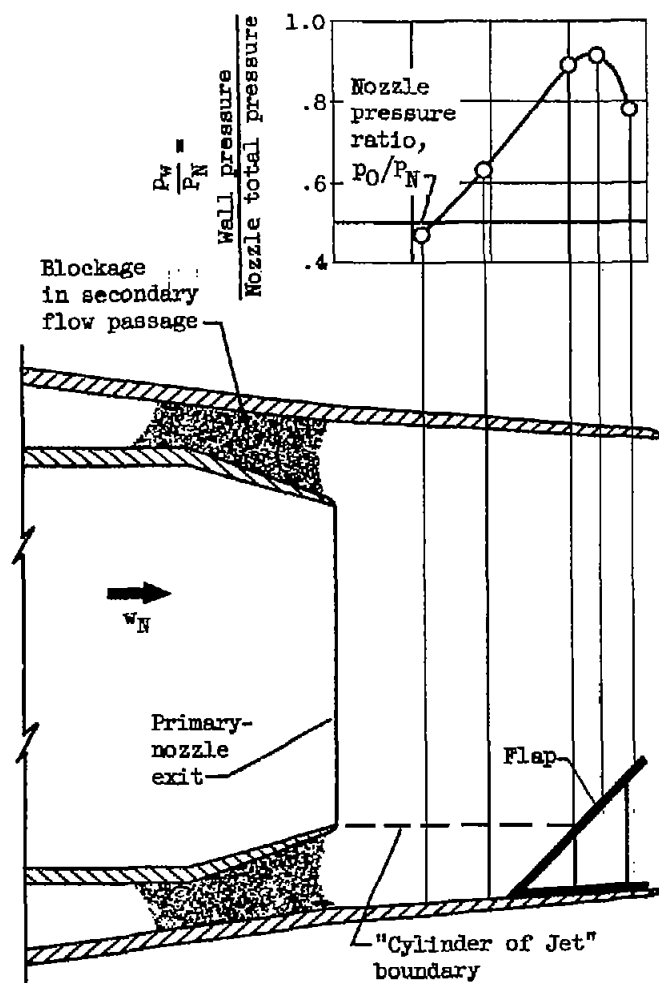
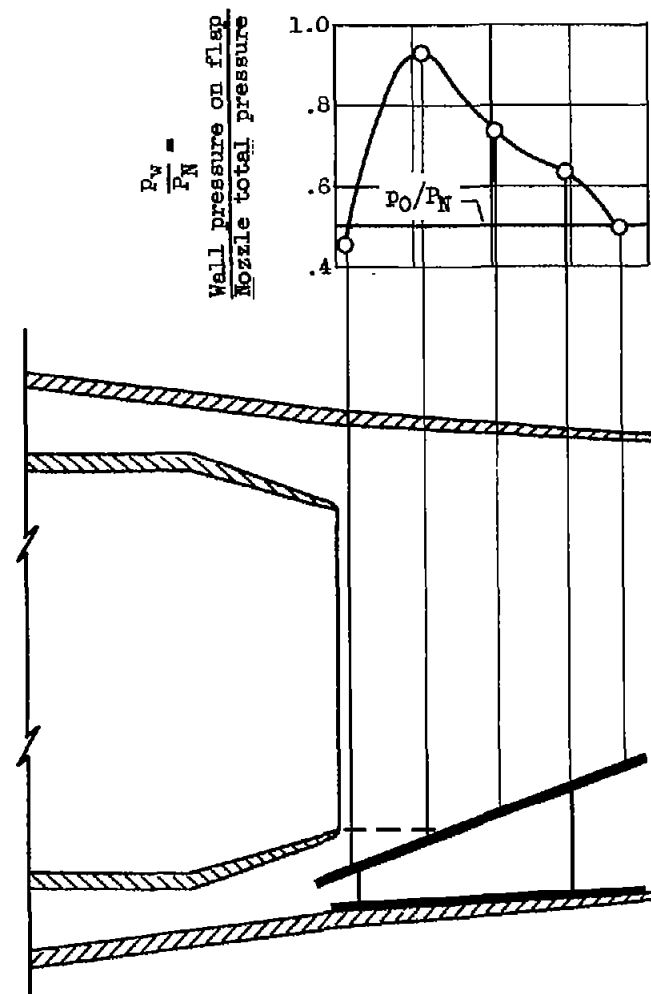


Figure 30. - Pumping characteristics of swivelled-ejector-shroud jet deflectors. Unheated primary airflow; ambient air secondary flow; secondary pressure ratio, P_s/P_0 , about 0.985.

Figure 31. - Performance of ejector with internal-flap jet deflectors. Fixed 20° and 45° flaps.



(a) $\alpha + \tau_{\max} = 45^\circ$.



(b) $\alpha + \tau_{\max} = 20^\circ$.

Figure 32. - Wall pressure distribution on flap and shroud in plane through longitudinal axis. Primary-nozzle pressure ratio, 2.0; ejector: diameter ratio, D_{sh}/D_N , 1.4; spacing ratio, S/D_N , 1.06; 3° conical shroud.

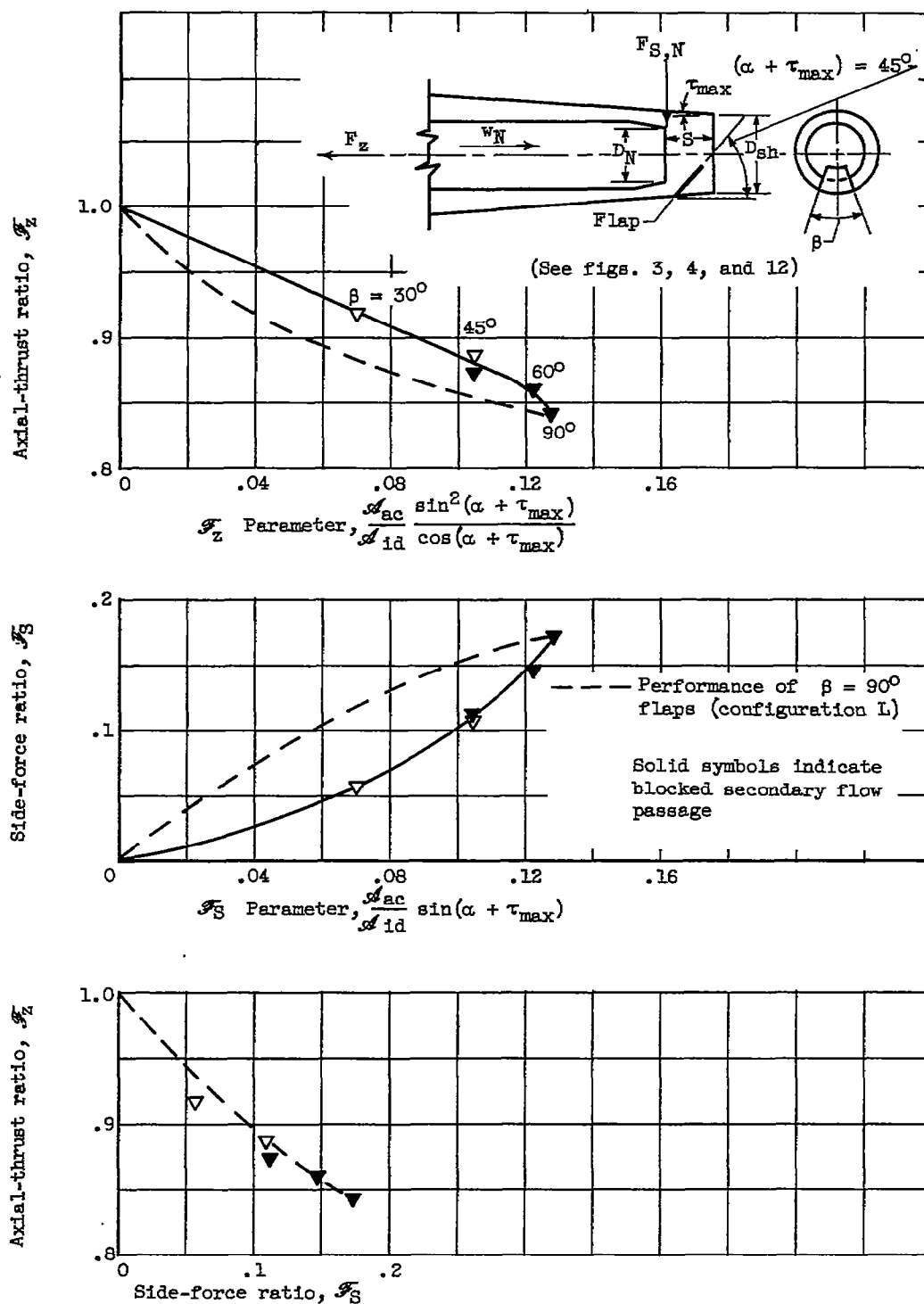


Figure 33. - Effect of reducing flap chord in configurations M. Primary-nozzle pressure ratio, 2.0; ejector: diameter ratio, D_{sh}/D_N , 1.4; spacing ratio, S/D_N , 1.06.

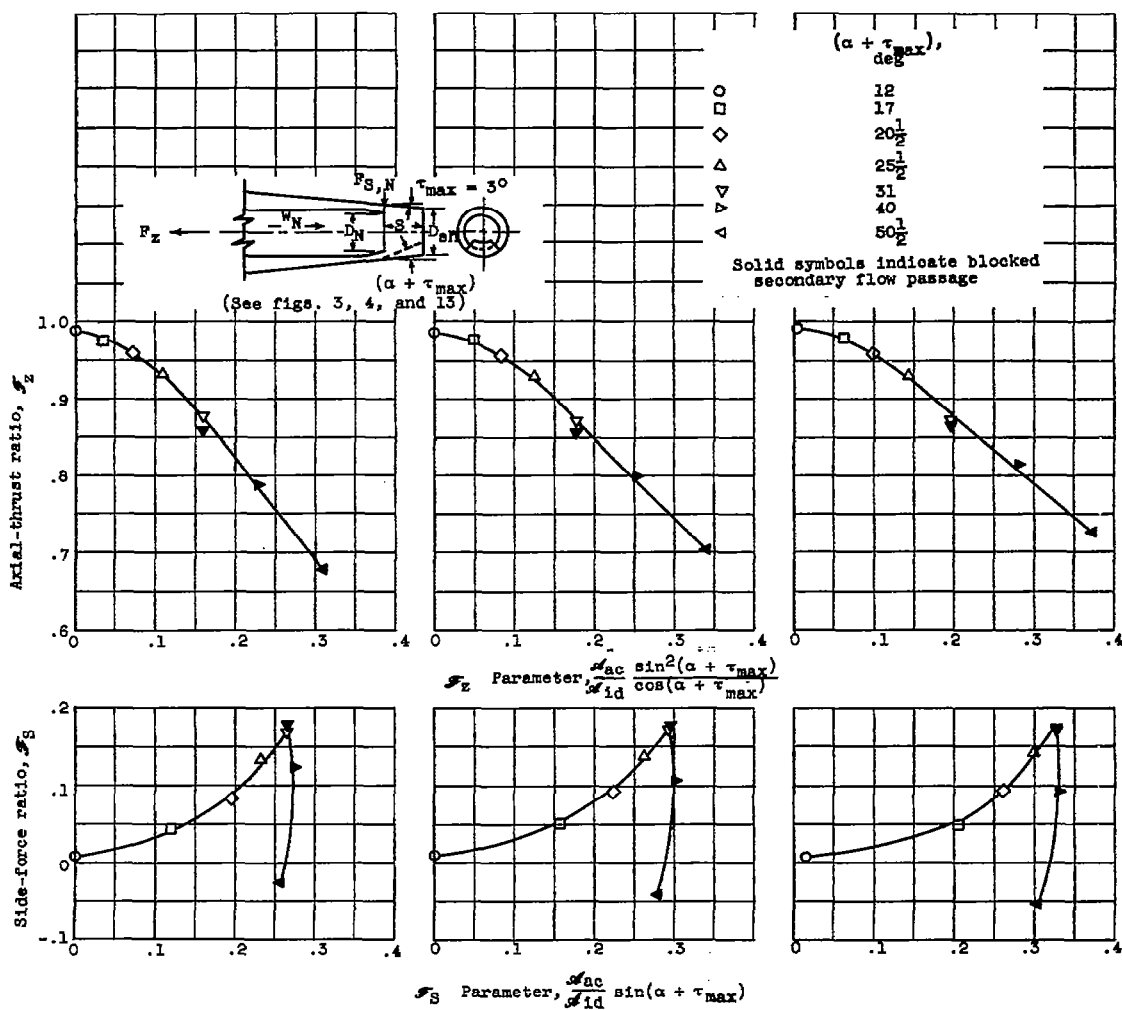


Figure 35. - Performance of ejector having pivoted internal flaps with two flaps actuated (configurations O). Ejector: diameter ratio, D_{sh}/D_N , 1.4; spacing ratio, S/D_N , 1.06.

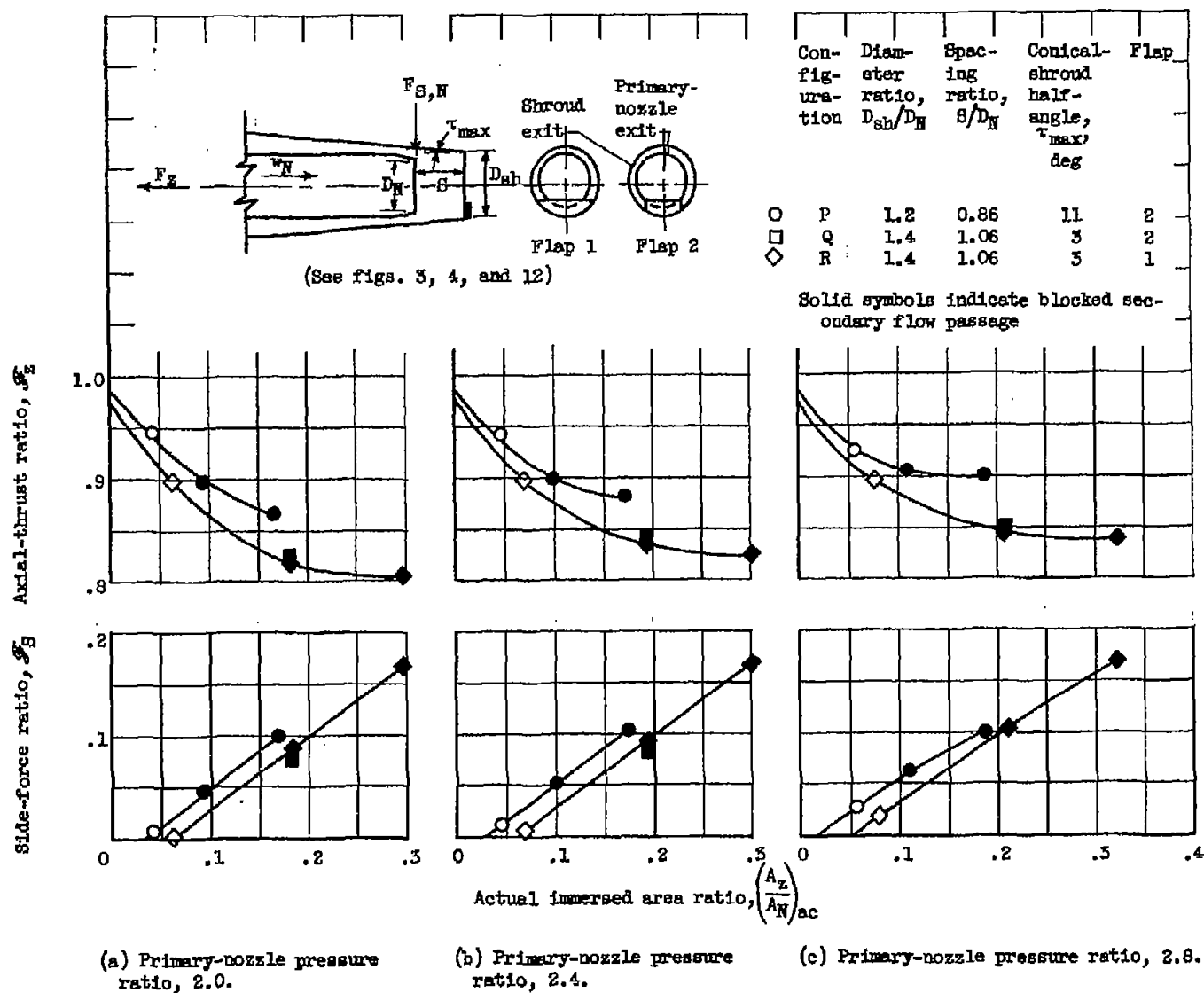


Figure 36. - Performance of ejector with flap normal to longitudinal axis at shroud exit.

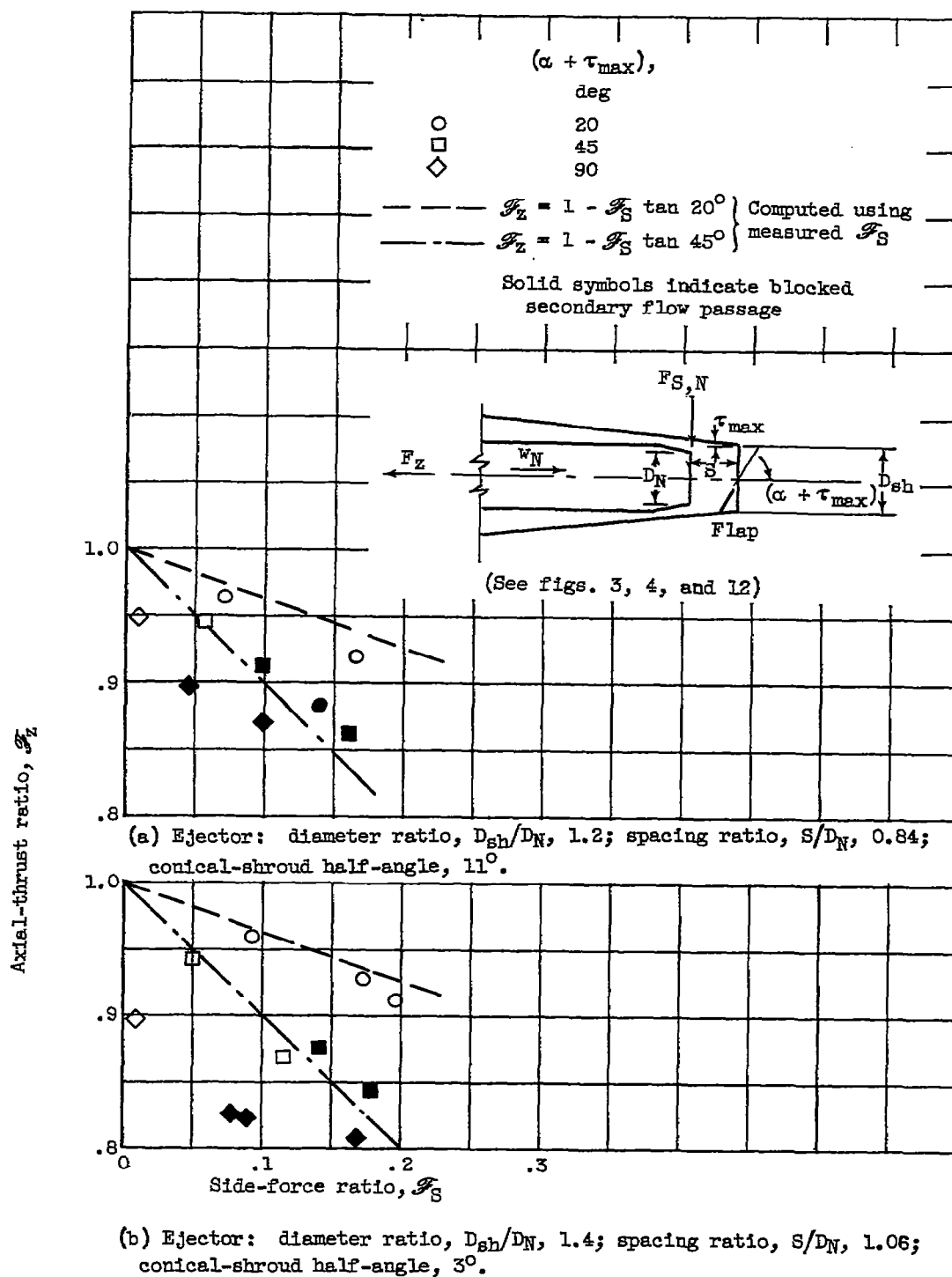


Figure 37. - Variation in axial-thrust ratio with side-force ratio for ejector with internal-flap jet deflectors. Fixed flaps; flap chord angle, β , 90° ; primary-nozzle pressure ratio, 2.0.

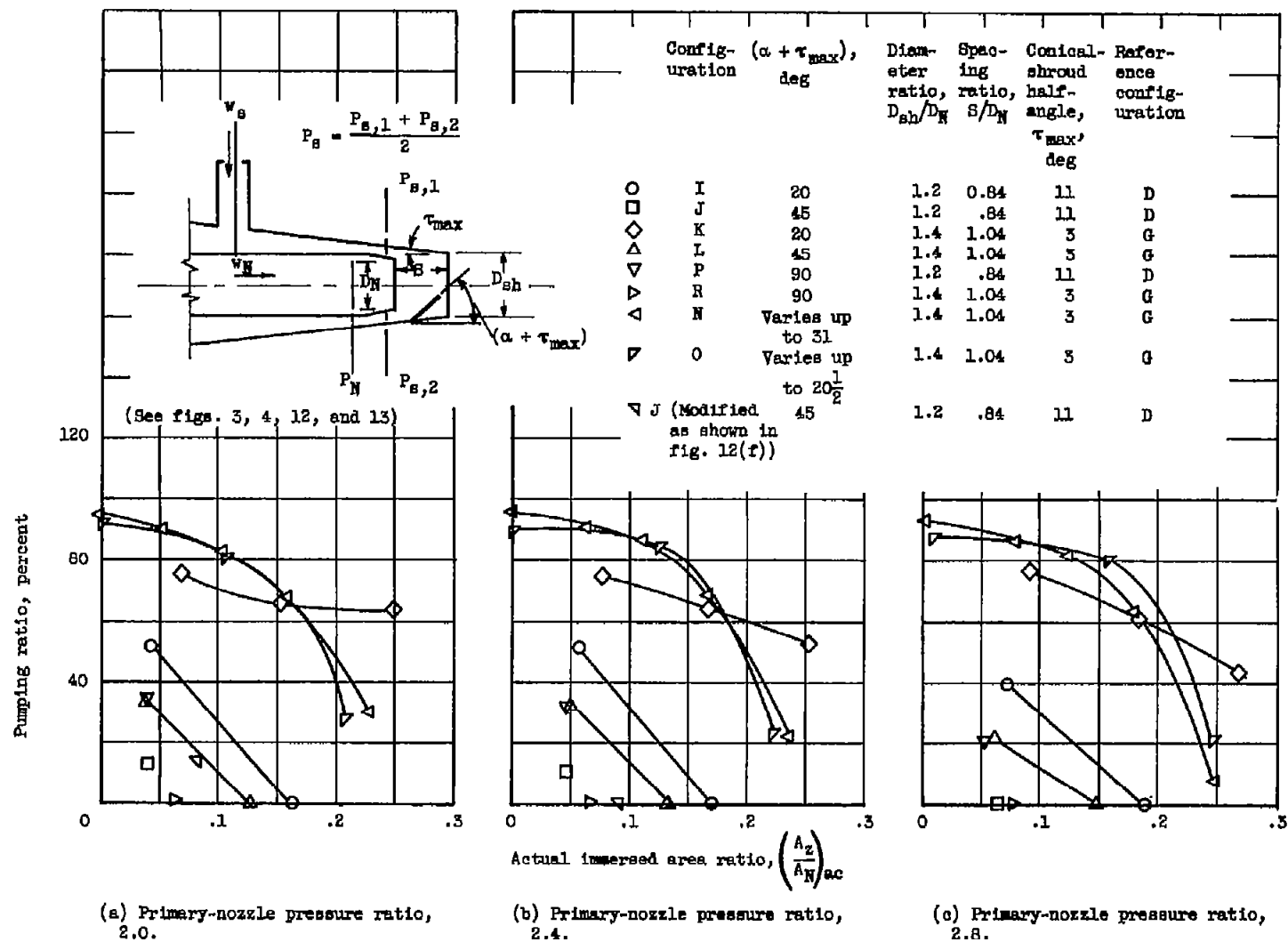
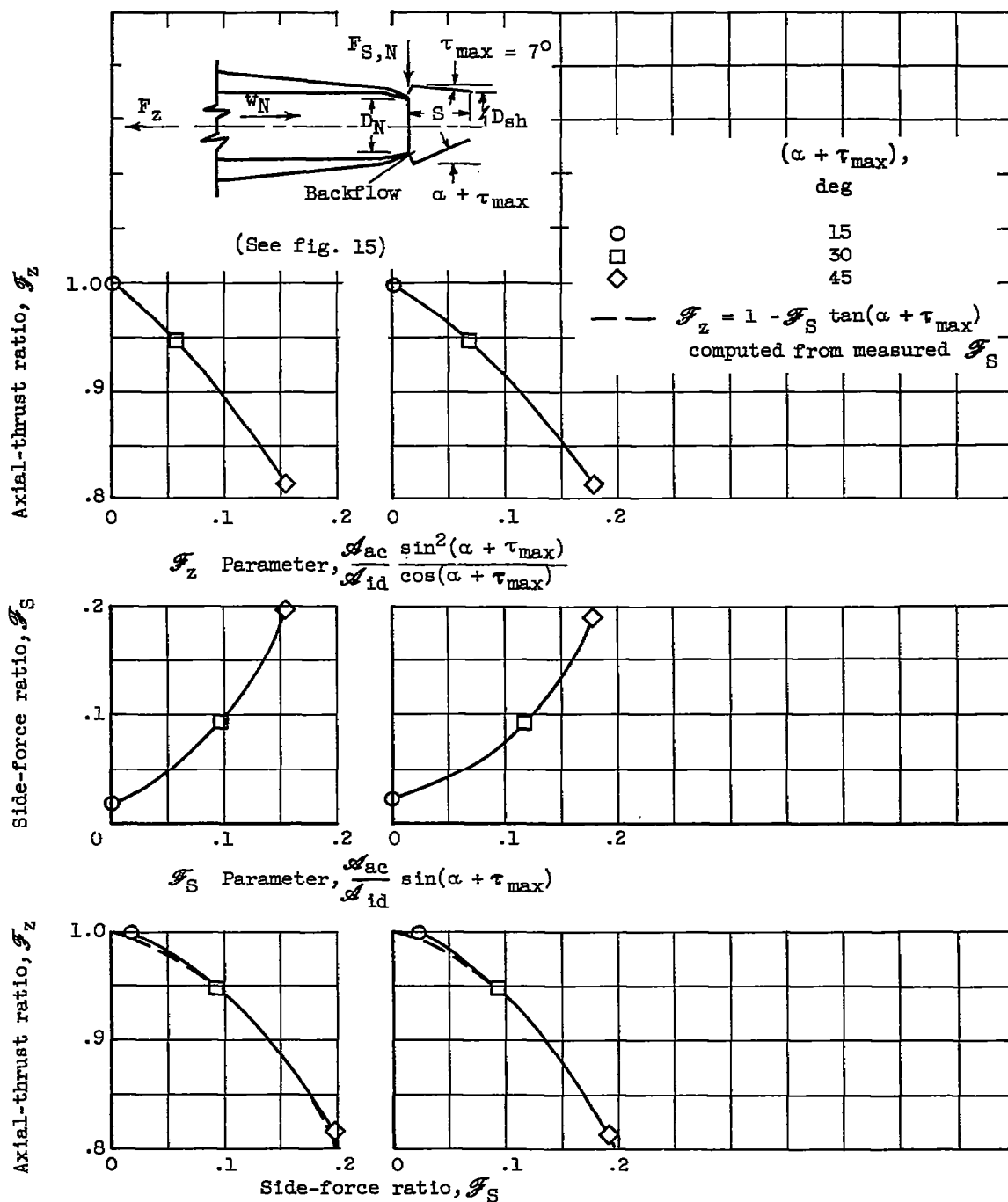


Figure 39. - Pumping characteristics for ejector with internal-flap jet deflectors. Unheated primary airflow, ambient-air secondary flow. Secondary pressure ratio, P_g/p_0 , about 0.985.



(a) Primary-nozzle
pressure ratio,
2.0.

(b) Primary-nozzle pressure ratio, 2.4.

Figure 41. - Jet deflector performance of cylindrical target-type thrust reverser (configuration U).

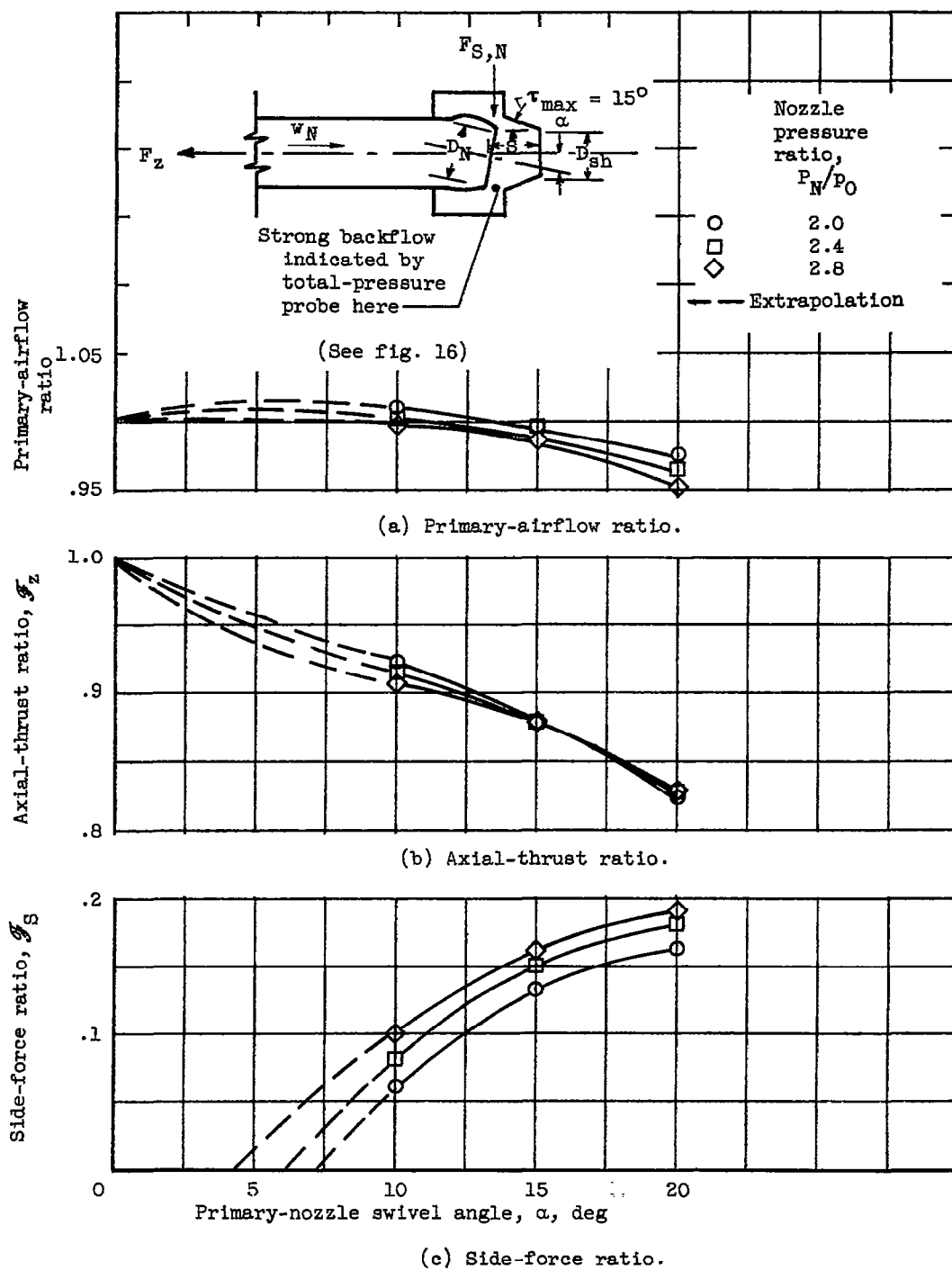
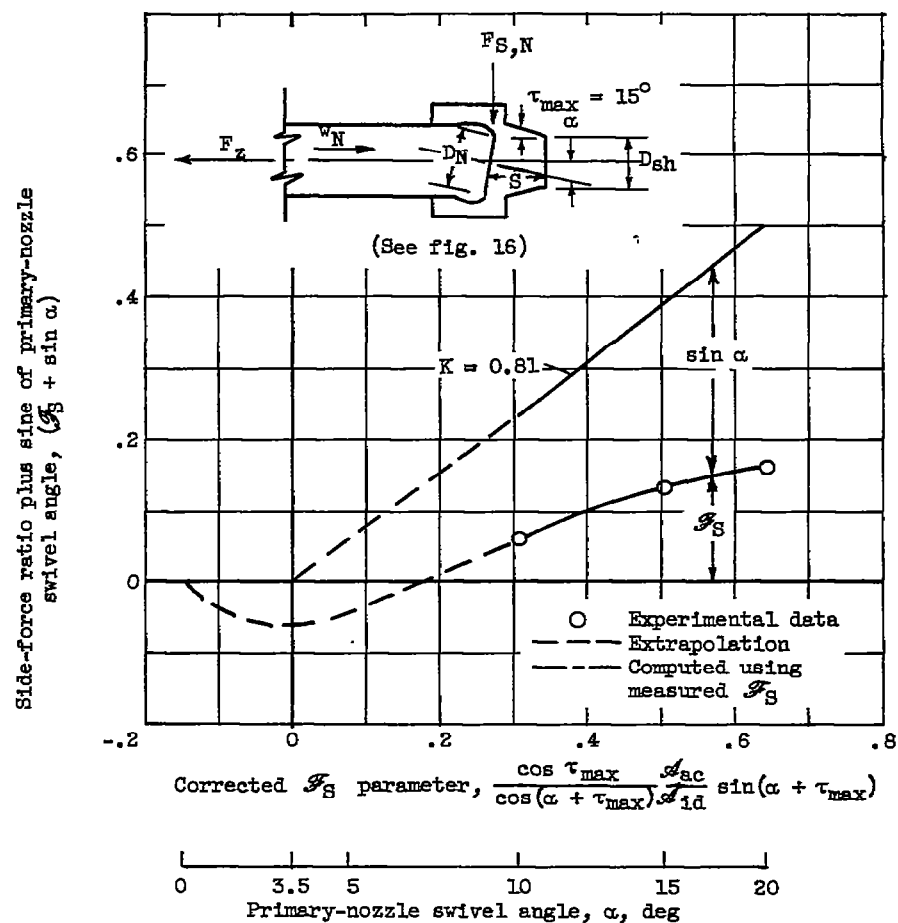
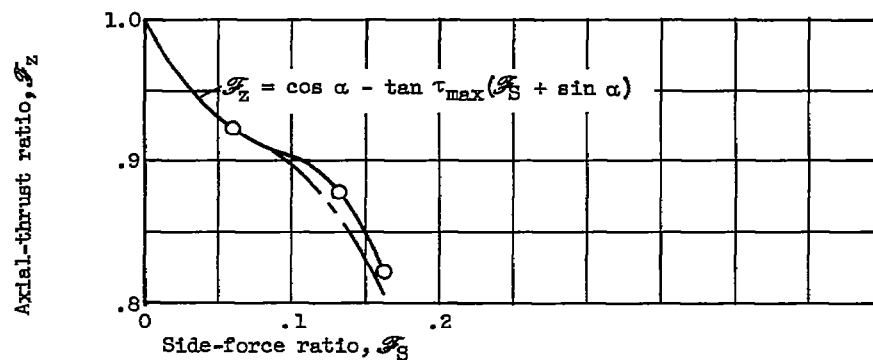


Figure 42. - Performance of ejector with swivelled-primary-nozzle jet deflector. Zero secondary flow; ejector: diameter ratio, D_{sh}/D_N , 1.1; spacing ratio, S/D_N , 0.78.



(a) Side-force ratio.



(b) Variation of axial-thrust ratio with side-force ratio.

Figure 43. - Comparison of computed and measured performance for ejector with swivelled primary nozzle. Zero secondary flow; primary-nozzle pressure ratio, 2.0.

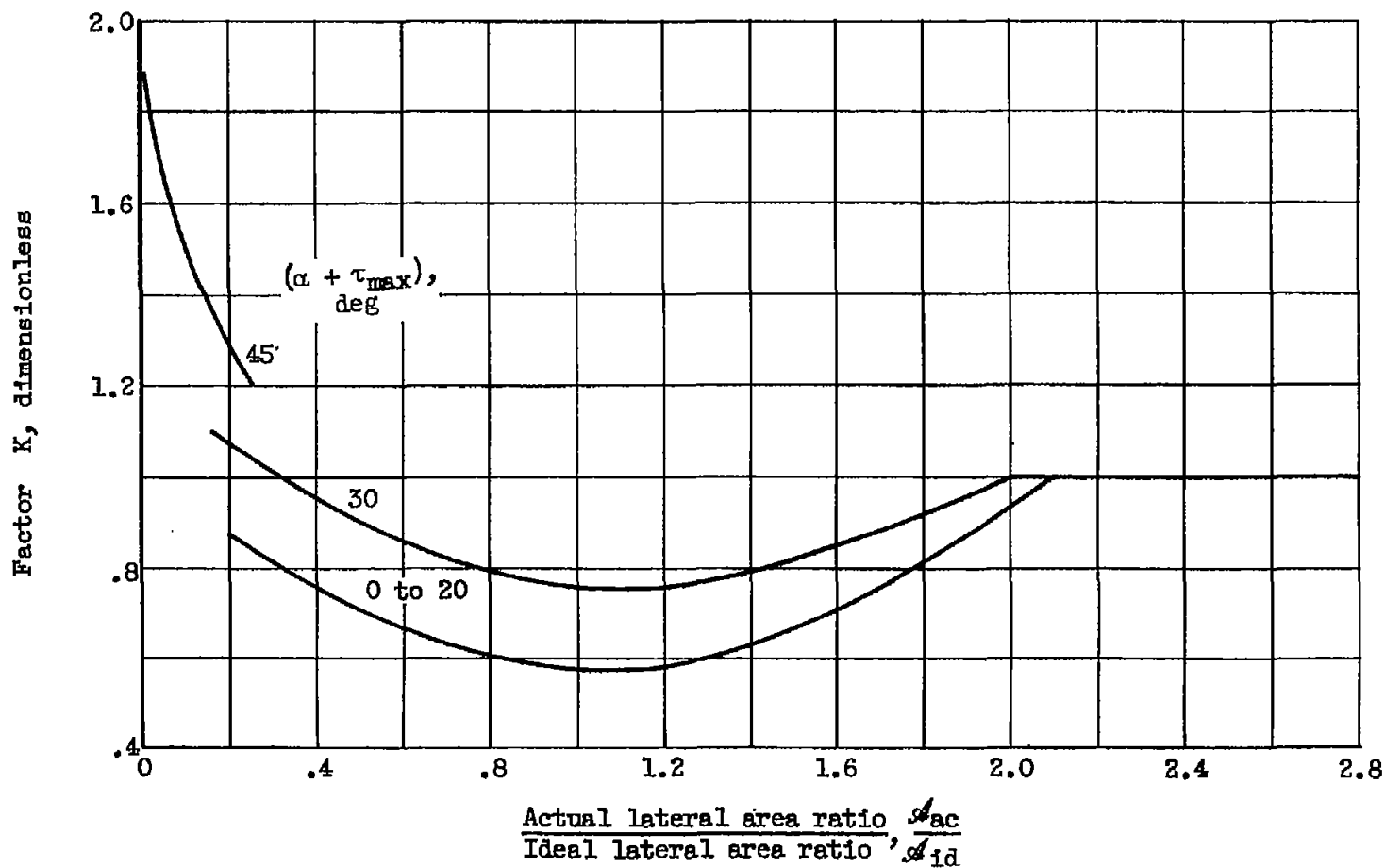


Figure 44. - Design chart for mechanical jet deflectors for primary-nozzle pressure ratios of 2.0 to 2.8 and flap chord angle $\beta \geq 90^\circ$.

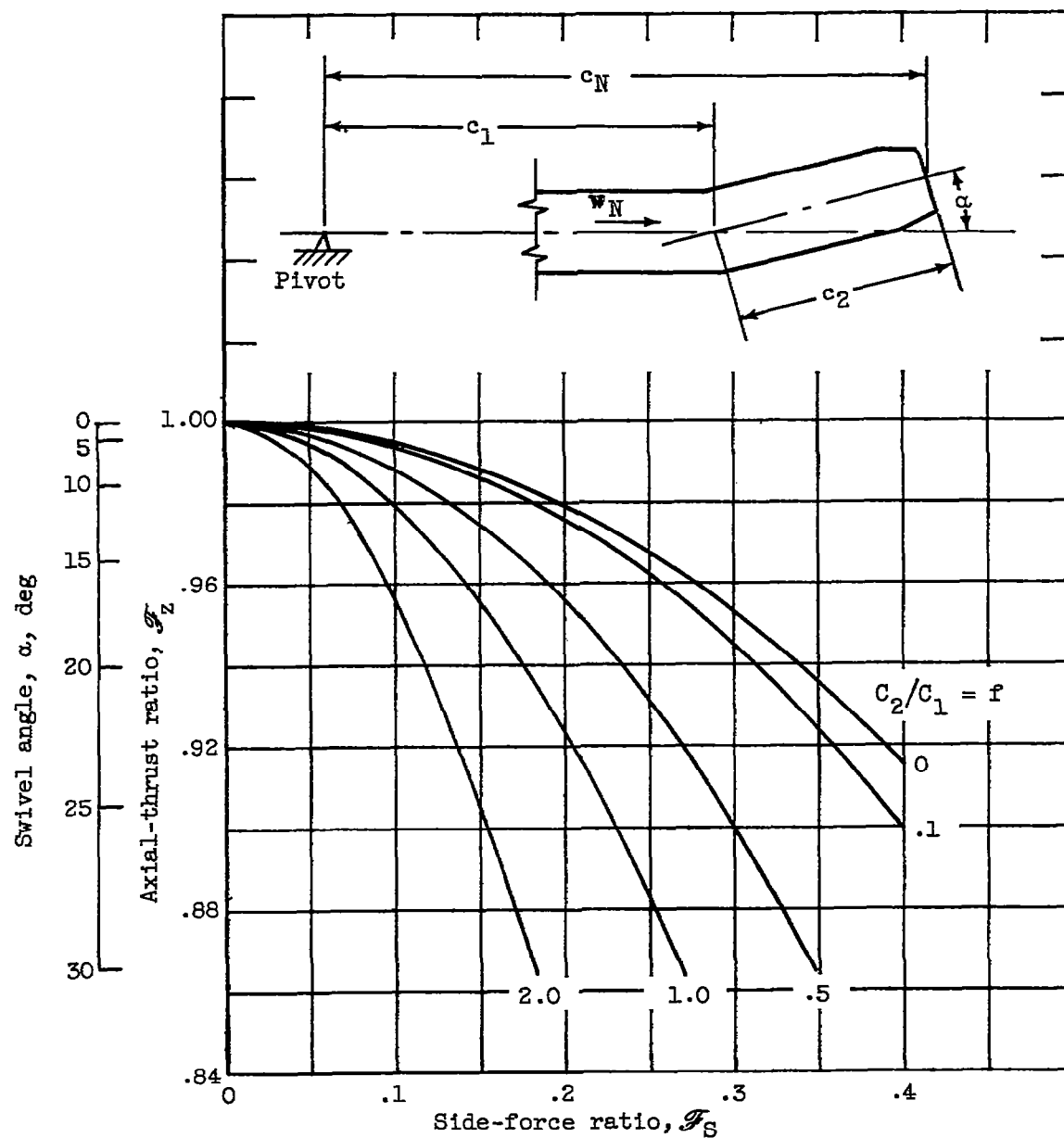


Figure 45. - Analytical performance of swivelled-nozzle-type jet deflectors.

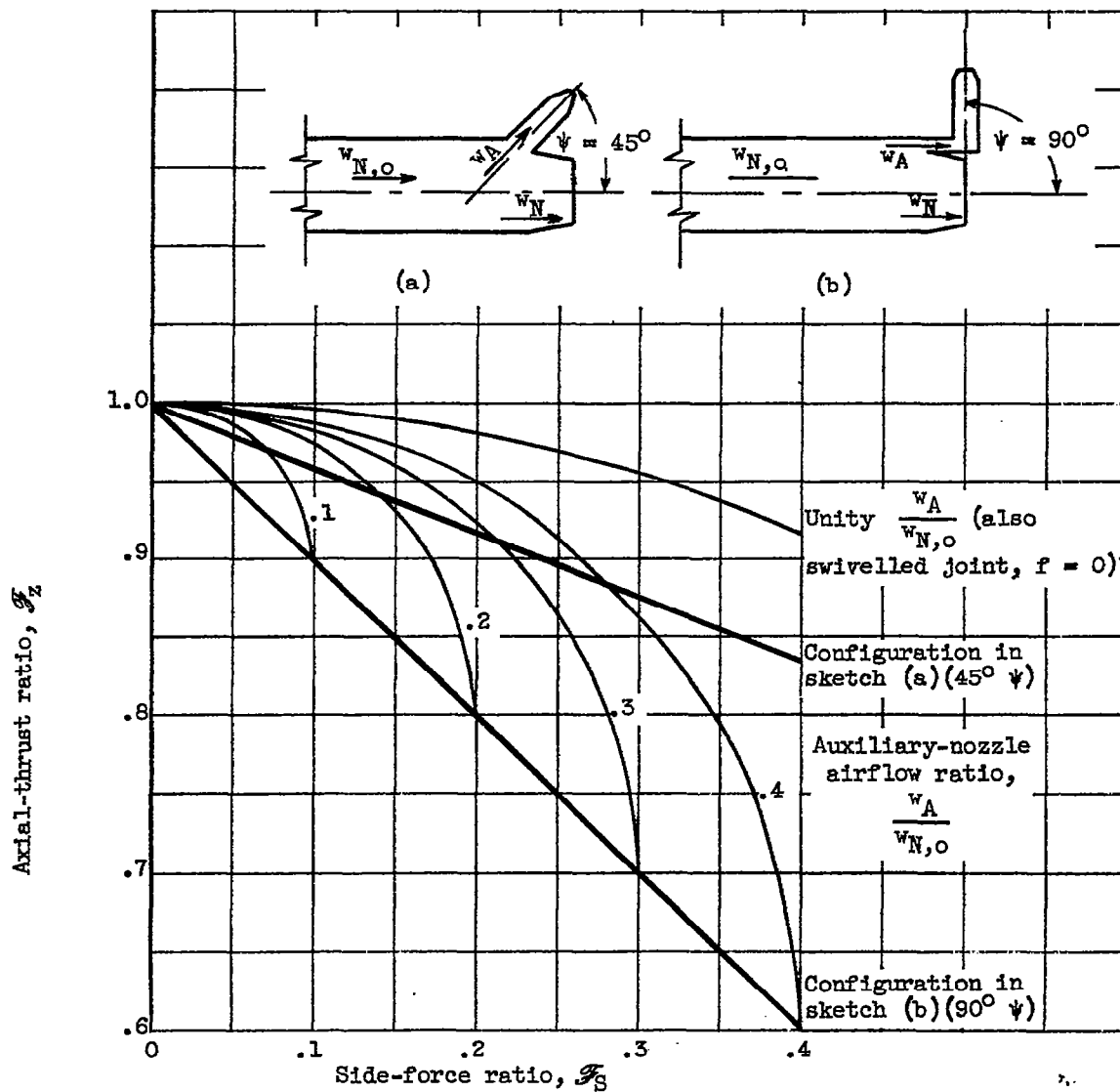


Figure 46. - Analytical performance of auxiliary-nozzle jet deflector.
 $w_A + w_N = w_{N,o}$; no turning losses; primary-exhaust-nozzle area reduced to maintain unactuated tailpipe pressure.

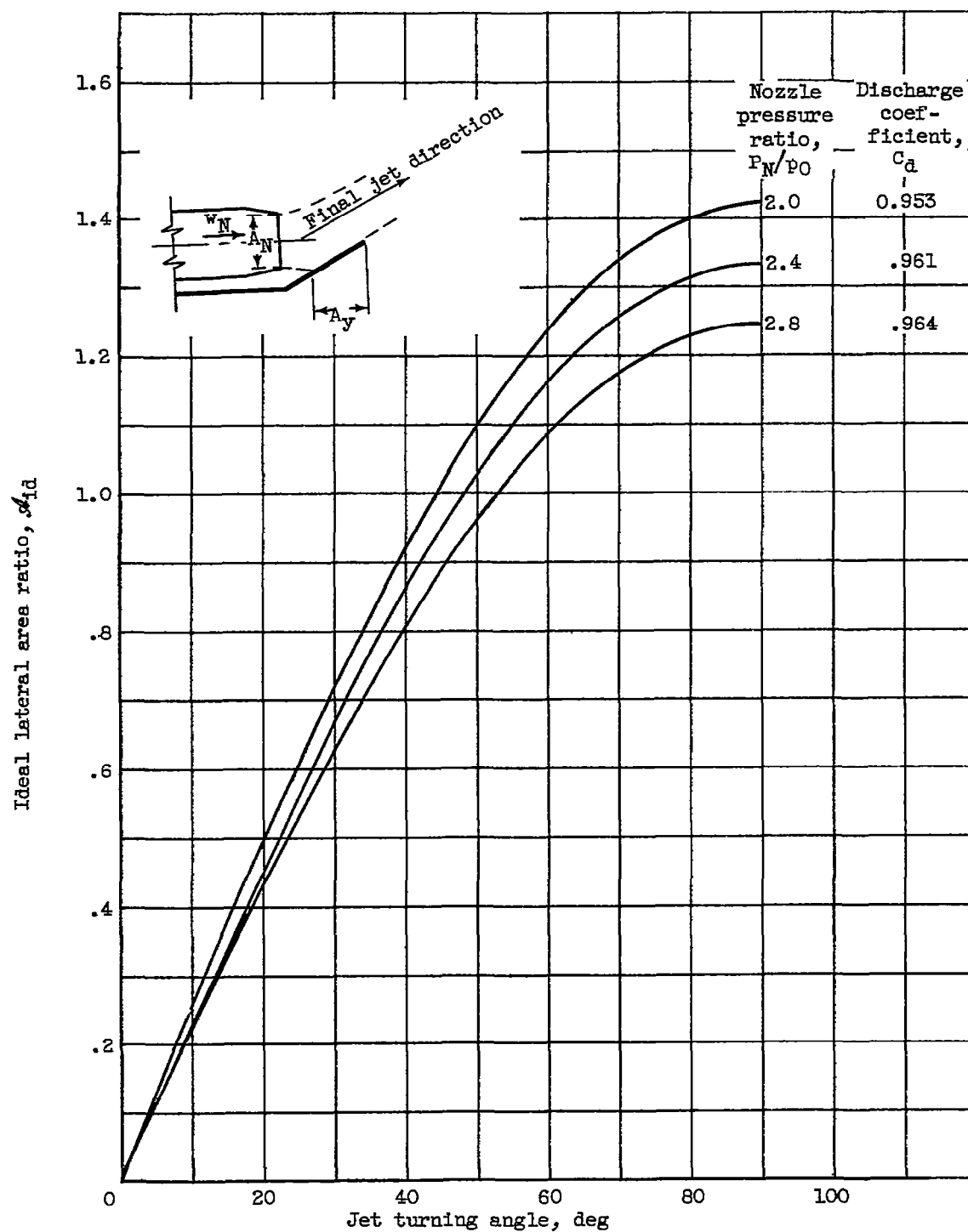


Figure 47. - Ideal lateral area ratio required to turn whole jet with mechanical deflector. Ratio of specific heats, γ , 1.40; primary-nozzle thrust coefficient, C_F , 0.976.

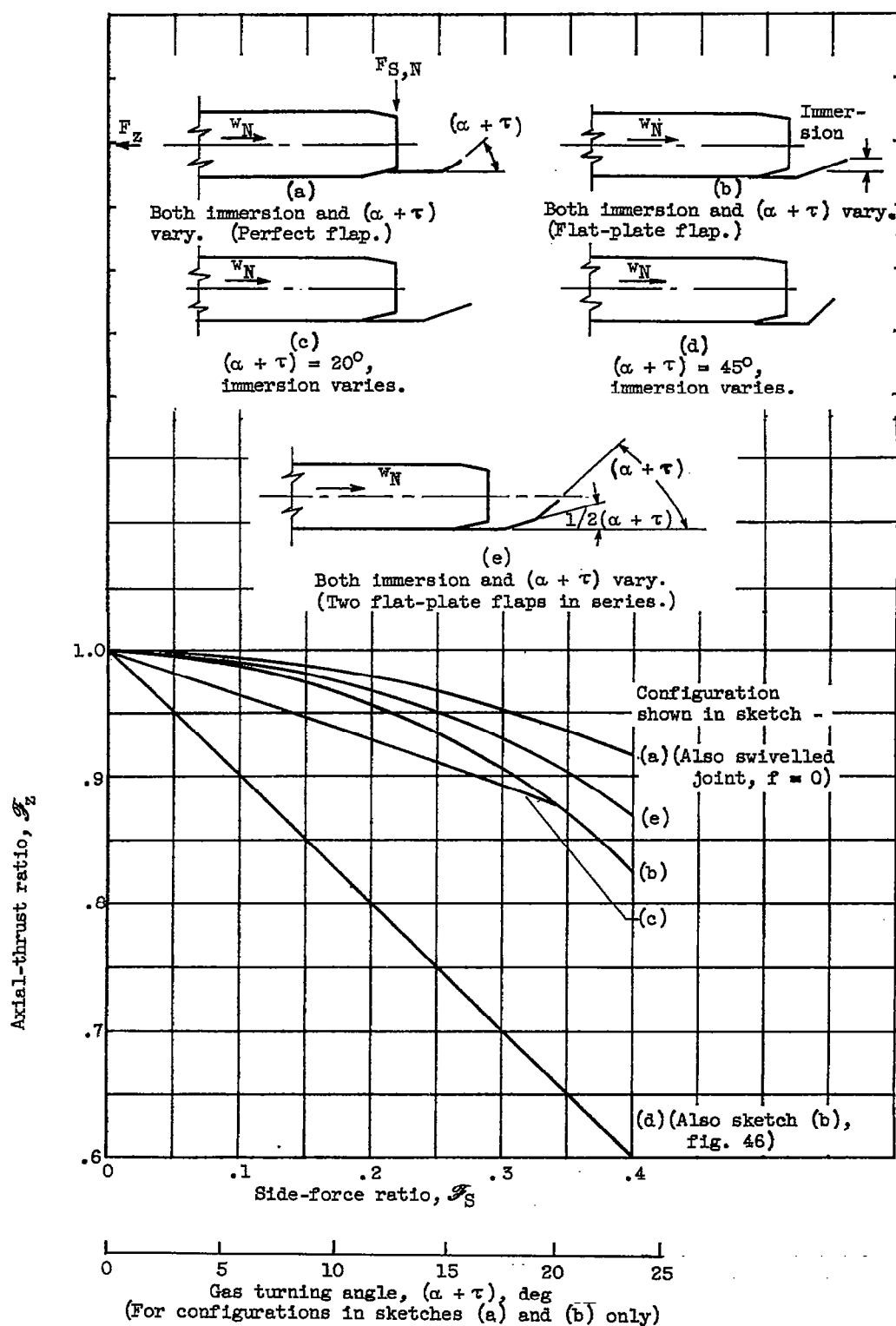
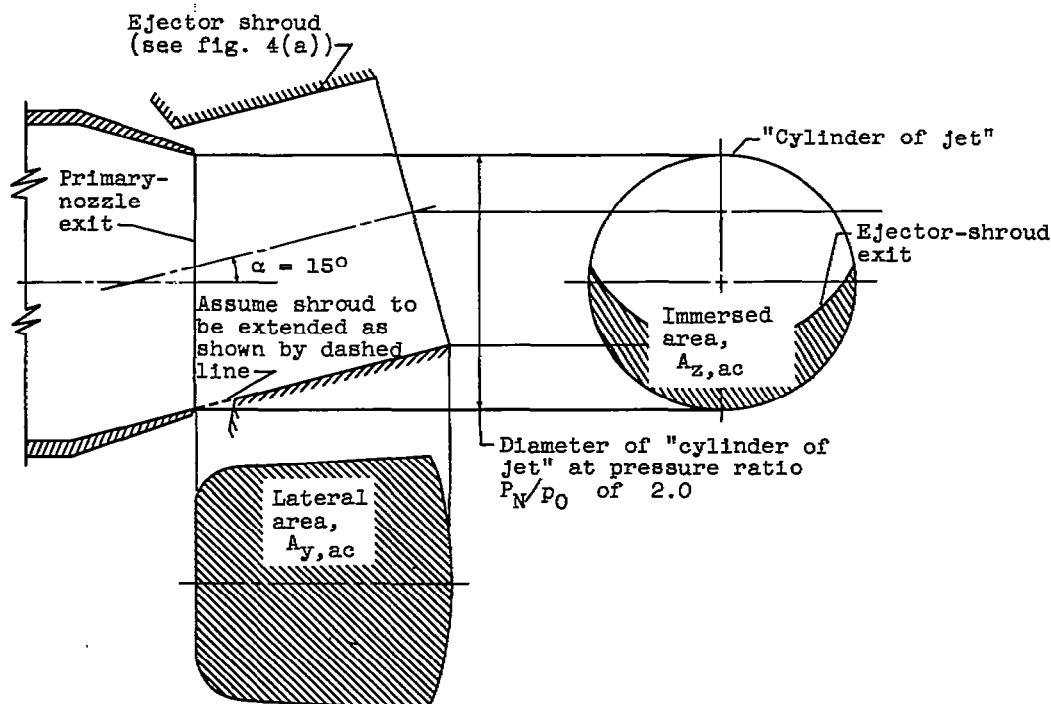
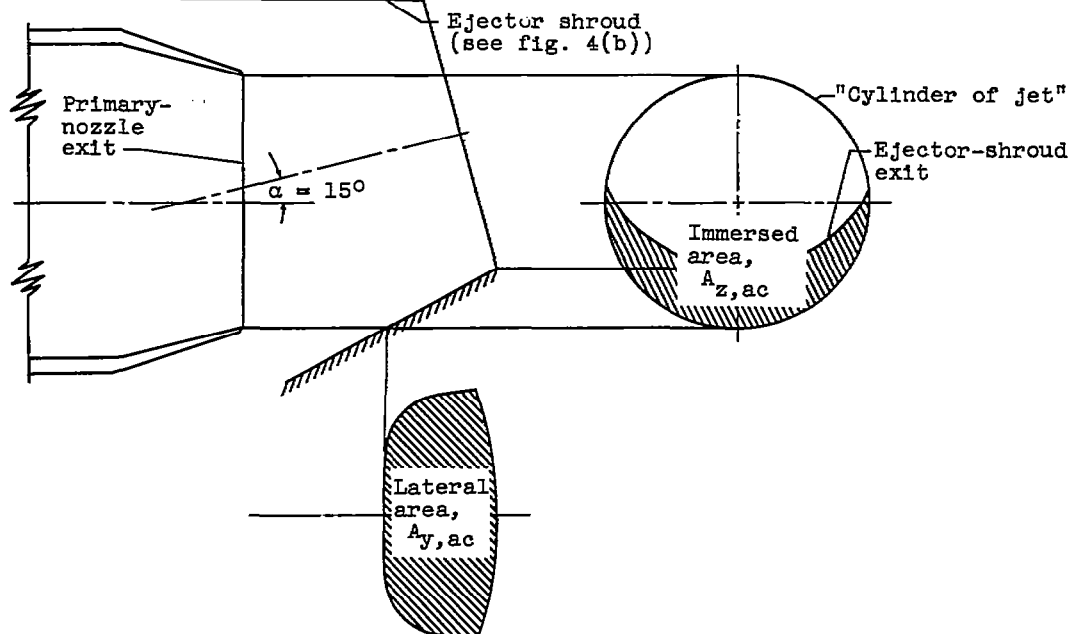


Figure 48. - Analytical performance of mechanical jet deflectors.



(a) Ejector: diameter ratio, D_{sh}/D_N , 1.1; spacing ratio, S/D_N , 0.86; cylindrical shroud.



(b) Ejector: diameter ratio, D_{sh}/D_N , 1.1; spacing ratio, S/D_N , 0.87; conical shroud.

Figure 49. - Immersed area and lateral area for ejector with shroud swivelled 15° . Primary-nozzle pressure ratio, 2.0.